Computer simulations of adsorption and molecular recognition phenomena in molecularly imprinted polymers

Eduardo Manuel de Azevedo Dourado

A thesis submitted for the degree of Doctor of Philosophy

The University of Edinburgh

2011

Abstract

Molecularly imprinted polymers (MIPs) are a novel, promising family of porous materials with potential applications ranging from separations, chemical sensing and catalysis to drug delivery and artificial immunoassays.

The unique feature of these materials is their biomimetic molecular recognition functionality. Molecular recognition is the biological phenomenon of specific, selective and strong association between a substrate and a ligand. In man made MIPs this functionality is implemented via templated synthesis protocol. MIPs are synthesized in the presence of additional template molecules which form complexes with functional monomers in the pre-polymerization mixture. After polymerization, the template is removed, leaving cavities in the structure which are complementary in shape and interaction patterns to the template molecules. These cavities act as mimics of biological receptors and are able to recognize and rebind template molecules.

Although the imprinting concept is simple in principle, synthesis of MIPs with precisely controlled characteristics and performance remains a challenging task. Composition, polymerization conditions, template removal process and application conditions all affect the properties of MIPs. The material is affected at different scales, but crucially at the microscopic level, the number, fidelity and accessibility of binding sites are dependent on all the factors mentioned. The full potential of these materials can only be achieved if researchers can control and optimize the properties of MIPs through detailed understanding of adsorption and molecular recognition processes in these materials.

The objective of this work is to, using computer simulations and statistical mechanics; develop a fundamental description of MIP formation and function, and to link morphological features of the model materials to their molecular recognition capabilities. In general, molecular simulations employed in this study should allow easier and more efficient exploration of a vast number of factors influencing the behaviour of MIPs.

At the heart of the approach developed in this thesis is a computational strategy that imitates all the stages of MIP formation and function. First, the model simulates the

pre-polymerization mixture, allowing the formation of template-functional monomer complexes. (This stage is implemented via canonical Monte Carlo simulation). Complexes can have different structures, depending on the chemical nature of template and functional monomer; therefore complexes can have a range of association constants. The distribution of template-functional monomer complexes also translates into a distribution of binding sites of different specificity after template removal. In the second stage of the process, adsorption simulations (grand canonical Monte Carlo) are performed for a variety of model MIPs prepared to assess the role of various processing conditions such as composition, density and binding sites degeneration.

This strategy was first applied to a simplified description of MIP species in order to identify the minimal model capable of molecular recognition and thus shed the light on the very nature of this phenomenon. In the developed model, the molecular species are constructed from hard spheres, featuring small interaction sites on their surfaces. The bond between two interaction sites has the strength and topological features of a typical hydrogen bond. The model exhibits molecular recognition, being able to preferentially adsorb template molecules. The associations between template and functional monomers were analyzed and classified to describe the distribution of binding sites and their heterogeneity. Using this model, several experimental trends typically observed in MIP studies could be explained, such as maximum in the selectivity as a function of monomer concentration. Using this model, we were also able to explore hypothetical, alternative protocols for MIP synthesis in order to improve their performance. These include the use of alternative templates and the post-synthetic surface modifications of MIPs.

The general strategy to modelling MIP, employed in this thesis, was then applied to a more detailed description of MIPs with realistic force field potentials for all the species involved. This more elaborate model is simulated with a combination of molecular dynamics (MD) and Monte Carlo techniques.

This detailed model provided a wealth of information on various types of complexes observed in the pre-polymerization mixture. Specifically, it revealed the relative weight of different interactions in the complex and their role in the binding energy of adsorbates. These simulations also provided the comparison of the relative contribution of different types of interactions (van der Waals, Coulombic) involved in a molecular recognition process.

We believe the insights gained in this work will contribute to the development of rational MIP design strategies. In the discussion of the results of the thesis we speculate on how these models can be further developed in order to generate quantitative predictions and what type of systems it would be interesting and important to investigate in the future.

Declaration

The work presented in this thesis was carried out in the School of Engineering, the University of Edinburgh, and is a result of the original work of the author, except where acknowledged in the text. The thesis was composed by the author and was not submitted to any other degree or professional qualification.

_____

Eduardo Manuel de Azevedo Dourado

June 2011, Edinburgh

Acknowledgments

I must thank my supervisor Lev for his patience, encouragement and his time. Your love of science and your practical view of research were re-assuring and inspiring.

I'd like to thank the IMP for their stimulating environment. Particularly, I am grateful to Prof. Nigel Seaton, Prof. Stefano Brandani and Dr. Tina Düren for their feedback during the adsorption group meetings. Many thanks also to Dr. Carmelo Herdes for his support and advice.

The vibrant and welcoming multinational environment of the post-graduate community was a great help in my life in Edinburgh, both academically and socially. I'd particularly like to thank Yavor, Christian, Jacqueline, Claudia, Carlos, Meropi, Milan, Jeniffer, Peyman, Panos, David and Alex.

I can't forget the vibrant smile and laughter that welcomed me every bleak cold morning in the Kenneth Denbigh Building. Thank you so much Agnes.

Very special thanks must go to these friends; they have enriched my life so much. In their own way, they helped my academic experience, but most of all they made my life happier.

Thank you Millie for always being there with a kind word and a smile.

Evi, thank you for so many engaging discussions and especially for all the trips and fun we had.

David Martins, your experience and advice were so valuable, but not as much as your friendship.

Jose Costa was more than the best flatmate I could have whished for. Your trust, confidence and drive were an inspiration. Thank you for being such a great friend.

To my family, what can I say…? You are the reason I am the man I am today. Thank you for your endless support and love.

Dissemination

The work described in this thesis has been subject of publication and presentation by the author; further dissemination is also being prepared.

Publications

Dourado, E. M. A., Sarkisov, L. "Computer simulation of adsorption in simple models of molecularly imprinted polymers", Modelling and Simulation of New Materials: Proceedings of Modelling and Simulation of New Materials: Tenth Granada Lectures, AIP Conf. Proc., 1091, pp. 256-261, January 21, 2009.

Dourado, E. M. A., Sarkisov, L. "Emergence of molecular recognition phenomena in a simple model of imprinted porous materials", J. Chem. Phys. 130, 2009.

Presentations

Dourado, E. M. A., Herdes, C., Sarkisov, L. "Characterization of molecularly imprinted polymers", insights from computer simulations; poster presentation; COPS VIII – 8th International Symposium on Characterization of Porous Solids , June 2008, Edinburgh, UK.

Dourado, E. M. A., Herdes, C., Sarkisov, L. "Theory and computer simulation of adsorption in templated molecular recognition materials", oral presentation, 10th Granada Seminar on Computational and Statistical Physics: Modelling and Simulation of New Materials, September 2008, Granada, Spain.

Dourado, E. M. A., Herdes, C., Sarkisov, L. "Computer Simulation of Adsorption and Molecular Recognition Phenomena in Imprinted Polymers", oral presentation, AIChE Annual Meeting 2009, November 2009, Nashville, USA.

Table of Contents

List of Figures

the Langmuir-Freundlich isotherms. a) AD for pyrazine rebinding in MIP_PRZ (solid line), and pyrimidine adsorption in MIP_PRZ (dashed line). b) AD for pyrimidine rebinding in MIP_PMD (solid line), and pyrazine adsorption in MIP_PMD (dashed line). c) Comparison of the characteristic ADs (from template rebinding) for both MIP_PRZ and MIP_PMD.

List of Tables

1.

Introduction

Functional porous materials have been playing an increasingly important role in a number of applications, from adsorption to sensing or drug delivery. The interest in materials capable of *biomimetic molecular recognition*, such as molecularly imprinted polymers (MIPs), is driven by the immense opportunities and applications that they offer. However, one of the challenges in the development of MIPs is the lack of adequate understanding of the adsorption and binding processes in these materials and of a description of the recognition binding phenomena on a molecular level.

The principal focus of this thesis is to increase the understanding of the molecular recognition phenomenon and its resulting effect on the adsorption behaviour of MIPs.

This chapter provides an introduction to the early studies of materials capable of molecular recognition. This is followed by a summary of the imprinting technology in polymers and their applications. Later, the challenges faced by researchers in the characterisation and optimization of MIPs, are presented. Molecular simulation has been shown to be an invaluable tool to address some of these challenges; we then outline simulation strategies and models used in previous studies. Finally, we formulate objectives for the present work and outline the structure of the thesis.

1.1. Historical perspective

Molecular recognition is a process of specific non-covalent interaction between a ligand and a substrate, exhibiting structural and interaction complementarities (host-guest interaction). It plays a vital role in processes in biological systems, especially at the cellular level, and is essential to life. DNA replication, enzyme-substrate complexes, antigen-antibody are examples of such interactions. The research on this phenomenon created the basic principles that lead to synthesis protocols for molecular imprinting, thus it is important to briefly examine molecular recognition from the biological perspective.

1.1.1. Understanding molecular recognition through lock-and-key analogy

While studying the characteristics and functions of enzymes, Fischer observed they could exhibit stereochemical selectivity. A mechanism he

explained with an analogy well fitted for the mechanical age he lived in. "To use a picture, I will comment that enzyme and glucoside must fit each other like a lock and key, in order to carry out a chemical result on each other" (Fischer 1894). It is a simple and remarkable observation considering that X-ray diffraction would not be discovered for 20 years and yet another 20 years would pass before the first organic and biological structures were discovered. Molecules have shapes (identity), they can interact (recognize) and fit (compatibility) "like a lock and key" (Meyer 1995).

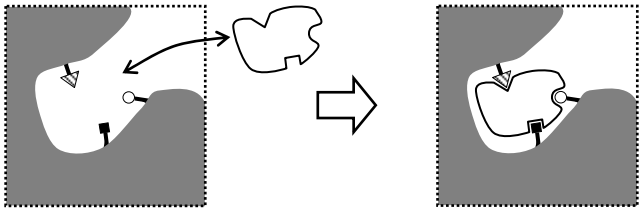

Figure 1.1: Schematic representation of the interaction between a ligand and a substrate that exhibit shape and interaction complementarity.

This analogy simply highlights the requirement for complementarity of the molecular shape as well as of the interaction patterns, represented schematically in Figure 1.1. Several attempts were made to replicate molecular recognition in man-made structures using cyclic hydrocarbons and other cage-like systems to create specific interactions and study the phenomenon. These attempts were generally too costly and impractical as alternatives to their biological equivalents (Marty and Mauzac 2005).

1.1.2. Early studies of molecular recognition in abiotic systems

The first report of a molecular imprinting phenomenon in an abiotic system was not a consequence of a deliberate molecular "construction", but rather a

chance observation. It was made by Polyakov in 1931. In his work, some silica gels samples were prepared with the inclusion of a solvent additive (Polyakov 1931). Later the adsorption studies of the silica showed preferential binding for the additive. In subsequent studies the selectivity was explained as arising from the structural properties of the silica due to the additive (Polyakov *et al.* 1933). This work went relatively unnoticed by western science.

At around the same time of Polyakov's studies, the nature of selectivity of antibodies was being debated. One explanation was that of instructional theory (Breinl and Haurowitz 1930; Mudd 1932) endorsed by Linus Pauling (Pauling 1940), where the formation of an antibody is induced by the presence of an antigen which serves as a template. Instructional theory was later eventually abandoned in favour of the clonal-selection theory (Burnet 1976). However, instructional theory principles were subsequently used in Pauling's group to examine how the same mechanism could work for inorganic systems. Dickey performed synthesis of silicas using a process very similar to Polyakov's, but using various dyes to create a templating effect (Dickey 1949). The results showed a significant selectivity of the materials produced towards the dye used during the polymerisation process. Further studies were done by Dickey and other groups and these selective materials soon found applications in chromatographic separations (Alexander *et al.* 2006).

The early methods of Polyakov and Dickey live on, albeit in a more developed form, in modern molecular imprinting procedures. The somewhat modest activity that continued in this area over several decades, after the

work of Polyakov and Dickey can be probably explained by rather low chemical specificity of the imprinted silica materials. In other words, it seems that the observed specificity in the materials was due solely to geometric molecular compatibility. This effect alone was not sufficient to generate materials with the true recognition functionality. Although studies in the area of imprinted silicas continue to emerge (particularly with the focus on surface functionalized silicas), the true potential of the imprinting technologies could be realized only with materials offering a more versatile chemistry and building blocks.

1.1.3. Development of molecularly imprinted polymers (MIPs)

The next significant step in molecular imprinting was the introduction of molecularly imprinted organic polymers by Wulff and Sarhan (Wulff and Sarhan 1972) and by Takagishi and Klotz (Takagishi and Klotz 1972), in 1972, independently. In the synthesis of these polymers, a template molecule is added to the pre-polymerization mixture. In this mixture, functional monomers are present which can interact and covalently bind with the template. Post-polymerization removal of the template leaves the matrix with imprinted cavities.

Another important landmark development in the field was the introduction of non-covalent molecular imprinting of organic polymers by Mosbach in 1981 (Arshady and Mosbach 1981). In this case the interactions between the template and functional monomers are non-covalent. This opened the possibility to use imprinting protocol for a much wider range of templates than what was previously possible since it does not require chemical bonds to be created or broken (Sellergren and Allender 2005).

1.2. MIPs: technology overview

One can better grasp the great technological potential of molecularly imprinted polymers, by understanding the synthesis protocol used to create them. MIPs are polymers which are synthesized in the presence of a template or imprint molecule. The presence of such an additive molecule has a structure directing effect (imprinting) on the polymer matrix resulting from polymerization. In the case of molecularly imprinted polymers, the functional monomers are chosen so that they interact with the template to form stable complexes. The template can be extracted from the MIP, leaving cavities in its place. These cavities have structure and interaction patterns complementary to the template. As a result, these cavities, or binding sites, possess specificity which makes them capable of exhibiting binding affinity and selectivity, mimicking biological molecular recognition. A schematic representation of the generic synthesis process is described in Figure 1.2.

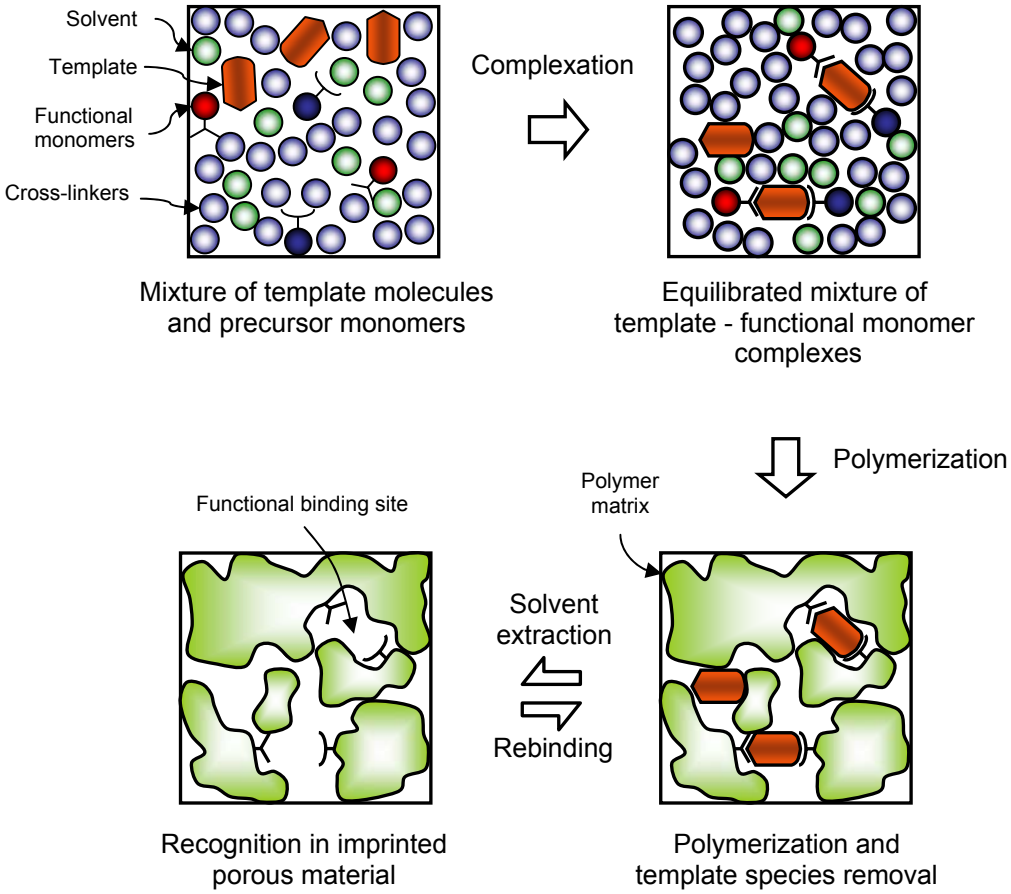

Figure 1.2: Schematic representation of the imprinting process in polymers.

This scheme also illustrates the possibilities of a more general use of molecular imprinting as the same approach can be employed (with different limitations) to imprint even very large templates, such as proteins, crystals, viruses and cells (Alexander *et al.* 2006).

1.2.1. Review of available MIP synthesis protocols

Although the idea of the imprinting procedure can be described by the generic scheme depicted in Figure 1.2, the ways by which the template-functional monomer complexes are formed can vary. Different imprinting

protocols fall into two general approaches, depending on the nature of the association between template and functional monomers: covalent or non-covalent.

As mentioned before, Wulff and Klotz designed MIPs imprinted covalently (Takagishi and Klotz 1972; Wulff and Sarhan 1972). This requires a pre-arrangement of template and functional monomer species and the creation of chemical bonds between them. For the case of the non-covalent strategy, the self-assembly of the species in a complex is governed by weaker electrostatic and Van der Waals interactions.

As expected, covalent imprinting creates complexes with much greater stability which can withstand the polymerization process. The chemical equilibrium is also much more favourable as lower concentrations of functional monomers are required to produce a good population of binding sites. The inherent stability leads to binding sites that are more homogeneous in their affinity and morphology.

For non-covalent imprinting the nature of the interactions involved leads to the demand for concentrations of functional monomer well above that of the template, the complexes are less stable and can have different conformations, which also increases heterogeneity of the binding sites. Polymerization can have adverse effects on the complex and lead to their degeneration and ultimately to poorly formed binding sites. However, two very important advantages of the non-covalent imprinting technique are the fact that the template can easily be extracted from the material and the very broad range of templates and functional monomers available, making this strategy very

versatile. In table 1.1, a summary of characteristics for covalent and non-covalent imprinting is presented.

Table 1.1: Characteristics of covalent versus non-covalent imprinting.

	Covalent	Non-covalent
Synthesis of template – functional monomer complex	Required	Not required
Structure of target binding site	Well defined	Not well defined
Polymerization conditions	Broad	Rather restricted
Removal of template	Difficult	Easy
Target-binding / Target-release	Slow	Fast

Overall, non-covalent imprinting is the most widely used, due to the sheer magnitude of template/functional monomer/cross-linker combinations possible. However, because of the limitations of both approaches, other options and developments upon these processes have been explored, such as semi-covalent imprinting. For an in-depth description of examples of synthesis protocols as well as more evolved techniques, the reader is directed to a recent review article (Alexander *et al.* 2006).

1.2.2. Typical non-covalently synthesized MIPs

To give the reader a better understanding of what MIPs are, an example of a typical MIP synthetic protocol as used by Andersson and co-workers (Andersson *et al.* 1996), is provided in the table below.

Table 1.2: Example of a typical MIP composition. Adapted from (Andersson *et al.* 1996).

Component	Chemical formula	Role	Composition
Methacrylic acid (MAA)	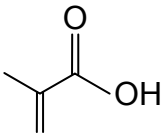	Functional monomer	0.39 M
Ethylene glycol dimethacrylate (EGDMA)	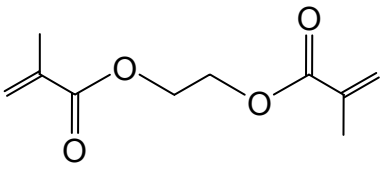	Cross-linker	1.96 M
Azobisisobutyronitrile (AIBN)	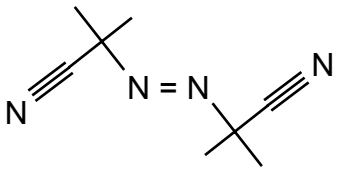	Initiator	0.03 M
Pyridine	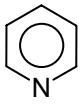	Template	0.10 M
Chloroform	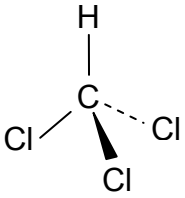	Solvent (porogen)	7.40 M

The monomer mixtures were cooled on ice and degassed in a sonicating bath followed by sparging for 15 min with nitrogen. Polymerization was initialized with ultraviolet (UV) light at 4°C for 44 h. The bulk polymers produced were white colour monoliths, which had to be ground and characterized.

Typical materials prepared in this manner are micro and mesoporous with areas ranging widely from ~40 to 400 m^2g^{-1}, depending on polymerization conditions (Al Kobaisi *et al.* 2007).

1. 3. Applications of MIPs

Separations and chromatography have historically been the most prominent applications of MIPs and other imprinted materials such as silicas. The reason for this is obvious: the remarkable selectivity in MIPs makes them ideal for the design of separation processes. A very successful commercial application has been solid phase separation, with products in medicinal and analytical chemistry (e.g. Biotage, former MIPtechnologies). Examples of application of MIPs for separations are numerous (Alexander *et al.* 2006), but one particularly interesting case is the separation of enantiomers, which is a well recognized challenge in the chemical industry (Maier *et al.* 2001). Separation of enantiomers has also been one of the key issues in the pharmaceutical industry, where often (and increasingly so) the final product must be in a single pure enantiomer form. A number of studies demonstrated the capability of MIPs to separate chiral mixtures. Recent progress in this area has been extensively discussed by Maier and co-workers (Maier *et al.* 2001; Maier and Lindner 2007).

MIPs can be used as artificial antibodies in pseudo-immunoassays. Typically they are used in a homologous competition format (two chemically similar species compete for binding sites). Because heterogeneity of binding sites is a pervasive problem, the results have to be interpreted in the view of polyclonal antibody mixtures (Pap and Horvai 2004). Although the use of MIPs can require a more complicated analysis of the results, still many advantages can be obtained by this alternative. MIP based assays are much more chemically, thermally and mechanically stable and can be more easily stored. They can also be re-used and there is no requirement for the use of

lab animals. The specificity of MIPs can in some cases rival that of their biological counterparts. Further details on the use of MIPs for immunoassays can be found, *e.g.* in (Lavignac *et al.* 2004) and (Ye and Haupt 2004).

Catalysis in porous adsorbents has a long history in the chemical industry. Several effects, such as confinement as well as the fixing of one or more reactants in place, results in the catalytic activity of a porous solid. In the case of MIPs, the binding site, with its restricted arrangement of functional groups and specific morphology, offers more precise arrangement/alignment of the reactants. A binding site can be optimized to create an environment that forces interaction between two or more reactants. It can also serve as a stabilizer for a transition state of the reaction (Ramstrom and Mosbach 1999). The binding site, mainly through conformational interaction energy gains, lowers the activation barrier required for the reactions to proceed. For this case, the template that imprints the binding site must usually be close in structure to the transition state of the product to be formed. For further insight and examples of catalysis in MIPs, the reader is directed to two recent articles (Alexander *et al.* 2003) and (Wulff 2002).

The high specificity of MIPs and the physical-chemical versatility of polymeric materials make them a promising tool for chemical sensing applications. Sensors operate by translating the interaction event (such as binding of a molecule to a substrate) into a quantifiable signal (mass change, fluorescence, electrochemical activity, etc). An example is TNT sensing, recently proposed using MIPs and detection from the gas phase (Moore 2007). A review of MIP sensing technology is outlined in (Hillberg *et al.* 2005) and (Ye and Haupt 2004).

Several truly fascinating and creative applications of MIPs in drug release have been contemplated. Most methods for administrating bioactive compounds still rely on frequent and repeated doses. This is required because a great portion of the dose degrades or is lost by diffusion to other parts of the organism. It is therefore desirable to release the drug closer to the location where it is necessary. This way, less of the drug is required and therapeutic activity is achieved quicker. Controlled drug release has been focusing mainly on slowing the rate at which the drug is released into the organism. This makes it possible to maintain therapeutic concentration of the drug over an extended period of time. This is particularly beneficial for conditions such as cancer, diabetes, etc. Furthermore, timed release can be used to preserve the drug for the release in a more appropriate location. The best known example of this involves polymeric capsules for oral intake, which degrade at a desired rate.

In its basic form, a biocompatible MIP can be imprinted and loaded with a drug molecule of interest. The high affinity of binding leads to slower release rates. Slow permeation of the drug through the pores of a MIP is another factor contributing to the extended release time. Such a setup was studied by Allender and co-workers (Allender *et al.* 2000) using a propranolol imprinted MIP. It was shown that, compared to non-imprinted polymer (NIP), the time required for a certain amount of propranolol to be released nearly doubled (Figure 1.3).

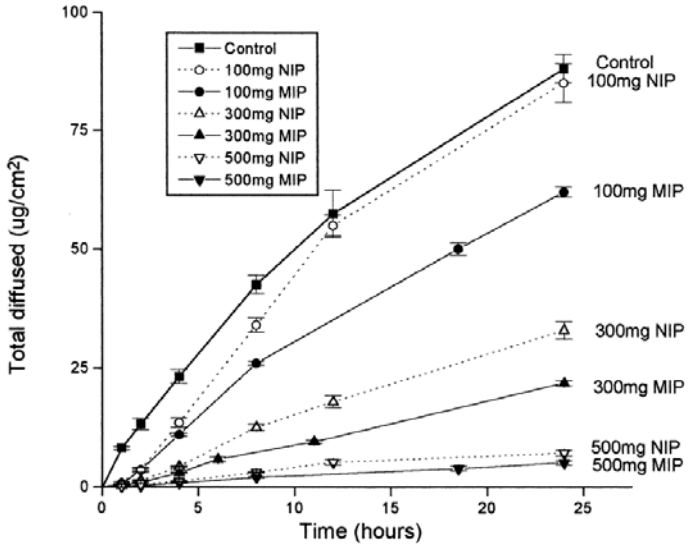

Figure 1.3: Permeation profiles for the transdermal controlled release devices loaded with 0.5 mg of propranolol and varying quantities of MIP and NIP (Allender *et al.* 2000). The imprinted polymers noticeably enhance retention of propranolol, compared to non-imprinted polymers.

Other studies (Piletsky *et al.* 1998; Piletsky *et al.* 1998; Yoshimi *et al.* 2001) have observed shrinking and expansion of the polymeric network due to binding and cleaving of template. The swelling and shrinking of hydro-gels can also be responsive to external stimuli. These can include pressure, pH, temperature or concentration changes, and can be exploited in sophisticated controlled release protocols.

Another interesting release protocol is as follows. One imprints a polymer with a certain template and loads that polymer with the drug molecule to be released. When in solution containing the template, the drug bound in the polymer is replaced by the template, thus releasing it. This has been studied by Sreenivasan using the competitive binding of hydrocortisone (template) and testosterone (drug to be delivered) (Sreenivasan 1999). Almost four times

the release rate of testosterone could be observed when the MIP was in the presence of the template (Figure 1.4).

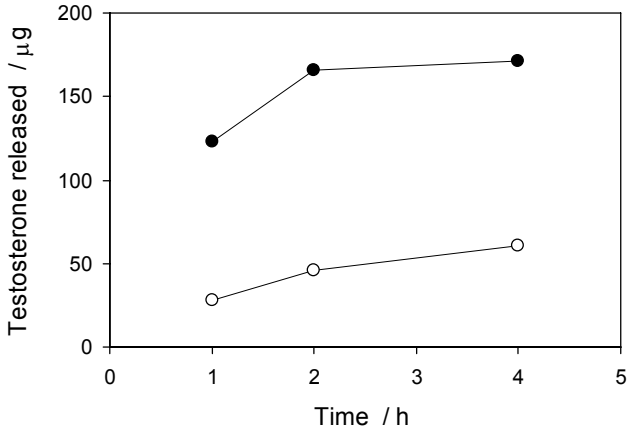

Figure 1.4: Effect of the presence of hydrocortisone in the aqueous medium on testosterone release rate (per 100 mg of MIP). Solid symbols indicate presence of hydrocortisone, whereas open circles indicate it is absent from the aqueous medium. Data taken from (Sreenivasan 1999).

While reviewing MIP applications, it is important to mention some considerations of cost. Consider, for example, the scope and application of MIPs to other porous materials, such as activated carbons and zeolites, commonly used in separations and catalysis. It is clear, that due to higher cost, it would be impractical to use MIPs in a conventional separation processes for which cheaper, efficient alternatives exist. It is the molecular recognition functionality of MIPs that sets them aside from other porous materials and opens a possibility for a number of unique, niche applications. In many of these applications, only a small amount of MIP is required (sensing), or the resulting product has a sufficiently high added value (enantioselective separation of racemic drug mixtures) to justify higher cost of MIPs. Furthermore, in the absence of MIPs, some of the reviewed

applications (immunoassays, biocatalytic processes) can be implemented only using some specialized enzymes. Compared to enzymes, MIPs offer a cheaper and more robust alternative.

1.4 Characterization of MIPs

Two tests are commonly carried out in experiments to characterize the performance of MIPs. In the first type of test, the ability of a MIP to bind and retain a particular species is compared to the same property for a similar non-imprinted polymer (NIP). A good illustration of this effect is observed in the work of Allender *et al.* (see Figure 1.3) where it is clearly shown that the MIP has a slower release rate of propranolol than the NIP, (Allender *et al.* 2000). This is evidence that higher affinity is induced by the binding cavities resulting from the imprinting process.

A different test examines the ability of the MIP to distinguish between two similar molecules. This is well exemplified in the work of Yin and co-workers (Yin *et al.* 2005), shown in Figure 1.5. They prepared a nateglinide-templated MIP and a NIP under the same conditions, with EGDMA and acrylamide (cross-linker and functional monomer, respectively) and some porogenic solvents.

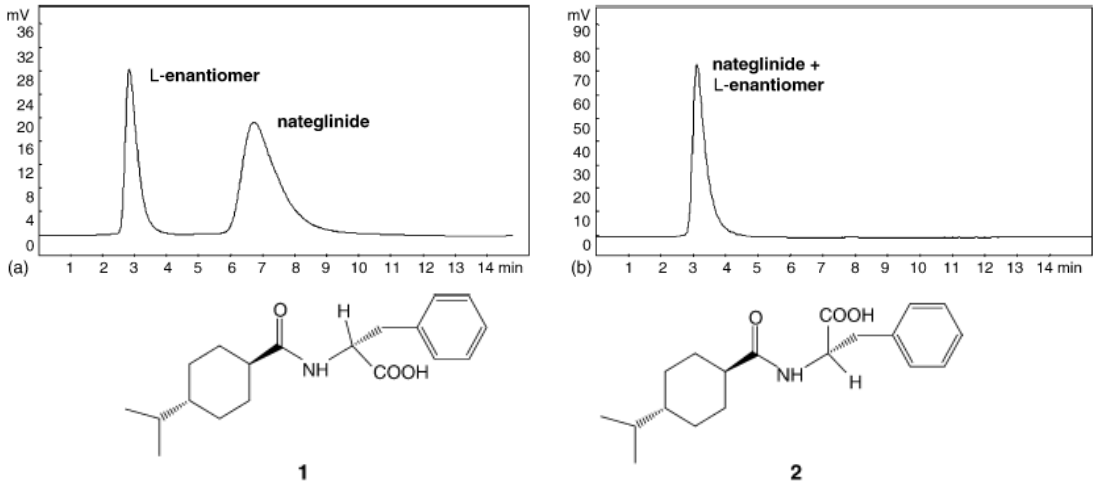

Figure 1.5: Separation of nateglinide (**1**) and its L-enantiomer (**2**) detected by absorption spectroscopy (machine signal as milivolts in yy axis). a) Enantioseparation of nateglinide and its L-enantiomer on monolithic MIP. b) Enantioseparation of nateglinide and its L-enantiomer on NIP. Adapted from (Yin *et al.* 2005).

High performance liquid chromatography studies show that non-imprinted polymer is unable to differentiate between the two enantiomers. The imprinted version of the polymer, on the other hand, displays the ability to retain nateglinide, much more strongly than its L-enantiomer.

One could say that the first type of test (MIP vs. NIP) provides circumstantial evidence of molecular recognition, since the only solid fact is that the imprinting changes the adsorption properties of the porous polymer. The separation of two similar compounds is a more conclusive evidence of *recognition* as it implies the imprinted cavities have some specificity towards the template that imprinted them.

1.4.1. Characterization of binding site affinity distribution

It is an inevitable result of current imprinting protocols that the produced materials will possess a distribution of binding sites. In fact, only a small fraction of binding sites have high enough affinity and specificity to exhibit molecular recognition. For the design and optimization of MIPs, it is vitally important to characterize the heterogeneity of binding sites in MIP structures. Here several methods available for this purpose will be reviewed.

A measure of the heterogeneity of binding sites is the affinity distribution (AD), which reports the number of binding sites N with a certain affinity K (plotted usually as N *vs.* log K). The AD is characterized by two parameters: N_T, the total number of binding sites and K_0, the average affinity.

Affinity distributions can be extracted from adsorption isotherms. These isotherms are obtained from rebinding experiments where the MIP is placed in a solution with a known concentration of the template. After equilibration the concentration in solution, F, can be measured and the adsorbed concentration, B, calculated. By fitting isotherm models to experimental data, the relation between N, the number of sites and K, the affinity, can be determined (Figure 1.6).

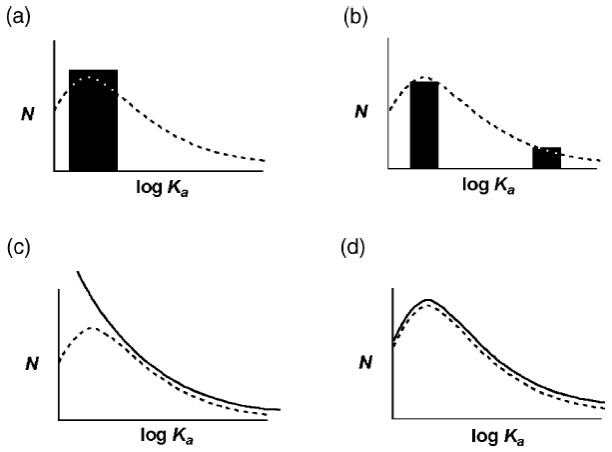

Figure 1.6: Binding models, shown as solid lines and bars, and the broad unimodal affinity distribution assumed for MIPs (dashed lines). Discrete models: a) Langmuir and b) Bi-Langmuir. Continuous models: c) Freundlich and d) Langmuir-Freundlich (Umpleby *et al.* 2004).

In discrete binding site models, the binding site distribution consists of several discrete types of sites. In the simplest case, only one type of sites is present, hence it models a homogeneous site population. This situation can be described by the Langmuir isotherm (Langmuir 1916):

$$B = \frac{NKF}{1+KF} \qquad \text{I.1,}$$

A more realistic picture is when two types of binding sites are considered. This leads to a Bi-Langmuir isotherm.

$$B = \frac{N_1 K_1 F}{1+K_1 F} + \frac{N_2 K_2 F}{1+K_2 F} \qquad \text{I.2}$$

This was the approach employed by Vlatakis and co-workers (Vlatakis *et al.* 1993). More types of sites can be added increasing the accuracy of the representation. A convenient way to analyse this type of isotherms is the Stratchard plot where B/F is given as a function of B. If the bi-modal binding

site distribution is adopted, the experimental points should fit two straight lines on the Stratchard plot (Figure 1.7). This can be used to validate if the bi-modal model is appropriate for a particular system.

These discrete models suffer from several drawbacks. They are poor representations of the porous space, as well as being subject to intuitive assumptions about how many types of sites should be considered, and in which concentration ranges.

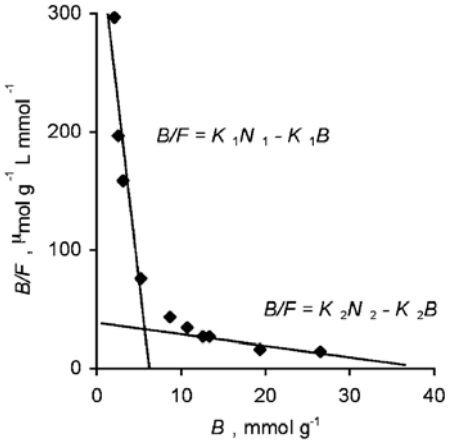

Figure 1.7: Example of a Stratchard plot for an ethyl adenine-9-acetate imprinted polymer, with a bi-Langmuir model fitted. Adapted from (Umpleby *et al.* 2004).

Recently, some researchers argued that a more accurate description of binding site distribution are continuous models, such as, for example, resulting from the Freundlich isotherm (Freundlich 1906):

$$B = aF^m \qquad \text{I.3,}$$

where *a* is a measure of the capacity and affinity of the surface, though N_T and K_0 cannot be deduced directly from it; m is an indicator of the heterogeneity of the surface varying from 0 (heterogeneous) to 1 (homogeneous) (Umpleby *et al.* 2004). An example of the distribution corresponding to this isotherm is given in Figure 1.6. Although, this continuous distribution is a more realistic representation of the binding site heterogeneity, the Freundlich model does not capture the low concentration regime where the Henry's law regime is approached. An improvement on this is the hybrid Langmuir-Freundlich (LF) isotherm:

$$B = \frac{N_T K_0^m F^m}{1 + K_0^m F^m} \qquad \text{I.4,}$$

where N_T is the total number of sites and K_0 is the median affinity. The fundamental assumption for the LF isotherm is that the surface consists of patches of different adsorption energies, wherein on each patch a Langmuir isotherm operates. The behaviour of this model is shown in Figure 1.6. Despite being a better description of the heterogeneity, these continuous models also have disadvantages: they are applicable only to a specific range of concentrations; the LF isotherm does not capture the behaviour in the Henry's law regime (low concentration region). Parameters *a* and *m* are fitting parameters, but *m* can be taken as an indication of heterogeneity. At m=1, equation I.4 reduces to the Langmuir isotherm, at values lower than this (>0) the isotherm changes towards a rectangular isotherm.

In general, affinity distribution analysis provides a useful tool to characterize an imprinted porous material and to distinguish it from similar non-imprinted structures. Affinity distributions in non-imprinted materials are

typically broader and skewed towards lower affinity sites compared to the imprinted material. Using the affinity distribution to distinguish between the two similar imprinted materials is a much more subtle issue, as affinity distribution methods suffer from several limitations. Specifically, recovering the affinity distribution is an ill posed problem and a particular affinity distribution is not a unique solution: in other words different affinity distributions (unimodal, bimodal) can reproduce the same rebinding isotherm. Accuracy of the affinity distribution methods to describe the behaviour in high saturation regimes (where all the specific binding sites should already be occupied) is also an issue to consider. This lack of robustness in the affinity distribution methods hinders their role in the rational design of MIPs.

1.5. Rational design and optimization of MIPs

Researchers have at their disposal a large array of cross-linkers, functional monomers and polymerisation conditions for MIP synthesis. Furthermore, the number of studies exploring MIPs and combinations of template and monomer pairs is vast.

Synthesis of a new MIP requires two key decisions. First, one must select the building blocks for the new material (functional monomers and cross-linkers). Secondly, optimize the processing conditions, such as concentrations of the components, to achieve a MIP with a desired property. These decisions will depend on the template and the desired functionality of

the material. Properties such as the porosity of the MIP, its binding site heterogeneity, site affinity, site specificity, site accessibility and other characteristics all depend on these decisions. Therefore synthesising a MIP for a specific purpose is not a trivial matter. Currently, no strategy exists to make these decisions in a rational way. In addition to this, a new material must be accurately characterized or described, and as we have seen, this is also riddled with a number of issues. As a result, optimization of MIP properties is reduced to tedious experimental trial and error effort.

To develop a more rational strategy for MIP design we first need to review the fundamental challenges associated with MIP synthesis and characterization. In the following sections the fundamental challenges associated with MIP synthesis and characterization are reviewed.

1.5.1. Nature of molecular recognition in MIPs

Molecular recognition is a process of strong and specific binding between a molecule and a substrate. Although molecular recognition is a common phenomenon, its nature is not well understood and this hinders design of artificial systems capable of mimicking the phenomenon. It is a complex process and involves a number of interactions. These include van der Waals, hydrophobic, Coulombic terms and steric effects. However, it is difficult to accurately calculate their relative contributions. Furthermore, some researchers suggest molecular recognition cannot be described by binding in a single cavity. They argue molecules in the neighbouring sites may affect the recognition process. Knowing these relative contributions could allow for a more systematic design of MIPs.

The study of molecular recognition phenomena is not new, and there has been considerable research done, particularly for biological systems to describe an association process between a protein and a ligand. The differences between binding processes in MIPs and proteins are well recognized. MIPs are predominantly rigid structures that feature a distribution of binding sites, contrary to proteins. However, in both cases, molecular recognition phenomenon takes place and it must have fundamentally the same origin. Naturally, there have been a number of efforts to construct a thermodynamic description of binding and molecular recognition processes in imprinted materials in the same spirit adopted for biological systems (Kollman 1993; Wang *et al.* 2001; Böhm and Schneider 2003; Brooijmans and Kuntz 2003).

The general starting point of these thermodynamic approaches is to consider a single event of a ligand binding to a molecular recognition site (either in a protein or in a MIP). The free energy of binding is the most fundamental measure that describes this process. The key idea of the thermodynamic description reviewed here is to formulate the free energy of binding in terms of individual contributions associated with the formation of new interactions, losses of some degrees of freedom and so on. For example, building on the previous considerations of Page and Jencks (Page and Jencks 1971), the following expression has been proposed by Williams and co-workers to describe the free energy change for the binding event between two species, A and B, in solution (Williams *et al.* 1991):

$$\begin{aligned}\Delta G_{bind} = {} & \Delta G_{trans+rot} + \Delta G_{rotors} + \Delta G_{conform} \\ & + \Delta G_{polar} + \Delta G_{vdW} + \Delta G_{hydro} + \Delta G_{vib}\,'\end{aligned} \qquad \text{I.5}$$

where the free energy changes are described by changes in translational and rotational degrees of freedom upon binding $\Delta G_{trans+rot}$, restriction of internal rotors in the complex/bound ligand ΔG_{rotors}, adverse conformational changes upon binding $\Delta G_{conform}$, interacting polar groups contribution ΔG_{polar}, van der Waals interactions ΔG_{vdW}, hydrophobic effects ΔG_{hydro}, and residual soft vibrational modes ΔG_{vib}. Thus, the objective is to estimate these individual contributions, and their role in the free energy of binding. Although there have been many studies aiming to quantify individual terms, here the author limits himself to a qualitative description of the behaviour of each term (*i.e.* favourable or unfavourable contribution to ΔG_{bind}). The reader is referred to the literature for further insights (Williams *et al.* 1991; Searle *et al.* 1992; Nicholls 1995; Nicholls 1998).

Considering the $\Delta G_{trans+rot}$ term, species A and B prior to complexation would have 12 degrees of rotational and translational freedom; these are reduced to 6 upon complexation. This is clearly an adverse entropic effect on binding which is accentuated for multi-coordinated complexes. The stabilization of the species in the complex implies the loss of internal rotational degrees of freedom, hence the presence of the ΔG_{rotors} term. One can expect that, other considerations ignored, larger and more flexible molecules, will incur a higher penalty than small and more rigid molecules. The conformational energy of the species in solution will typically be lower than that of the complex: since the species are free in solution, the minimum energy accessible to them will hardly be available in the constrained complex. The term $\Delta G_{conform}$, will be negligible if the binding molecules are able to associate in or near their energy minimum conformations, that is to say, if the species are "naturally" complementary. Strong electrostatic

interactions between the species in the complex mean a favourable contribution of the term ΔG_{polar}. Species capable of stronger interactions in the complex will form more stable complexes and higher affinity binding sites. One can also deduce that species that compete with the template for these interactions will hinder complex formation, hence polar solvents are usually avoided as the medium for MIP synthesis. Weak van der Waals interactions typically have a favourable contribution ΔG_{vdW}, as a result of molecular complementarity. This term should be further enhanced by higher density of the polymer, as a result of stronger confinement. In aqueous solvent there is an additional entropic effect when water is removed from the hydrophobic regions of the ligand surface upon binding to the substrate/MIP. This contribution ΔG_{hydro}, becomes more significant for larger non-polar species. In practice this term is reflected in changes to the direct interactions ΔG_{vdW} and ΔG_{polar} wich arise from the presence of hydrogen bonded water molecules. Finally, the last term, ΔG_{vib}, is associated with the formation of the new soft vibrational modes upon binding.

The key challenge in this approach is systematic separation and estimation of these terms. Often, very different levels of theory are involved in the calculation of individual terms, with the type of approximations used at each level not clearly specified or appreciated. Thus, this thesis is based on molecular modelling approach rather than on the thermodynamic analysis of individual terms presented here. However, from time to time, the author will refer to the language of individual contributions to the free energy of binding and thus it was important to introduce this language.

1.5.2. Heterogeneity of binding sites

The binding sites created during the imprinting process do not all have the same properties. In addition, many can be disrupted or blocked during polymerization or may degenerate during the template extraction. Thus, an imprinted material features a distribution of binding sites.

An example of this heterogeneity is provided in one of the earlier works on MIPs by Vlatakis *et al.* (Vlatakis *et al.* 1993). They synthesised two MIPs: one templated with theophylline and the other with diazepam. They performed rebinding experiments on the MIPs. The adsorption data, they observed, could be modelled by considering two and three classes of sites for theophyline and diazepam, respectively. This work was revisited by Davis and co-workers (Davis *et al.* 1996), who concluded that only a very small fraction of the sites in the MIPs corresponded to very high affinities (Figure 1.8). This description is believed to apply to most imprinted materials.

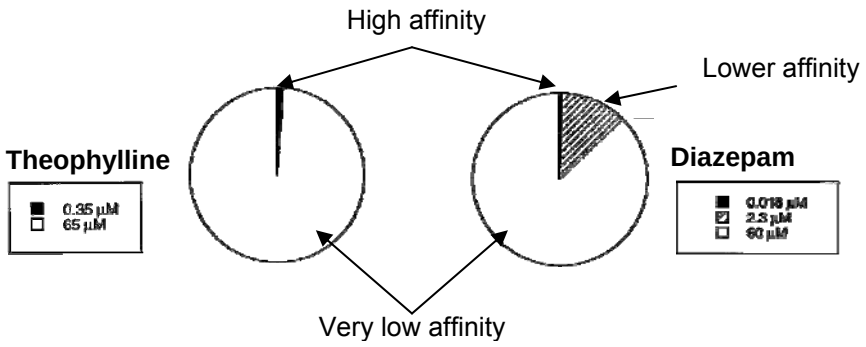

Figure 1.8: Fraction of sites of different types with a given dissociation constant for theophylline and diazepam. For theophylline two types of sites were considered while for diazepam three types were used.

Heterogeneity of binding sites is the most significant disadvantage of MIPs compared to biological examples of molecular recognition. As was shown, even characterization of this heterogeneity in a robust and consistent fashion poses several challenges. Study and control of this heterogeneity has been subject of some of the most intense research efforts in MIP community. This still remains, in the author's view, the most serious issue in MIP design, for most applications.

1.5.3. What factors to customize for different applications

Although it is tempting to concentrate on one figure of merit to evaluate the performance of a MIP (selectivity, affinity distribution), this may not provide the whole picture. Different applications may require different additional parameters to be optimized. For example, for separations one should consider the polymerization conditions that affect porous morphology in order to maximize capacity and allow reasonably favourable adsorption dynamics (particularly for large industrial applications) all this while maximizing the selectivity over a broad range of pressures. For catalysis, one favours a high number of binding sites while the specificity is less important for MIP to perform the function desired. Sensing on the other hand would demand both very high specificity and affinity. The optimization of a MIP demands the juggling of all the interdependent factors that define the behaviour of a MIP and this has been a well recognized challenge in MIP design.

This section outlined the different issues researchers face when studying and developing MIPs. Optimization of these materials is currently done mostly by rules of thumb and trial and error processes. It is a very costly approach

because of the sheer weight of combinations of polymer mixture components coupled with the influence of numerous and cumulative effects of different parameters in the synthesis and application of MIPs. More rational strategies in MIP design are required and the development of these strategies should start with a better understanding of adsorption and binding phenomena in MIPs on a molecular level. Molecular recognition is a phenomenon on a molecular scale, therefore, it is difficult to analyze in experiments. In this situation, molecular simulations present themselves as an expedient and flexible way to explore the problem in an in-depth fundamental perspective.

1.6. Molecular simulations of MIPs

Several computer simulation studies have recently emerged focusing on adsorption and binding phenomena in MIPs. In principle, computer simulations offer a detailed description of adsorption and recognition phenomena in porous materials on a detailed molecular level; they allow the decoupling of various factors influencing molecular recognition functionality and assessment of their role. In addition, in computer simulations, adsorption experiments can be mimicked on a model MIP material and thus various structure characterization models can be tested. This way, one could link the information concerning the structure of the material and the binding site distributions extracted from the isotherms using the conventional methods discussed earlier. Depending on the property being studied, different models and simulation methods can be employed. This has originated a number of studies with a range of simulation strategies and

levels of model detail and complexity. A brief review of some of these studies is presented here.

Qualitative studies have the species involved in the system represented in a simplified manner as hard sphere or Lennard-Jones particles or even lattice sites. For example, in a recent study, Yungerman and Srebnik have considered a model of a polymerizing Lennard-Jones fluid templated with rigid dimers, also made of two Lennard-Jones sites (Yungerman and Srebnik 2006). Polymerization was modelled as the formation of harmonic bonds between the particles representing monomers. This model allowed the authors to investigate porosity and pore size distribution in the final structure as function of the template concentration and degree of polymerization. Wu and co-workers, recently proposed a simple 2D square lattice model of MIPs (Wu *et al.* 2008). In the model each lattice site can be either empty or occupied by a cross-linker, functional monomer or template species. Each functional monomer can form an association with only one out of four adjacent lattice sites. Template sites can have up to four monomers associated with it. This leads to binding sites of different types and quality, depending on the number of monomers associated with the site. This model is clearly well suited to explore binding site distributions in MIPs and how this characteristic depends on the relative concentrations of the template and monomer species and on the strength of the template-functional monomer association. It was also applied to a specific case of enantioselective recognition.

Early fully atomistic studies focused on the accurate description of the formation and function of a single binding site. The procedure is to consider

a molecule (template), surrounded by several molecules of the monomer, and minimize the energy of the system. This procedure is repeated for a series of monomers. The complexes with the lowest potential energies are selected for synthesis. The idea is that stronger complexes between the functional monomers and templates should lead to better defined, more selective binding sites and therefore the procedure can be used as a computational design tool to guide synthesis of MIPs. For example, Chianella *et al*. used this approach to simulate several abacavir-monomer pairs, with three of them selected for synthesis (Chianella *et al.* 2006). They used bisacrylamide and acrylamide mixture as functional monomers for MIP1, while itaconic acid and acrylamide were used for MIP2 and MIP3, respectively. From the potential energy criteria the strongest binding monomers should be ordered in the following manner: MIP1 > MIP3 > MIP2. Their rebinding experiments show that the order is not followed in binding experiments results. Furthermore, this approach cannot explain further variations in the behaviour of the materials under different conditions as shown in Figure 1.9.

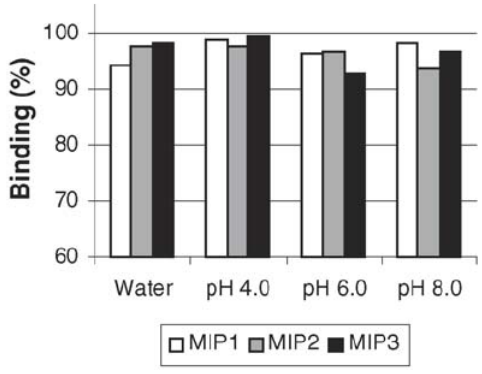

Figure 1.9: MIP binding (%) for 10 mg l^{-1} of abacavir hemi-sulphate prepared in different solutions. From left to right in the graph: water, 50 mM Na-phosphate buffer (pH 6.0 and 8.0) and 50 mM Na-acetate buffer (pH 4.0) (Chianella *et al.* 2006).

The behaviours of different materials are very similar to each other, therefore one cannot state conclusively that the trends observed have been directly predicted by Chianella and co-workers (Chianella *et al.* 2006). There are several possible issues with this approach that may lead to the discrepancies between the computational predictions and the experiments. The first issue is associated with the use of the potential energy as the selection criteria in application to the binding process. This does not correctly describe the thermodynamics of the complexation or re-binding process. As has been already discussed, free energy of complexation or binding, ΔG, is a more appropriate characteristic of this process (or Helmholtz free energy ΔA, if we believe that volume variations are not important). It accounts for both the enthalpic and the entropic energy effects in the process. Free energy of binding is also a measure directly linked to properties observed in experiments, and thus seems more appropriate. In the rebinding experiment from solution, the equilibrium between the bound molecules and free molecules in solution is characterized by the binding constant Kc:

$$Kc = \frac{a_B}{a_F} \qquad \text{I.6}$$

where a_B and a_F are the activities of the template in the bound state and in solution, respectively. For ideal solutions (or dilute solutions), this expression is simplified to:

$$Kc \approx \frac{B^*}{F} \qquad \text{I.7}$$

where B* is concentration of the template in the adsorbed phase (mol/dm^3, or M). We use the star to distinguish this property from B, defined earlier as the amount adsorbed per gram of solid (mol/g). F is defined as before, and is the concentration of the free template in solution (mol/dm^3, or M). The

relationship between an equilibrium constant and the standard free energy of the process as formulated in classical thermodynamics is:

$$Kc = e^{-\frac{\Delta G_{bind}}{RT}} \qquad \text{I.8}$$

In the MIP community, the rebinding data is quite often characterized using the following partition coefficient:

$$K = \frac{B}{F} \qquad \text{I.9}$$

This expression above is not a dimensionless number (as the equilibrium constant should be) and actually can not viewed as a proper equilibrium constant, such as K_c. Two properties are related to each other via a constant:

$$K = \phi K_C \qquad \text{I.10}$$

where ϕ is the porosity of the material (volume per gram). Selectivity of a porous material with respect to a mixture of two components *A* and *B* can be characterized through the separation factor:

$$S = \frac{K_{C,A}}{K_{C,B}} = \frac{K_A}{K_B} = e^{-\frac{(\Delta G_A - \Delta G_B)}{RT}} \qquad \text{I.11}$$

From the expressions above, it is also clear that in the low concentration (or pressure) of adsorbate regime, K is nothing but the slope of the rebinding (adsorption) isotherm, or in other words, the Henry's coefficient K_H.

$$K_H = \lim_{\substack{P \to 0 \\ F \to 0}} K \qquad \text{I.12}$$

In this regime, equation I.1 for the Langmuir isotherm also reduces to 1.9, and the Langmuir constant is the Henry's coefficient (within a factor of N, the number of binding sites).

During re-binding experiments, the concentration of template in solution, F, is measured. From this, one can calculate the concentration of bound template, B. Selectivity as given above through the ratio of K for two MIPs prepared with two different monomers describes how much better one adsorbs the target species compared to the other.

For computationally modelled MIPs, one can obtain K through simulated adsorption experiments and by using equation I.10, as in experiments. In the Henry's law regime the ratio of two Henry's constants can be also calculated using the virial expression for the Henry's constant and the Widom test particle insertion method (Frenkel and Smit 2002) . However, it is important to emphasize that the properties of MIPs measured in experiments do not describe behaviour of a single type of a binding site, but a distribution of binding sites of varying affinities. This brings us to the second issue associated with the approach.

The simulations done in the work of Chianella *et al*. mimic only one template-monomer complex, and therefore only one binding site. It is not possible in this way to simulate the real complexity of the MIP porous space and surface. Since only one type of site is defined, there is no assessment of the affinity distribution the simulated MIP recipe might produce.

Recently, more sophisticated models have been developed. Nicholls and co-workers proposed fully atomistic models of the association processes in pre-polymerization solutions (Karlsson *et al.* 2009). For this, they used the AMBER (Case *et al.* 2005) suite of molecular simulations programs [with

AMBER99 (Wang *et al.* 2000) and GAFF (Wang *et al.* 2004) force-fields] to simulate mixtures of bupivacaine and methacrylic acid in chloroform with and without an ethylene dimethacrylate cross-linker. Insight into complex heterogeneity revealed that the presence of cross-linker affects the nature of template-functional monomer complex. Other effects such as self association and varying internal structures of the species involved were found. It has then been observed, in agreement with experiments, that association of functional monomer with the template species is, in some cases, strongly influenced by other possible association processes in the system. These can include those between two functional monomers, functional monomer and cross-linker, cross-linker and template and so on. This leads to a broad range of possible complexes in the system and, as a result, it leads to a broad range of binding sites. Although modelling of porous materials and adsorption processes were not studied explicitly by Nicholls and co-workers, their studies highlight that models limited to only functional monomer – template interactions are not sufficient to describe processes in pre-polymerization mixtures.

Thus, it follows from these studies that the association processes in solution among the various species of the pre-polymerization mixture are complex and competitive. Upon polymerization, this leads to a complex porous morphology featuring a distribution of binding sites. The molecular recognition functionality of a MIP is a function of this structure and the MIP optimization cycle, most likely, can not be reduced to the sole focus on template - functional monomer interaction. These observations motivate the current work, where the aim is the development of a model of a molecularly imprinted polymer that reflects the actual process of material formation,

featuring complex disordered porous space, and the capability for molecular recognition. Depending on the specific parameters being studied, either a simplified representation of the species or a more accurate approach based on the available atomistic force fields, is adopted. To the best of the author's knowledge, the study of such a model MIP in terms of its binding sites characteristics and adsorption behaviour, is presented for the first time.

The inspiration for this approach originated in a more general model of a fluid confined in a disordered porous media. In this model, the matrix is treated as a collection of prearranged quenched particles. The adsorbate fluid will occupy the free spaces and will be in an annealed, thermodynamic equilibrium state. These models are often called quenched-annealed models of adsorption in porous materials (Madden and Glandt 1988; Fanti *et al.* 1990; Given and Stell 1992; Madden 1992; Sarkisov and Van Tassel 2005). A theoretical treatment of the simplest system of this kind (involving only hard-sphere interaction) was proposed by Madden and Glandt within the replica Ornstein-Zernike approach (Madden and Glandt 1988). The most important feature of a quenched-annealed model is that it captures the 3D complexity of disordered materials which cannot be mimicked by a collection of simple pores.

Zhang and Van Tassel extended this model to study the effect of templating on a porous material (Zhang and Van Tassel 2000). Concentrating on simple species, they used hard sphere interactions for both template and matrix, and tested different template diameters. The general procedure to mimic templating was to place a binary mixture (matrix + template) of particles on a lattice. This was followed by a canonical MC simulation to melt and

equilibrate the structure. After this, the template particles were removed. Grand canonical Monte Carlo (GCMC) simulations were then performed to simulate adsorption and to study the effects of templating on the material properties. Zhang and Van Tassel also developed theoretical tools based on the integral equation theory to describe adsorption in this model. Both in simulations and theory they found that adsorption is increased in templated systems, compared to non-templated systems.

The model delivered a correct description of the effect of templating, but the geometries studied were quite simple. A significant development was recently introduced by Sarkisov and Van Tassel (Sarkisov and Van Tassel 2005; Sarkisov and Van Tassel 2007). While still using simple potentials such as hard-sphere and Lennard-Jones, Sarkisov and Van Tassel extended the previous approach to molecules of complex geometries. These molecules were represented as rigid clusters of interacting sites. Adsorption simulations were performed with geometries equal to and different from the template. The model allowed the authors to investigate the effects of molecular shape complementarity and indeed, some selectivity effects were observed in the model materials. However, since the model does not feature any specific interactions (such as polar and hydrogen bond interactions, characteristic for MIPs), the molecular recognition effects in the model were limited to few specific cases. Nevertheless, this approach is an important milestone in the development of a model with molecular recognition capabilities. This will be the foundation for the development of the present model.

1.7. Outline and objectives of this thesis

In this thesis we use computer simulations and modelling to investigate molecular recognition phenomena in imprinted polymers, ultimately gaining insights into the rational design of these novel materials.

This goal can be expanded into the following objectives:

a) develop a model of molecularly imprinted polymers, which would reflect the actual process of their formation, feature complex, disordered porous space, and be capable of molecular recognition;

b) employ the model to study the imprinting and recognition processes in MIPs; provide a detailed description of the phenomena on molecular a level;

c) investigate the interplay between the morphology of the porous matrix and molecular recognition characteristics of the material;

d) investigate binding site structure and affinity, site distribution and robustness of molecular recognition under various conditions;

e) employ the proposed simulation strategy in combination with accurate atomistic potentials to construct predictive models of adsorption in MIPs. Use computer simulations to investigate the scope and the applicability of conventional affinity distribution characterization methods.

In the next chapter, the statistical mechanics fundamentals are presented and the computer simulation strategy employed in this project is introduced. Chapter 3 presents the application of the developed molecular model, the emergence of molecular recognition in this model, and its subsequent implications. In chapter 4, the model is further explored to assess the factors affecting molecular recognition in MIPs. Hypothetical MIP design scenarios are explored in chapter 5, towards the optimization of the characteristics of the MIPs generated. Chapter 6 deals with the application of the developed simulation strategy with more realistic potentials, with a focus on MIPs templated with different isomers. The implications of this study and further potential research directions are discussed in chapter 7.

1.8. References

Al Kobaisi, M. *et al*. (2007). "The effect of molecular imprinting on the pore size distribution of polymers." Adsorption-Journal of the International Adsorption Society **13**(3-4): 315-321.

Alexander, C. *et al*. (2006). "Molecular imprinting science and technology: a survey of the literature for the years up to and including 2003." Journal of Molecular Recognition **19**(2): 106-180.

Alexander, C. *et al*. (2003). "Imprinted polymers: artificial molecular recognition materials with applications in synthesis and catalysis." Tetrahedron **59**(12): 2025-2057.

Allender, C. J. *et al*. (2000). "Pharmaceutical applications for molecularly imprinted polymers." International Journal of Pharmaceutics **195**(1-2): 39-43.

Andersson, H. S. *et al.* (1996). "Study of the nature of recognition in molecularly imprinted polymers." Journal of Molecular Recognition **9**(5-6): 675-682.

Arshady, R. and K. Mosbach (1981). "Synthesis of Substrate-Selective Polymers by Host-Guest Polymerization." Macromolecular Chemistry and Physics-Makromolekulare Chemie **182**(2): 687-692.

Böhm, H.-J. and G. Schneider (2003). Protein-Ligand Interactions: From Molecular Recognition to Drug Design, Volume 19. Weinheim, WILEY-VCH Verlag GmbH & Co. KGaA.

Breinl, F. and F. Haurowitz (1930). "Chemische Untersuchung des Präzipitates aus Hämoglobin und Anti-Hämoglobin-Serum und Bemerkungen über die Natur der Antikörper." Hoppe-Seyler´s Zeitschrift für physiologische Chemie **192**(1-3): 45-57.

Brooijmans, N. and I. D. Kuntz (2003). "Molecular recognition and docking algorithms." Annual Review of Biophysics and Biomolecular Structure **32**: 335-373.

Burnet, F. M. (1976). "A Modification of Jerne's Theory of Antibody Production using the Concept of Clonal Selection." CA Cancer J Clin **26**(2): 119-121.

Case, D. A. *et al.* (2005). "The Amber biomolecular simulation programs." Journal of Computational Chemistry **26**(16): 1668-1688.

Chianella, I. *et al*. (2006). "Computational design and synthesis of molecularly imprinted polymers with high binding capacity for pharmaceutical applications-model case: Adsorbent for abacavir." Analytica Chimica Acta **559**(1): 73-78.

Davis, M. E. *et al*. (1996). "Rational catalyst design via imprinted nanostructured materials." Chemistry of Materials **8**(8): 1820-1839.

Dickey, F. H. (1949). "The Preparation of Specific Adsorbents." Proceedings of the National Academy of Sciences of the United States of America **35**(5): 227-229.

Fanti, L. A. *et al*. (1990). "Fluids in Equilibrium with Disordered Porous Materials - Integral-Equation Theory." Journal of Chemical Physics **93**(8): 5945-5953.

Fischer, E. (1894). "Einfluss der Configuration auf die Wirkung der Enzyme." Berichte der deutschen chemischen Gesellschaft **27**(3): 2985-2993.

Frenkel, D. and B. Smit (2002). Understanding molecular simulation : from algorithms to applications. London, Academic Press.

Freundlich, H. M. E. (1906). "Over the adsorption in solution." Journal of Chemical Physics **57**: 385-470.

Given, J. A. and G. Stell (1992). "Comment on: Fluid Distributions in 2-Phase Random-Media - Arbitrary Matrices." Journal of Chemical Physics **97**(6): 4573-4574.

He, J. F., Q. H. Zhu, et al. (2007). "Investigation of imprinting parameters and their recognition nature for quinine-molecularly imprinted polymers." Spectrochimica Acta Part a-Molecular and Biomolecular Spectroscopy **67**(5): 1297-1305.

Herdes, C. and L. Sarkisov (2009). "Computer Simulation of Volatile Organic Compound Adsorption in Atomistic Models of Molecularly Imprinted Polymers." Langmuir **25**(9): 5352-5359.

Hillberg, A. L. *et al*. (2005). "Molecular imprinted polymer sensors: Implications for therapeutics." Advanced Drug Delivery Reviews **57**(12): 1875-1889.

Karlsson, B. C. G. *et al*. (2009). "Structure and Dynamics of Monomer-Template Complexation: An Explanation for Molecularly Imprinted Polymer Recognition Site Heterogeneity." Journal of the American Chemical Society **131**(37): 13297-13304.

Kollman, P. (1993). "Free-Energy Calculations - Applications to Chemical and Biochemical Phenomena." Chemical Reviews **93**(7): 2395-2417.

Lavignac, N. *et al*. (2004). "Current status of molecularly imprinted polymers as alternatives to antibodies in sorbent assays." Analytica Chimica Acta **510**(2): 139-145.

Lev, S. and R. V. T. Paul (2005). "Replica Ornstein-Zernike theory of adsorption in a templated porous material: Interaction site systems." The Journal of Chemical Physics.

Madden, W. G. (1992). "Fluid distributions in random media: Arbitrary matrices." The Journal of Chemical Physics **96**(7): 5422-5432.

Madden, W. G. and E. D. Glandt (1988). "Distribution-Functions for Fluids in Random-Media." Journal of Statistical Physics **51**(3-4): 537-558.

Maier, N. M. *et al*. (2001). "Separation of enantiomers: needs, challenges, perspectives." Journal of Chromatography A **906**(1-2): 3-33.

Maier, N. M. and W. Lindner (2007). "Chiral recognition applications of molecularly imprinted polymers: a critical review." Analytical and Bioanalytical Chemistry **389**(2): 377-397.

Marty, J. D. and M. Mauzac (2005). "Molecular imprinting: State of the art and perspectives." Microlithography - Molecular Imprinting **172**: 1-35.

Meyer, E. F. (1995). "Emil Fischer: then and now." Pharmaceutica Acta Helvetiae **69**(4): 177-183.

Moore, D. (2007). "Recent Advances in Trace Explosives Detection Instrumentation." Sensing and Imaging: An International Journal **8**(1): 9-38.

Mudd, S. (1932). "A Hypothetical Mechanism of Antibody Formation." J Immunol **23**(6): 423-427.

Nicholls, I. A. (1995). "Thermodynamic Considerations for the Design of and Ligand Recognition by Molecularly Imprinted Polymers." Chemistry Letters(11): 1035-1036.

Nicholls, I. A. (1998). "Towards the rational design of molecularly imprinted polymers." Journal of Molecular Recognition **11**(1-6): 79-82.

Page, M. I. and W. P. Jencks (1971). "Entropic Contributions to Rate Accelerations in Enzymic and Intramolecular Reactions and Chelate Effect." Proceedings of the National Academy of Sciences of the United States of America **68**(8): 1678-1683.

Pap, T. and G. Horvai (2004). "Binding assays with molecularly imprinted polymers-why do they work?" Journal of Chromatography B, Analytical Technologies in the Biomedical and Life Sciences **804**(1): 167-172.

Pauling, L. (1940). "A theory of the structure and process of formation of antibodies." Journal of the American Chemical Society **62**: 2643-2657.

Piletsky, S. A. *et al*. (1998). "The rational use of hydrophobic effect-based recognition in molecularly imprinted polymers." Journal of Molecular Recognition **11**(1-6): 94-97.

Piletsky, S. A. *et al*. (1998). "Imprinted membranes for sensor technology: Opposite behavior of covalently and noncovalently imprinted membranes." Macromolecules **31**(7): 2137-2140.

Polyakov, M. V. (1931). "Adsorption properties of silica gel and its structure." Zhurnal Fizicheskoi Khimii **6**: 799-805.

Polyakov, M. V. *et al.* (1933). "On the structure of silica gel." *Zhurnal Fizicheskoi Khimii*, **4,** 454-456.

Ramstrom, O. and K. Mosbach (1999). "Synthesis and catalysis by molecularly imprinted materials." Current Opinion in Chemical Biology **3**(6): 759-764.

Sarkisov, L. and P. R. Van Tassel (2005). "Replica Ornstein-Zernike theory of adsorption in a templated porous material: Interaction site systems." The Journal of Chemical Physics **123**(16): 164706-10.

Sarkisov, L. and P. R. Van Tassel (2007). "Integral equation theory of adsorption in templated materials: Influence of molecular attraction." Journal of Physical Chemistry C **111**(43): 15726-15735.

Searle, M. S. *et al*. (1992). "Partitioning of Free-Energy Contributions in the Estimation of Binding Constants - Residual Motions and Consequences for Amide-Amide Hydrogen-Bond Strengths." Journal of the American Chemical Society **114**(27): 10697-10704.

Sellergren, B. and C. J. Allender (2005). "Molecularly imprinted polymers: A bridge to advanced drug delivery." Advanced Drug Delivery Reviews **57**(12): 1733-1741.

Sreenivasan, K. (1999). "On the application of molecularly imprinted poly(HEMA) as a template responsive release system." Journal of Applied Polymer Science **71**(11): 1819-1821.

Sulitzky, C. *et al*. (2002). "Grafting of molecularly imprinted polymer films on silica supports containing surface-bound free radical initiators." Macromolecules **35**(1): 79-91.

Takagish.T and I. M. Klotz (1972). "Macromolecule-Small Molecule Interactions - Introduction of Additional Binding-Sites in Polyethyleneimine by Disulfide Crosslinkages." Biopolymers **11**(2).

Umpleby, R. J. *et al*. (2004). "Characterization of the heterogeneous binding site affinity distributions in molecularly imprinted polymers." Journal of Chromatography B, Analytical Technologies in the Biomedical and Life Sciences **804**(1): 141-149.

Vlatakis, G. *et al*. (1993). "Drug assay using antibody mimics made by molecular imprinting." Nature **361**(6413): 645-647.

Wang, J. *et al.* (2000). "How well does a restrained electrostatic potential (RESP) model perform in calculating conformational energies of organic and biological molecules?" Journal of Computational Chemistry **21**(12): 1049-1074.

Wang, J. *et al.* (2004). "Development and testing of a general amber force field." Journal of Computational Chemistry **25**(9): 1157-1174.

Wang, W. *et al*. (2001). "Biomolecular simulations: Recent developments in force fields, simulations of enzyme catalysis, protein-ligand, protein-protein, and protein-nucleic acid noncovalent interactions." Annual Review of Biophysics and Biomolecular Structure **30**: 211-243.

Williams, D. H. *et al*. (1991). "Toward the Semiquantitative Estimation of Binding Constants - Guides for Peptide Peptide Binding in Aqueous-Solution." Journal of the American Chemical Society **113**(18): 7020-7030.

Wu, X. *et al.* (2008). "Stochastic Lattice Model Simulations of Molecularly Imprinted Polymers." Chem. Mater.

Wulff, G. (2002). "Enzyme-like catalysis by molecularly imprinted polymers." Chemical Reviews **102**(1): 1-27.

Wulff, G. and A. Sarhan (1972). "Use of Polymers with Enzyme-Analogous Structures for Resolution of Racemates." Angewandte Chemie-International Edition **11**(4).

Yan, H. Y. and K. H. Row (2006). "Characteristic and synthetic approach of molecularly imprinted polymer." International Journal of Molecular Sciences **7**(5-6): 155-178.

Ye, L. and K. Haupt (2004). "Molecularly imprinted polymers as antibody and receptor mimics for assays, sensors and drug discovery." Analytical and Bioanalytical Chemistry **378**(8): 1887-1897.

Yin, J. F. *et al*. (2005). "Rapid and efficient chiral separation of nateglinide and its L-enantiomer on monolithic molecularly imprinted polymers." Journal of Chromatography A **1090**(1-2): 68-75.

Yoshimi, Y. *et al*. (2001). ""'Gate effect'' of thin layer of molecularly-imprinted poly(methacrylic acid-co-ethyleneglycol dimethacrylate)." Sensors and Actuators B: Chemical **73**(1): 49-53.

Yungerman, I. and S. Srebnik (2006). "Factors Contributing to Binding-Site Imperfections in Imprinted Polymers." Chem. Mater. **18**(3): 657-663.

Zhang, L. and P. R. Van Tassel (2000). "Theory and simulation of adsorption in a templated porous material: Hard sphere systems." The Journal of Chemical Physics **112**(6): 3006-3013.

2.

Molecular Simulations

Statistical mechanics relates the properties of a system at the atomistic scale, such as intermolecular interactions, to macroscopic characteristics and properties of the system. This provides the basic framework for the construction of the fundamental description of molecular recognition and adsorption processes in MIPs. In this thesis, a detailed treatment of statistical mechanics is not intended and the reader is directed to the general textbooks in the field such as those of Hill (Hill 1986) and McQuarrie (McQuarrie 1975) for a deeper insight and explanation on the subject. Here we are concerned only with the application of statistical mechanics in computer modelling of the systems and phenomena of interest.

Thus, this chapter begins with the introduction of the general simulation strategy. The basic philosophy of this thesis is that the simulation strategy must realistically reflect various stages of MIP formation and function. An

overview of the simulation strategy is provided, wherein the statistical mechanics concepts and simulation tools appropriate for each stage are identified. The chapter continues with the description of the molecular model defined for the present work, with the corresponding interaction potentials. Finally, since relating the function of MIPs to their morphology is of great interest, some general methods for structural characterization of model materials are discussed.

2.1 Simulation strategy

In the previous chapter we reviewed several recent studies focused on modelling the processes associated with formation and function of MIPs. Although the reviewed approaches generated a number of useful insights, none of them describes an actual molecular recognition event in a realistic model of a porous MIP. Thus, we aim to adopt a molecular simulation strategy which would satisfy several key requirements. Specifically:

1) it should allow one to generate realistic three dimensional porous structures, reflecting the essential features of MIP morphology;

2) the model should allow the examination of the actual adsorption and binding phenomena in model MIPs;

3) the strategy should be general enough to be applied to a broad range of molecular models with a view to establish the simplest model capable of molecular recognition effect.

The foundation of this strategy has been laid out in the approach proposed by Zhang and Van Tassel, within the quenched-annealed formalism (Zhang and Van Tassel 2000). This strategy requires essentially three simulation steps.

A. In the first step, simulation of the equilibrium pre-polymerization mixture is performed; in the most general case, this mixture includes template, functional monomers, cross-linkers and solvent species.
B. In the second step, the equilibrium mixture of pre-polymerization components is frozen (quenched) in a specific configuration (this crudely models polymerization process), followed by the removal of template and solvent species.
C. The final structure obtained in the previous step serves as a model templated disordered porous structure in the consequent adsorption studies.

As discussed in the Introduction, in the original work of Van Tassel and co-workers, this approach was applied to simple hard sphere species. At this level of description it was possible to investigate the templating effects using integral equation methods (within the replica Ornstein-Zernike theory), however naturally no molecular recognition effects were detected for such simple components.

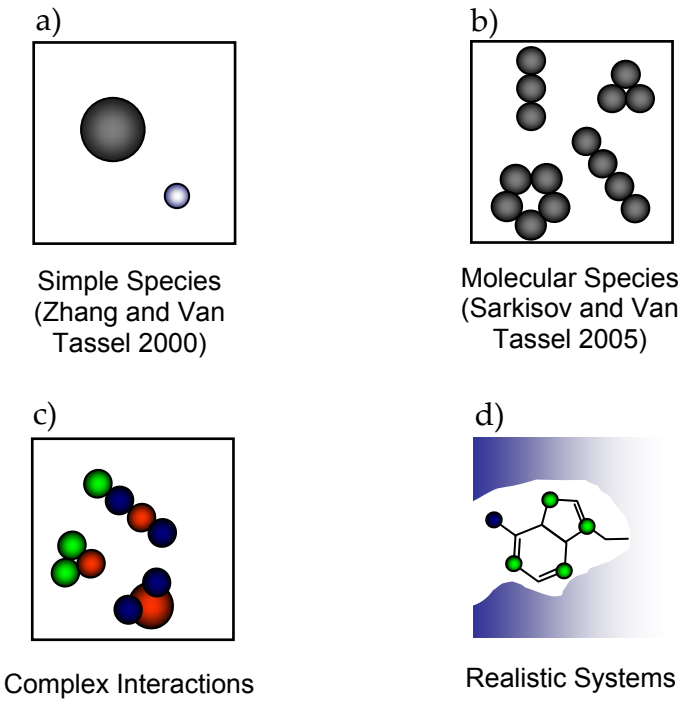

Figure 2.1: Schematic representation of different levels of detail possible in the model of a MIP. a) Simple monatomic hard-sphere interactions. b) Polyatomic and nonlinear species with hard-sphere interactions. c) Polyatomic species with complex interactions. d) Coarse-grained or fully atomistic representations.

Hence, in order to develop a model capable of molecular recognition, more complex potentials should be considered. (It is important to note, that the proposed strategy is general and does not depend on the particular potential form.) Figure 2.1 schematically depicts a natural evolution of the complexity of the molecular model from simple hard-sphere species towards realistic molecular force-fields, where molecular recognition effects are expected to manifest themselves.

A natural extension of the model based on simple hard sphere species is to consider rigid *clusters* of hard spheres, or rigid clusters of Lennard-Jones interaction sites. In the schematic shown in Figure 2.1 this corresponds to

evolution steps b and c (to some extent). Sarkisov and Van Tassel considered these models and observed that preferential adsorption can occur, particularly for geometrically different species. This derives from steric compatibility of the matrix, rather than consistent molecular recognition behaviour (Sarkisov. and Van Tassel 2005).

Thus, the idea of this thesis is to continue to extend complexity of the interaction patterns (stages c and d in Figure 2.1) to identify an appropriate model for studies of molecular recognition. Having said this, several potential models may lead to model materials capable of molecular recognition. These models are not mutually exclusive, as they may be used to answer or tackle different issues. For example, qualitative models, based on simplified potentials may be used to outline the minimum set of conditions for the molecular recognition to occur. Models based on accurate, fully atomistic potentials on the other hand could be used to provide more quantitative insights (for example on the values of the association constants between different components in solution). This thesis will use a different level of description detail depending on a particular task at hands.

Finally, it is clear that the proposed strategy is missing one fundamental realistic element; specifically it does not explicitly describe the polymerization process. Although it is possible to construct such a description within, for example, a kinetic Monte Carlo scheme, it is beyond the scope of this thesis and should be considered in the future work. It is important, however, to understand the role of the polymerization processes so we have a better appreciation of the effects possibly missing in the model. Polymerization helps to stabilize the complexes, locking the components of

the complexes in their relative positions and onto the matrix, without it no recognition would be observed. Particularly important is the level of cross-linking.

High level of cross-linking is desired so that the structure of the complexes is stable and well defined, and rigid enough to withstand extraction of template and still maintain recognition in the resulting cavity. In the literature, high levels of cross-linker in the mixture are reported to improve the performance of MIPs (Wulff *et al.* 1982; Spivak 2005). For example, Noss and co-workers studied testosterone imprinted MIPs with different types of cross-linkers and cross-linking percentages (Noss *et al.* 2008). Cross-linking agent was varied from 50 to 90% and the resulting MIPs exhibited a doubling of the uptake capacity and a fourfold increase in affinity. In Figure 2.2 the increase in association constant is shown for MIP systems poly(MAA-co-EGDMA), as a function of an increasing degree of cross-linking, whereas no such effect is seen with a different cross-linker in poly(MAA-co-PEG200DMA) MIP.

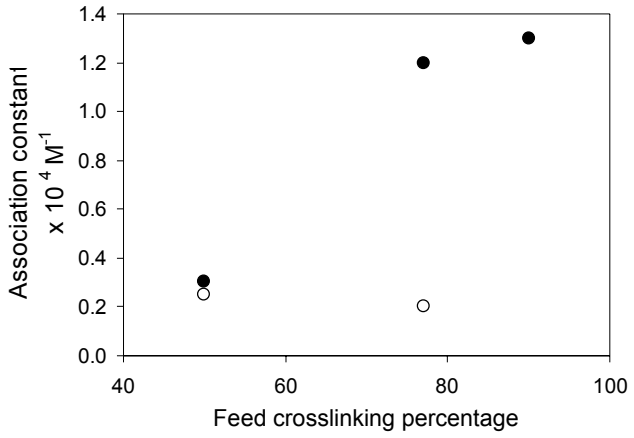

Figure 2.2: Testosterone binding affinity constants for poly(MAA-co-EGDMA) and poly(MAA-co-PEG200DMA) networks at various feed cross-linking percentages. Solid circles are for poly(MAA-co-EGDMA) MIP and open circles are for poly(MAA-co- PEG200DMA).

However, not all complexes "survive" the polymerization process. In other words, polymerization process, with its competing associations, may destroy some of the complexes that could become the binding sites. Polymerization may also lead to some of the binding sites and regions of the porous space becoming inaccessible. While for covalent imprinting the stable complex allows for very high degree of (>80%) cross-linking, in non-covalent imprinting average to high (50-80%) values of the degree of cross-linking are more common (Spivak 2005).

Naturally the "freezing" of a matrix configuration, as it is done in this work, reflects only one aspect of the cross-linkers function. Polymerization (with the presence of solvent) must be modelled to capture realistically the effects in the porous network and the deviation form the equilibrium population of complexes. This thesis focuses on an extreme, ideal case, where the pre-polymerization complexes become binding sites without any detrimental structural effects. Compared to this ideal case, introduction of an explicit polymerization process in the simulation, would most likely lead to model MIPs with lower performance in terms of molecular recognition and selectivity. Where appropriate, we will return to and discuss the implication of not modelling explicitly the polymerization process.

Simulation of a system in the first step of the outlined strategy involves a multi-component mixture of a known number of molecules of each species. In principle, reproduction of experimental conditions would imply that the system is maintained at constant temperature and pressure, corresponding to the isobaric-isothermal (NPT) ensemble. However, if the density fluctuations of the system are not expected to be significant (or important), as in dense

liquid systems, an adequate description can be obtained using the NVT, or canonical ensemble, which is simpler to implement.

Step C, on the other hand, implies that simulations are carried at constant temperature and volume, using the matrix obtained in step B as a model porous structure. Molecules of interest adsorb in the matrix, so their number in the system fluctuates, whereas the multi-component matrix species have fixed number of quenched molecules. Thus, it is an open system corresponding to the grand canonical (μVT) ensemble. For each chemical potential of adsorbate species, a simulation in the grand canonical ensemble generates the equilibrium adsorbed density in a particular matrix realization. A sequence of increasing chemical potentials results in a series of increasing density values, constituting an adsorption isotherm.

In this thesis, pure component adsorption simulations are performed. This makes the simulations somewhat simpler to implement, and vitally, allows us to investigate the re-binding process in a fashion similar to that of experiments. Using re-binding data, one can establish a better link between the observations for the pre-polymer mixture complexes (evaluating population of complexes) and adsorption binding sites (evaluating binding site population, heterogeneity, and affinity distribution). Many experiments on MIPs, such as chromatographic studies analyse a mixture of two or more components. In practice, MIPs will mostly be used to recognise one component from a mixture, but as we are characterizing its functionalities, it is more useful and practical to start with studies with one component.

It is vital to note that, however simple or complex one chooses or is allowed to make the model, the statistical mechanical description of the model is the same throughout. It is only the particular representation of molecules and the ways they interact that vary, altering the terms of the equations, but not their nature.

In the following sections we will expand on the simulation and statistical mechanics details required to describe each of the steps mentioned prior. This will be done with emphasis on the Monte Carlo approach to the molecular model since this was the approach implemented by the author. Molecular Dynamics (MD) was also used (in Chapter 6) as a third party tool. In MD, Newton's laws of motion describing the molecules in the system are solved, which simply involves determining the velocity of the particles from the forces applied and from this determine the new position of said particles after an arbitrarily small time interval δt. Once the system's properties no longer change in time, the system is in equilibrium. Sampling at given time intervals generates configurations which populate the ensembles that describe the system under specific conditions. The pre-polymerization stage can be simulated using either a Monte-Carlo or molecular dynamics approach (either in canonical or isothermal-isobaric ensemble). Adsorption in a porous structure, on the other hand, implies variable number of molecules in the system under consideration. Discrete addition and removal of particles poses a challenge for molecular dynamics, as it creates a sudden perturbation in the interactions, leading to the Hamiltonian of the system not being conserved. Although, alternative approaches exist (based on the Gibbs ensemble, and so called open molecular dynamics), simulation of adsorption using Monte Carlo in grand canonical ensemble remains the most

straightforward approach to implement. This also justifies the implementation of the canonical Monte Carlo for the pre-polymerization stage, since simulation of the both stages can be performed with essentially the same simulation code.

2.2. Simulation of pre-polymerization mixture

In this section we examine the canonical partition function describing the pre-polymerization mixture and explain the basic principles of the Metropolis Monte Carlo method, employed in this work to simulate the first step of the protocol.

2.2.1. Canonical partition function

Consider a multi-component system of *c* species with constant volume V and temperature T. Each of the species has N_c number of rigid molecules. Each particular configuration of the system can be characterized by generalized coordinates $\mathbf{q}_c$ (which specifies location and orientation of all molecules of any species *c*) and momenta $\mathbf{p}_c$ (which is associated with both translational and rotational motions of molecules of any species *c*). To make our considerations more concrete, the species in this system correspond to the multi-component pre-polymerization mixture, which in the most general case consists of template, functional monomer of different types, cross-linker and solvent. Thus, in our notation *c* can take values *t* (for template), *fm* (for functional monomer), *x* (for cross-linker) and *s* for solvent. For the purpose of

future discussion, it is also convenient to group together functional monomers and cross-linkers together (as these are the species that will constitute the resulting porous material) and treat them collectively as species *m* for matrix. Finally, to reduce the notation, the generalized coordinates, orientation and momenta for all species, c, in the system will be labelled simply as **q** and **p**.

The probability to observe the system with molecules in a particular location and orientation **q**, and momenta **p** is given by:

$$\rho(\mathrm{q},\mathrm{p})d\mathrm{q}d\mathrm{p} = \frac{e^{-\frac{H(\mathrm{q},\mathrm{p})}{kT}} d\mathrm{q}d\mathrm{p}}{N_1!...N_c!h^{d_1N_1}...h^{d_cN_c}Q(N_1,...,N_c,V,T)} \qquad \text{II.1,}$$

where $H(\mathbf{q},\mathbf{p})$ is the Hamiltonian of the system and

$$Q(N_1,...,N_c,V,T) = \frac{1}{N_1!...N_c!h^{3dN_1}...h^{3dN_c}} \int ... \int e^{-\frac{H(\mathbf{q},\mathbf{p})}{kT}} d\mathbf{q}d\mathbf{p} \qquad \text{II.2}$$

is the canonical partition function. d_i corresponds to the number of degrees of freedom of any species *i*.

Equations II.1 and II.2 show that the probabilities of observing the system in any given microstate, depends on the energy of that microstate and on the total partition function of the ensemble. Furthermore, the partition function is the most fundamental property of an ensemble, and it can be used to establish the link between microscopic properties of the system and classic thermodynamic properties.

If the system was constituted by simple monatomic species the Hamiltonian could simply be decomposed in the following manner

$$H(\mathbf{q},\mathbf{p}) = K(\mathbf{p}) + U(\mathbf{q}) \qquad \text{II.3}$$

where $K(\mathbf{p})$ term is the kinetic energy of the system and it depends on the momenta only, and $U(\mathbf{q})$ term is the potential energy of the system and it depends on the positions $\mathbf{q}$ of molecules only. This separation of the Hamiltonian into different contributions, allows one to perform their integration separately, and factorizes the partition function into its ideal (kinetic, rotational) and excess (potential) parts. This results in:

$$Q(N_1,...,N_c,V,T) = \frac{1}{N_1!...N_c!h^{d_1N_1}...h^{d_cN_c}} \int e^{-\frac{K(\mathrm{p})}{kT}} d\mathrm{p} \int e^{-\frac{U(\mathrm{q})}{kT}} d\mathrm{q} \qquad \text{II.4}$$

However, for rigid polyatomic species, the factorization of the Hamiltonian, although still possible, is much more involved. The reader is directed to (Gray and Gubbins 1984) for the description of this step. For the system discussed in this thesis the partition function results:

$$Q = Q_t Q_r Q_c \qquad \text{II.5}$$

where Q_t is the translational partition function defined as

$$Q_t = \frac{1}{h^{3N_1}...h^{3N_c}} \int e^{-\frac{\mathbf{p}^2/2m}{kT}} d\mathrm{p} = \Lambda_{t,1}^{-3N_1}...\Lambda_{t,c}^{-3N_c} = \prod_{i=1}^{c} \Lambda_{t,i}^{-3N_i} \qquad \text{II.6}$$

$$\text{with } \Lambda_{t,i} = \left(h^2/2\pi m_i kT\right)^{1/2} \qquad \text{II.7;}$$

Q_r, the rotational partition function is described as

$$Q_r = \prod_{i=1}^{c} \left(\sigma_{SN,i}\Lambda_{r,i}\right)^{-N_i} \qquad \text{II.8,}$$

where $\sigma_{SN,i}$ is the symmetry number for species i and Λ_r can be described as

$$\Lambda_r = \pi^{-1/2}\left(\frac{h^2}{8\pi^2 I_x kT}\right)^{1/2}\left(\frac{h^2}{8\pi^2 I_y kT}\right)^{1/2}\left(\frac{h^2}{8\pi^2 I_z kT}\right)^{1/2} \qquad \text{II.9}$$

for non-linear molecules, or

$$\Lambda_r = \frac{h^2}{8\pi^2 IkT} \qquad \text{II.10}$$

for linear molecules. I_α describes the αα component of the moment of inertia tensor; Q_c, the configurational partition function, is given by

$$Q_c = \frac{1}{N_1!...N_c!\Omega_1^{N_1}...\Omega_c^{N_c}} \int e^{-\frac{U(\mathrm{q})}{kT}} d\mathrm{q} = \frac{1}{N_1!...N_c!\Omega_1^{N_1}...\Omega_c^{N_c}} Z_c \qquad \text{II.11}$$

in which $\Omega = 8\pi^2$ for non-linear molecules, 4π for linear molecules and 1 for monatomic species.

In case of an ideal gas, $U(\mathbf{q}) \equiv 0$, leading to:

$$Q_c^{id}(N_1,...,N_c,V,T) = \frac{V^{N_1}...V^{N_c}}{N_1!...N_c!} \qquad \text{II.12}$$

Finally, equation II.11 becomes:

$$Q(N_1,...,N_c,V,T) = Q^{id} Z_c, \qquad \text{II.13}$$

where Q^{id} is

$$Q^{id} = \prod_{i=1}^{c} \frac{\Lambda_{t,i}^{-3N_i}}{\Omega_i^{N_i} N_i!} \Lambda_{r,i}^{-N_i}, \qquad \text{II.14}$$

and Z_c is the configurational integral:

$$Z_c = \int e^{-\frac{U(\mathbf{q})}{kT}} d\mathbf{q} \qquad \text{II.15}$$

which depends on positions and orientations of molecules only.

2.2.2. Thermodynamic properties

If we are interested in a static property (A) of a system (*i.e.* a property that depends on the positions but not on the momenta), its ensemble average value is:

$$\langle A \rangle = \frac{\int A(\mathbf{q}) e^{-\frac{U(\mathbf{q})}{kT}} d\mathbf{q}}{\int e^{-\frac{U(\mathbf{q})}{kT}} d\mathbf{q}} \qquad \text{II.16}$$

The energy of a system is related to the canonical partition function in the following fashion:

$$E = kT^2 \left(\frac{\partial \ln Q}{\partial T} \right)_{N,V} \qquad \text{II.17}$$

One can also easily derive:

$$p = kT \left(\frac{\partial \ln Q}{\partial V} \right)_{N,T} \qquad \text{II.18}$$

for pressure, and

$$S = kT \left(\frac{\partial \ln Q}{\partial T} \right)_{N,V} + k \ln Q \qquad \text{II.19}$$

for entropy. If one can extract energy, pressure (p) and entropy (S) from the partition function, it follows that any thermodynamic property can also be determined. Thus, the partition function is the fundamental link between the microscopic description of the states of a system and the classical thermodynamics by which we describe its bulk properties (McQuarrie 1975).

2.2.3. Simulation of (NVT) ensemble

The preceding derivation has established a link between statistical mechanics principles and the macroscopic thermodynamic properties of the system we

want to study. However the integrals, as defined in the complete partition functions, cannot be calculated directly, except for some special cases. An alternative approach is provided by a numerical Monte Carlo procedure. Next, we present the basic elements of the Metropolis Monte Carlo protocol that allows the estimation of the average properties of the system.

The principal idea of the Monte Carlo method is to generate a sufficiently large sample N_{conf} of microstate configurations of the system with the appropriate probability distribution density $\rho(\mathbf{q})$. In this case, any property of the system, such as the adsorbed density, can be calculated simply from averaging this property over all the microstates generated:

$$\langle A \rangle = \frac{\sum_{i=1}^{N_{conf}} A_i}{N_{conf}} \qquad \text{II.20}$$

thus alleviating the need to calculate the complete partition function all together. An efficient way to generate this series of microstates has been proposed by Metropolis and co-workers and this is what is now known as the Metropolis importance sampling protocol (Metropolis and Ulam 1949; Metropolis *et al.* 1953). Consider a system with *c* components, N_c molecules for each species, in a particular configuration $\mathbf{q}^o$ (here and throughout *o* is for old and *n* is for new). The probability density of observing this particular microstate (*o*) is given by:

$$\rho(\mathbf{q}^o) = \frac{e^{-\frac{U(\mathbf{q}^o)}{kT}}}{\int e^{-\frac{U(\mathbf{q})}{kT}} d\mathbf{q}} \qquad \text{II.21}$$

This configuration of the system can be perturbed by randomly displacing one of the particles, leading to a new microstate *(n)* with the probability density of occurrence:

$$\rho(\mathbf{q}^n) = \frac{e^{-\frac{U(\mathbf{q}^n)}{kT}}}{\int e^{-\frac{U(\mathbf{q})}{kT}} d\mathbf{q}} \qquad \text{II.22}$$

In order to decide if the new configuration (*n*) is accepted or not, we need to introduce a set of rules to construct the Markov chain.

This chain of states reflects sampling of states with the Boltzmann distribution. We are interested in the equilibrium properties of the system and therefore the phase space must be sampled with a stationary distribution. For this, the condition of balance must be imposed. This means that, in equilibrium, the number of accepted moves that make the system leave any state *(o)* must be exactly equal to the number of accepted moves that make the system return to state *(o)*:

$$\sum \rho(\mathbf{q}^n)\pi(n \to o) = \sum \rho(\mathbf{q}^o)\pi(o \to n) \qquad \text{II.23}$$

where $\pi(o \to n)$ represents the transition probability matrix to go from state (*o*) to state (*n*), and $\pi(n \to o)$ represents the opposite process of going from *(n)* to *(o)*. It is convenient to impose a much stronger condition (although not necessary); namely, that in equilibrium the number of accepted moves from a *(o)* to a new particular state *(n)* is exactly cancelled by the number of moves from that state *(n)* back to *(o)*. This is called the detailed balance condition:

$$\rho(\mathbf{q}^o) \cdot \pi(o \to n) = \rho(\mathbf{q}^n) \cdot \pi(n \to o) \qquad \text{II.24}$$

This implies that, not only is the balance condition maintained in the whole Markov chain, it is also valid for any discrete set of states in the chain.

The transition probability matrix is composed of two factors:

$$\pi(o \to n) = \alpha(o \to n) \cdot acc(o \to n) \qquad \text{II.25}$$

where $acc(o \to n)$ is the probability of accepting the change from (*o*) to (*n*), and $\alpha(o \to n)$ the probability of selecting a particular type of move. Equation II.24 then becomes:

$$\rho(\mathbf{q}^o) \cdot \alpha(o \to n) \cdot acc(o \to n) = \rho(\mathbf{q}^n) \cdot \alpha(n \to o) \cdot acc(n \to o) \qquad \text{II.26}$$

In the original Metropolis protocol α is a symmetric matrix, *i.e.* $\alpha(o \to n) = \alpha(n \to o)$. Consequently, equation II.26 can be rewritten:

$$\frac{acc(o \to n)}{acc(n \to o)} = \frac{\rho(\mathbf{q}^n)}{\rho(\mathbf{q}^o)} = e^{-\beta \Delta U} \qquad \text{II.27}$$

where $\Delta U = U(\mathbf{q}^n) - U(\mathbf{q}^o)$. In practice, this term is calculated based on treating the molecules in the system as rigid clusters of interaction sites. In this case, total potential energy of the system is:

$$U = \sum_{i=1}^{c} \sum_{j=i}^{c} U_{ij} \qquad \text{II.28}$$

where U_{ij} is the potential energy of interaction between species *i* and *j*. In terms of site-site interactions, each of these terms is equal to:

$$U_{ij} = \left(1 - \frac{1}{2}\delta_{ij}\right) \sum_{n_i=1}^{N_i} \sum_{n_j=1}^{N_j} \sum_{\lambda=1}^{M_i} \sum_{\eta=1}^{M_j} u_{ij}^{\lambda\eta}\left(\left|\mathbf{r}_{i,n_i}^{\lambda} - \mathbf{r}_{j,n_j}^{\eta}\right|\right) \qquad \text{II.29}$$

where *i* and *j* represent species labels as usual, δ_{ij} is the Kronecker delta function, N_i is the number of molecules of species *i*, M_i is the number of interaction sites in a molecule of species *i*, $u_{ij}^{\lambda\eta}$ is the pair interaction energy between site λ on a molecule n_i of type *i* and site η on molecule n_j of type *j*, $\mathbf{r}_{i,n_i}^{\lambda}$ and $\mathbf{r}_{j,n_j}^{\eta}$ are position vectors of these sites λ and η.

Thus, the idea of any Monte Carlo scheme is to suggest a set of rules for the acceptance criteria that would follow II.27. Specifically in the Metropolis scheme, the acceptance criteria can be represented as:

$$acc(o \to n) = \min\left(1, e^{-\beta \Delta U}\right) \qquad \text{II.30}$$

For the case of rotational moves, the Euler angles describing the orientation of a molecule i (ϕ_i,θ_i,π_i) could be sampled from a uniform distribution, however the ratio of acceptance probabilities described in II.27 becomes:

$$\frac{acc(o \to n)}{acc(n \to o)} = \frac{\rho(\mathrm{q}^n)}{\rho(\mathrm{q}^o)} = e^{-\beta \Delta U} \frac{\sin(\theta_i^n)}{\sin(\theta_i^o)} \qquad \text{II.31}$$

To use the same acceptance criteria as before, the probability of generating the new state must be biased. This is done by sampling from a uniform distribution for $\cos(\theta_i)$ rather than θ_i (Allen and Tildesley 1987).

2.3. Creation of the porous matrix

In real experimental synthesis of molecularly imprinted polymers, the mixture is equilibrated, followed by polymerization and then by removal of solvent and the template. Detailed modelling of these steps, and in particular of the polymerization step, is beyond the scope of this thesis, as the development and validation of the appropriate models for polymerization process is a separate project in itself. Here we adopt a simplified approach, where a particular configuration of cross-linker, functional monomer, template and solvent (if present) species is quenched (*i.e.* molecules are "frozen" in their respective locations and orientations), followed by removal of template and solvent species. This model is a clear oversimplification, as it ignores a number of details, such as the actual links between molecules in the polymerized structure, possibility for matrix expansion and contraction, and so on. On the other hand, it is very simple and generates realistic disordered

imprinted morphologies. Finally, it generates structures that preserve formed pre-polymerization arrangements of functional monomers around templates, and thus it should be capable of molecular recognition. Validation of this assumption is one of the key objectives of this thesis.

Two important aspects of characterization of any adsorbent are the affinity of the porous surface and the structure of the porous network. Both characteristics depend on the components of the mixture: template, functional monomers, cross-linker, solvent and porogen, as well as polymerisation conditions. The porosity, connectivity, pore diameters of the porous network do not generally affect the extent of recognition binding in MIPs, although they will affect their performance in terms of capacity and dynamics (Yan and Row 2006; He *et al.* 2007).

Polymerisation, the level of cross-linking and the type of solvent and/or porogen will play an important role in defining the porous structure of a MIP. Solvents for non-covalent imprinting are desirably of very low polarity as they weaken the hydrogen bonds in the template – functional monomer complexes. A large volume of solvent (or porogen) is typically desirable to create large pores and help diffusion. The surface area and pore size distribution can be customized via judicious selection of solvent, favouring large pore sizes or high surface area depending on the application intended. Many complexes may become inaccessible or have such high steric restrictions that extraction of template becomes impossible. The result of this is the reduction of the number of high affinity binding sites.

Accessibility in these materials is a dual problem, the accessibility of the pore network, which depends on its topology; and binding site accessibility,

which will dictate how much of the pore surface is functionalized with well formed binding sites. A way to determine connectivity and accessibility is through percolation theory and the examination of diffusion dynamics of the adsorbates (via molecular dynamics simulations).

Of course, it is evident from the description of the model MIP matrices, together with the omission of solvent (see justification in chapter 3) that the current model lacks realism in its porous morphology. The molecular structures generated in the current model MIP material are aimed at assessing and characterizing the molecular recognition functionality of the model MIPs. At this stage in the model's development, all binding sites are considered to be accessible, which is not the case in real MIP structures.

2.4. Simulation of adsorption in MIPs

The system under consideration at this stage consists of one fluid adsorbing in a porous multi-component matrix; which is modelled as a configuration of prearranged molecules, fixed in their positions and orientations. The volume of the system is also fixed, and so is the temperature. The number of matrix molecules and their positions and orientations are known and fixed (N_m and $\mathbf{q}_m$). The chemical potential of the adsorbate μ_a is specified. In statistical mechanics, this system is described within the grand-canonical ensemble.

2.4.1. Grand-canonical partition function

Considering the derivations performed for the canonical ensemble in section 2.2.1., for a particular matrix realization $(\mathbf{q}_m)$ the probability density of observing the system in a given microstate $(\mathbf{N}_a, \mathbf{q}_a)$ (*i.e.* the microstate corresponding to the specific number of adsorbed molecules N_a) is described by:

$$\rho(\mu_a, N_a, \mathbf{q}_a) = \frac{z_a^{N_a} V^{N_a} q_{rot}^{N_a} e^{-\beta U(\mathbf{q}_a, \mathbf{q}_m)}}{N_a!\, \Xi(\mu_a, \mathbf{q}_m, V, T)} \qquad \text{II.32}$$

where $z_a = e^{\beta\mu_a}/\Lambda^3_a$, index a denotes adsorbate species, $\mathbf{q}_a$ describes positions and orientations of adsorbate molecules using the notation adopted at the end of section 2.2.1 and $\mathbf{q}_m$ represents the same for all molecules corresponding to the matrix. The grand-canonical ensemble can be viewed as an ensemble of canonical ensembles. Therefore the grand partition function is the sum of contributions of canonical partition functions for each varying number N_a of molecules in the system. For a particular matrix realization $\mathbf{q}_m$ (that can be viewed as an external field here), the grand canonical partition function in the denominator of equation II.32 can be expressed as:

$$\Xi(\mu_a, \mathbf{q}_m, V, T) = \sum_{N_a=0}^{\infty} e^{\beta\mu_a N_a} Q(N_a, \mathbf{q}_m, V, T) \qquad \text{II.33}$$

or, expanding the canonical partition function:

$$\Xi(\mu_a, \mathrm{q}_m, V, T) = \sum_{N_a=0}^{\infty} \frac{q_{rot}^{N_a} V^{N_a} e^{\beta\mu_a N_a}}{N_a! \Lambda^{3N_a}} \int e^{-\beta U(\mathrm{q}_a, \mathrm{q}_m)} d\mathrm{q}_a \qquad \text{II.34}$$

One can describe the potential energy of the system $U(\mathbf{q}_a, \mathbf{q}_m)$ as the sum of the separate interaction terms between species:

$$U(\mathbf{q}_a, \mathbf{q}_m) = U_{a,a}(\mathbf{q}_a) + U_{a,m}(\mathbf{q}_a, \mathbf{q}_m) \qquad \text{II.35}$$

where $U_{a,a}(\mathbf{q}_a)$ is the potential energy corresponding to interactions between adsorbate molecules (fluid-fluid interactions) and $U_{a,m}(\mathbf{q}_a,\mathbf{q}_m)$ is the potential energy between adsorbate and matrix molecules (fluid-solid interactions).

2.4.2. Thermodynamic properties

Again, a thermodynamic property, *A*, of the adsorbing fluid can be obtained by averaging its value across the ensemble.

$$\left\langle A(\mathrm{q}_m)\right\rangle = \frac{\sum_{N_a=0}^{\infty} \frac{q_{rot}^{N_a} V^{N_a} e^{\beta\mu_a N_a}}{N_a!\Lambda^{3N_a}} \int A(\mathrm{q}_a,\mathrm{q}_m,N_a) e^{-\beta U(\mathrm{q}_a,\mathrm{q}_m)} d\mathrm{q}_a}{\Xi(\mu_a,\mathrm{q}_m,V,T)} \qquad \text{II.36}$$

This property of the adsorbed fluid will be specific for the particular matrix configuration used. In fact, to obtain the thermodynamic properties of fluids confined in a macroscopic sample of porous material, equation II.36 is insufficient, as the properties of the fluid must be further averaged over canonical distribution of matrix realizations. This leads to:

$$\left\langle A\right\rangle = \frac{\int \left\langle A(\mathbf{q}_m)\right\rangle e^{-\frac{U(\mathbf{q}_m,\mathbf{q}_t,\mathbf{q}_s)}{kT}} d\mathbf{q}_m d\mathbf{q}_t d\mathbf{q}_s}{Z_p} \qquad \text{II.37}$$

where property $\left\langle A(\mathbf{q}_m)\right\rangle$ is averaged over canonical realizations of the pre-polymerization mixture, defined through the generalized coordinates of matrix (functional monomer + cross-linker), template and solvent species: $\mathbf{q}_m, \mathbf{q}_t, \mathbf{q}_s$. Z_p is the configuration integral of the equilibrium pre-polymerization mixture. In the most general case, we are interested in the grand potential of the confined fluid:

$$\Phi = -k_B T \ln \Xi = -PV \qquad \text{II.38}$$

and therefore

$$\left\langle \ln \Xi \right\rangle = \frac{\int \ln \Xi(\mathbf{q}_m) e^{-\frac{U(\mathbf{q}_m,\mathbf{q}_t,\mathbf{q}_s)}{kT}} d\mathbf{q}_m d\mathbf{q}_t d\mathbf{q}_s}{Z_p} \qquad \text{II.39}$$

which also serves as a starting point in the replica Ornstein-Zernike theoretical approach to thermodynamics of adsorbed species.

2.4.3. Simulation of adsorption in (μVT) ensemble

The simulation procedure in (μVT) ensemble relies on the Metropolis scheme described earlier. However, in addition to canonical perturbations (translations and rotations), insertions and deletions of molecules are also performed. Insertions are done by placing a particle in a random position and orientation with the following acceptance criteria:

$$acc(N \to N+1) = \min\left(1, \frac{V q_{rot} e^{\beta\mu_a} e^{-\beta[U_n(N_a+1)-U_o(N_a)]}}{(N_a+1)\Lambda_a^3}\right) \qquad \text{II.40}$$

Again, the term $U_n(N_a+1)-U_o(N_a)$, corresponding to the difference in the potential energy between the system with newly added adsorbate molecule and the unperturbed system is calculated using the site-site description of intermolecular interactions employed in the canonical treatment. Deletions are done by selecting a particle at random. This trial is approved in the same form, with the probability of accepting the transition as follows:

$$acc(N \to N-1) = \min\left(1, \frac{N_a \Lambda_a^3}{V q_{rot} e^{\beta\mu_a}} e^{-\beta[U_n(N_a-1)-U_o(N_a)]}\right) \qquad \text{II.41}$$

In these formulae, there are several quantities which for simplified models cannot be readily determined, or their actual values are not of principal importance. Specifically, to evaluate the translational and rotational partition

functions of a single molecule, we would need to specify the masses of constituent sites. Instead it is convenient to define the configurational chemical potential as follows:

$$e^{\beta\mu_a^*} = \frac{q_{rot} e^{\beta\mu_a}}{\Lambda_a^3} \qquad \text{II.42}$$

and treat it as a single parameter in the simulations. For simplicity, throughout the thesis, terms "chemical potential" and "βμ" refer to the configurational chemical potential.

In order to obtain a property of a confined fluid averaged over canonical realizations of the matrix structure, the grand-canonical simulation must be repeated for several matrix realizations.

$$\langle A \rangle = \frac{\sum_{i=1}^{N_m} \langle A(\mathbf{q}_{mi}) \rangle}{N_m} \qquad \text{II.43}$$

where $\langle A(\mathbf{q}_{mi}) \rangle$ is property of a fluid confined in a particular matrix realization $\mathbf{q}_{mi}$, N_m is the number of matrix realizations used, <*A*> is the value of property *A* averaged over canonical realizations of the matrix. In practice, sampling over only a few realizations is computationally feasible.

2.4.4. Biased grand-canonical Monte Carlo

For simulation of high density fluids or for adsorption problems in low porosity solids, the conventional GCMC protocol can be very inefficient due to high number of trial rejections caused by strong overlaps. To alleviate this problem, a number of biased Monte Carlo schemes have been proposed. These allow sampling within available space of sufficient size, in the porous

matrix. In this study the energy bias method is adopted. Snurr and co-workers (Snurr *et al.* 1993) investigated rotation, cavity and energy biased methods in application to adsorption in zeolites and observed that predominant gain in efficiency arises from energy biasing. This method consists of dividing the simulation box into $(n \times n \times n)$ small cubelets. Sampling is then done from the n^3 cubelets according to a weight assigned to each cubelet. In the energy biased protocol, this weight is based on the energy of interaction u_i of a probe molecule (placed in the centre of cubelet *i)* with the matrix:

$$\eta_i = \frac{e^{-\beta u_i}}{\sum_k e^{-\beta u_k}} \qquad \text{II.44,}$$

where the sum in the denominator is the sum over all cubelets and $\beta=1/k_BT$ as usual. This is very similar to the construction of an excluded volume bias map described by Deitrick (Deitrick *et al.* 1989).

For the case of the molecular model used in this study, interactions are based on a hard-sphere potential. The numerator in equation II.44 can only take two values: 1 or 0. If a probe placed in a cubelet *i* overlaps with matrix molecules, the cubelet is said to be not accessible and given η_i = 0. If the probe does not overlap with the matrix structure, the cubelet is said to be accessible (free) and is assigned weight $\eta_i = 1/N_f$, where N_f is the total number of accessible cubelets. A simpler bias is done by sampling only those cubelets considered accessible, *i.e.* portions of the system not occupied by the matrix. In the insertion trial, a cubelet is selected randomly from N_f available cubelets and a molecule is placed randomly within the cubelet.

Naturally, because the molecules are not inserted randomly in the whole volume V of the simulation box, the acceptance criteria presented in equations II.40 and II.41, must be biased as well. For insertions:

$$acc(N \to N+1) = \min\left(1, \frac{V_{cubelet}}{\eta_i} \frac{e^{\beta\mu^*_{ads}}}{N_{ads}+1} e^{-\beta[U_n(N_{ads}+1)-U_o(N_{ads})]}\right) \qquad \text{II.45}$$

where $V_{cubelet}$ is the volume of a single cubelet. To maintain microscopic reversibility, deletions must be biased also:

$$acc(N \to N-1) = \min\left(1, \frac{\eta_i}{V_{cubelet}} N_{ads} e^{-\beta\mu^*_{ads}} e^{-\beta[U_n(N_{ads}-1)-U_o(N_{ads})]}\right) \qquad \text{II.46}$$

Naturally in this method, the lower the value of $V_{cubelet}$, the higher the definition of the accessible volume will become.

2.4.5. Periodic Boundary Conditions

Due to storage and computational time restrictions, computer simulations consider systems of fairly small number of molecules (not exceeding tens of thousands of molecules, but usually limited to just thousands of molecules). Even small real systems such as micro droplets are many times larger than a typical system that can be handled by simulation. If the boundaries of the simulation system were defined by impenetrable walls, to a significant extent the simulated properties would be affected by the interaction with the walls (surface effects), whereas one is usually interested in the bulk properties of the system. A way around this is to define the simulation box as being an open subsystem in an infinite periodic array of its own replicas, or images (see Figure 2.3). This eliminates surface effects, and, if the simulation box is of adequate size, periodicity effects are negligible. The molecules are free to

move across the faces of the simulation box, which in practical terms means that a molecule exiting through one face is compensated by its replica re-entering the system through the opposite face. This behaviour corresponds to the application of the *periodic boundary condition*.

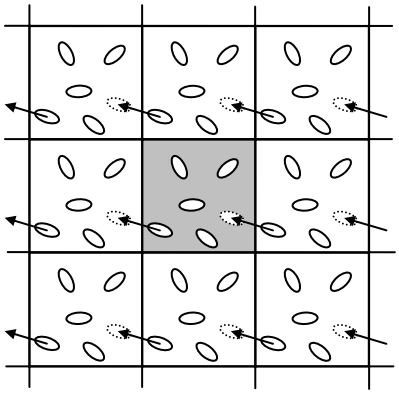

Figure 2.3: Two dimensional representation of the periodic boundary condition. A translation move of a molecule across the simulation box is exemplified.

Any molecule in the system behaves as interacting with the whole space surrounding it, not only the specific subspace (simulation box). Therefore, a molecule interacts with all molecules within the cut-off radius of its potential, whether they are in the simulation box or in one of its replicas. A requirement of this scheme is that the interaction between a molecule *i* and its neighbour *j* be calculated with respect to the image of *j* closest to *i*, (see Figure 2.4). This is called the *minimum image convention*.

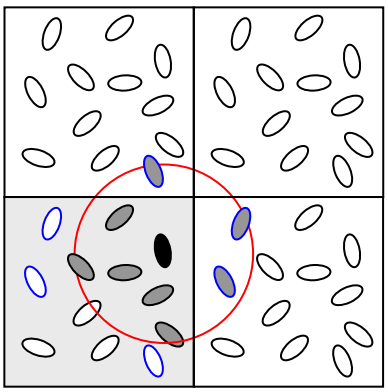

Figure 2.4: Schematic representation of minimum image convention in two dimensions. Black particle denotes the molecule *i*; any molecule *j* within its potential cut-off (red) are marked in grey. The molecules in blue are those whose image is closer to *i* than the "original" molecule.

2.4.6. Cell list scheme

In large systems of N molecules with a atoms the calculations of interaction energies amounts to $\frac{1}{2}a^2N(N-1)$. This makes these calculations the most expensive step in the simulation. However, for each cycle in the simulations, the calculation of the total energy is not necessary. Once the total energy is calculated, all that is needed is to calculate the difference in the energy originating from the attempted move. The energy gap is dependent only on one molecule, therefore only $a^2(N-1)$ calculations are now needed. For large systems, however, this is still woefully inefficient since most molecules are outside the cut-off radius of the energy potential, especially if one does not consider long range interactions.

To help further reduce the number of unnecessary calculations, a list of neighbour molecules can be composed, so that only molecules within the cut-off range are on the list, and only members of the list are considered when

calculating energies. This technique adds complexity to the code, but for systems exceeding 1000 molecules, it also increases the efficiency of the computation (Allen and Tildesley 1987).

A form of creating this neighbour list is to divide the simulation box into cells. In a three dimensional cubic simulation box, the system has $M \times M \times M$ cells whose dimensions are defined so that the side of each cell, d, is at least greater or equal to the cut-off radius $r_{cut\ off}$. Figure 2.5 shows a schematic 2D representation of the cell list scheme.

For a molecule located in a particular cell, the energy calculation is then restricted to only molecules in the 26 neighbouring cells plus its own cell. At every move accepted, the cell list must be updated in terms of its contents.

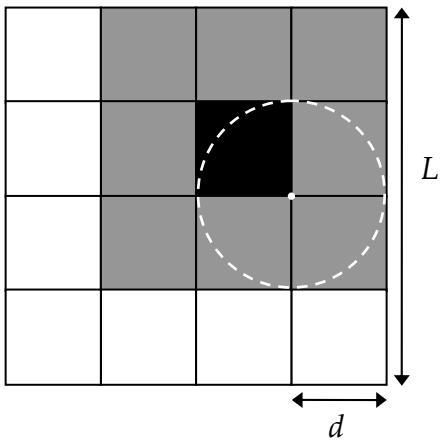

Figure 2.5: Two dimensional representation of a cell list scheme with an extreme case of an atom at edge of the cubicle, exemplifying the requirement for $d > r_{cut\ off}$.

2.5. Molecular Model

The strategy in this thesis is, using the approach and tools described before, to first develop the simplest model capable of molecular recognition and then relate its behaviour to various characteristics of the model porous materials. These include composition, binding site structure, overall morphology and others. The model must be sufficiently realistic to be capable of molecular recognition, while at the same time being simple enough so its outcomes are general and its computational cost modest. It is clear, that besides shape recognition (purely steric effect), intermolecular forces such as van der Waals, hydrogen bonds and ionic interactions must play a role in the emergence of the molecular recognition phenomena. Previous models (a and b in Figure 2.1) did not account for these forces, and in keeping with the philosophy of a simple model, further model development must be obtained by a simple alteration to the interaction between the molecules.

Hydrogen bonds, due to their directionality, short range and specificity (*i.e.* hydrogen bonds form between specific groups of atoms) seem to be particularly important in formation of complementary energetic patterns. These interactions seem to be a good candidate for the first additional element to be incorporated in the model of Sarkisov and Van Tassel (Sarkisov and Van Tassel 2005). The inspiration for the model used in this work comes from the model of water proposed by Kolafa and Nezbeda (Kolafa and Nezbeda 1987).

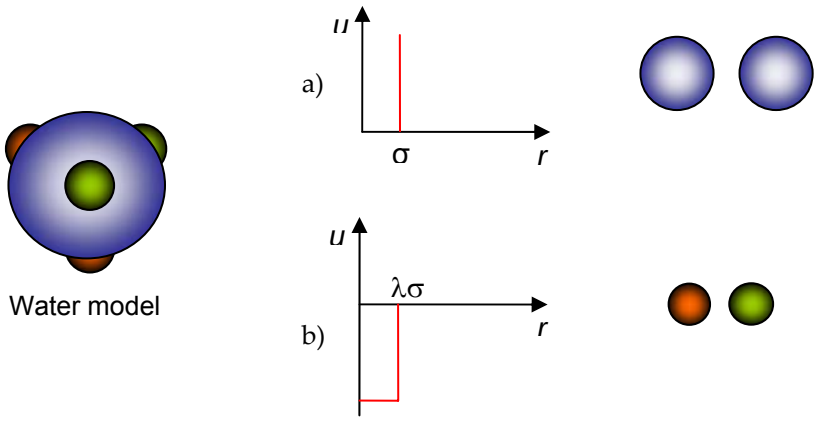

Figure 2.6: In the model of water by Kolafa and Nezbeda each molecule consists of a hard sphere particle (hard sphere potential is shown in subset (a), decorated with four associative sites interacting with each other through a strong short range square well potential (b).

This model considers a spherical particle of diameter σ decorated by four association sites in tetrahedral arrangement on or near its surface. Interaction between particles is a hard sphere (HS) interaction, whereas the association sites interact via a square well potential (SW), represented in Figure 2.6 and in the formulae below:

$$u_{HS}(r) = \begin{cases} \infty & r \le \sigma \\ 0 & r > \sigma \end{cases} \qquad \text{II.47}$$

$$u_{SW}(r) = \begin{cases} -\varepsilon & r < \lambda\sigma \\ 0 & r \ge \lambda\sigma \end{cases} \qquad \text{II.48}$$

This model can be seen as spheres with sticky sites, to put it in colloquial terms. The short range of the square well interactions coupled with the hard-sphere potential of the particle leads to directional bonding, imitating hydrogen bond associations. This model belongs to a broader class of association models and patchy particles which have been used to simulate hydrogen bonds in water as well as diamond structures and polymers chains

(Zhang *et al.* 2005; Sciortino *et al.* 2007). This attests to the versatility and capability of this simple approach. Using this model we can construct various species to describe a MIP system as shown in Figure 2.7.

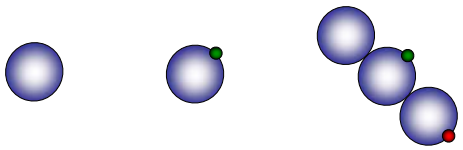

Figure 2.7: Schematic representation of several molecular species constructed from hard spheres and associative sites as building blocks.

Specific systems and species constructed in this study will be introduced in Chapter 3 along with the corresponding results.

2.6. Structural characteristics of model materials

One of the advantages of molecular modelling and computer simulations is the detailed information one can obtain about the microstructure of the model materials. An important avenue of research, in computational material design, is to relate adsorption capabilities (or other functionality) of model materials to various morphological features of their structure. A number of properties can be designated to characterize the model matrices. Among them are porosity, pore size distribution, accessibility and binding site geometry. Some of these characteristics have also direct analogues in the

experimentally measured properties (although not always necessarily defined in the same fashion).

2.6.1. Porosity

In experiments porosity and pore volume can be obtained from porosimetry experiments, where a fluid (typically mercury) is forced into the porous network. Although X-ray tomography can allow the visualization of the empty volume inside a solid, only when the material is sufficiently crystalline, can a relevant measurement be made.

In computer simulations, the microstructure is well defined: the number, geometry and the location of the molecules constituting the material are perfectly known. One can easily calculate porosity

$$\phi = \frac{V_{empty}}{V} \qquad \text{II.49}$$

where V_{empty} is the volume not occupied by the molecules ($V_{empty} = V - V_{molecules}$). This constitutes the absolute porosity of our system of molecules, in other words volume accessible to a point probe. This porosity is not of interest though, since many regions included in absolute porosity are not accessible to an adsorbate molecule of finite size.

The porosity of interest is in fact the *apparent* or *accessible porosity*, which represents the porosity as seen by a specific adsorbing molecule. To calculate accessible volume fraction one can use a single molecule as a probe and a Monte Carlo simulation to evaluate the following integral:

$$\frac{V_{acc}}{V} = \frac{\int e^{-\beta U(\mathbf{q})} d\mathbf{q}}{V} \qquad \text{II.50}$$

where $U(\mathbf{q})$ is the energy of interaction of the probe molecule with the matrix of the material. The apparent porosity presented in II.50 can be calculated by averaging $e^{-\beta U(\mathrm{q})}$ over a series of trial insertions of a single particle in the matrix (no other particles are present or included in the interaction):

$$V_{acc} = \int e^{-\beta U(\mathbf{q})} d\mathbf{q} \approx < e^{-\beta U(\mathbf{q})} > V \qquad \text{II.51}$$

This is, in fact, an application of the Widom insertion method to the calculation of the excess chemical potential. For a more extensive description of the Widom method, the reader is directed to (Frenkel and Smit 2002). Below we summarise the relationships between the accessible volume, excess chemical potential and the Henry's constant. The excess chemical potential is (Frenkel and Smit 2002):

$$\beta\mu_{ex} = -\ln < e^{-\beta U(\mathbf{q})} > \qquad \text{II.52}$$

In the limit of the pressure or concentration of adsorbing species approaching zero the Henry's constant is:

$$K_H = \beta < e^{-\beta U(\mathbf{q})} > \qquad \text{II.53}$$

and related to the excess chemical potential as:

$$K_H = \beta e^{-\beta\mu_{ex}} \qquad \text{II.54}$$

In the limit of one molecule in the matrix, the Henry's constant and the accessible volume are related as:

$$V_{acc} = K_H V / \beta \qquad \text{II.55}$$

For Lennard-Jones or other continuous potentials, $U(\mathbf{q})$ will have negative values in accessible space, and high positive values when there is an overlap with the solid structure. For the case of species interacting via hard sphere potential, $e^{-\beta U(\mathrm{q})}$ is 0 when the probe is overlapping with the solid and 1 when it is not. This somewhat simplifies the Monte Carlo protocol. The sampling of random insertions of a probe molecule (at random orientations) is done throughout the whole volume of the simulation box. The position can

either be occupied, leading to overlaps with the probe molecule (rejected insertion) or a free space (accepted insertion). By evaluating the ratio of accepted insertions to total samples taken, for a very large number of samples, one approximates the true value of the ratio of available volume to the total volume.

2.6.2. Pore Size Distribution

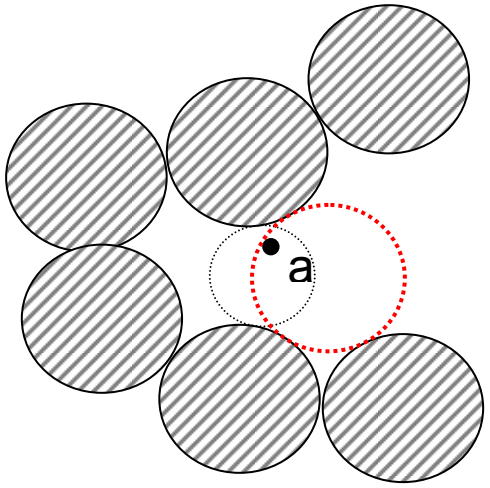

Figure 2.8: Schematic representation of pore size distribution assessment routine.

The pore size distribution is an important morphological characteristic of a porous material. In experiments this characteristic typically is extracted from nitrogen sorption experiments using methods such as Barret-Joyner-Halenda (Barrett *et al.* 1951). For molecular models it is also an important characteristic as it serves as a unique fingerprint of a particular model and also provides some important insights on the typical sizes of cavities present in the system.

A FORTRAN program has been developed in Sarkisov's group that calculates pore size distribution of a porous solid, given the coordinates of the atoms and their collision diameters. Previously, this program has been applied in the studies of metal organic frameworks, imprinted polymers and other materials.

The basic idea is described by Gelb and Gubbins in application to characterization of porous glasses (Gelb and Gubbins 1999). The protocol works as follows. Consider a porous solid (adsorbent) structure, as shown in Figure 2.8, with adsorbent atoms shaded grey. Suppose $V_p(r)$ is the volume of the void space that can be covered by spheres of radius r or *smaller*. A point **a** is in $V_p(r)$ if and only if one can construct a sphere of radius r that overlaps **a** and does not overlap any adsorbent atoms (this is schematically depicted in Figure 2.8). $V_p(r)$ is a monotonically decreasing function of r, and corresponds to the cumulative pore volume function. The derivative $dV_p(r)/dr$ is the fraction of volume coverable by spheres of radius r but *not* by spheres of radius $r+dr$. In other words - $dV_p(r)/dr$ is the pore size distribution function (PSD).

To calculate this function the following Monte Carlo procedure is involved. The pore range of interest is divided into small bins. A test point **a** is randomly placed in the simulation cell and tested for no overlaps with structure atoms. If no overlaps are observed, in the second round of Monte Carlo procedure, the vicinity of the point is probed to find the *largest* sphere that contains point **a** *and* does not overlap with the atoms of the structure. In Figure 2.8 this sphere is schematically depicted as a red dashed circle, while the black dashed circle satisfies the criteria, but is not of the largest possible

radius. Once the largest sphere has been identified, the value of the bin corresponding to that radius *and* all the preceding bins (corresponding to all smaller radii) are incremented by one. The normalized bin distribution corresponds to cumulative $V_p(r)$.

2.7. References

Allen, M. P. and D. J. Tildesley (1987). Computer simulation of liquids. New York, Clarendon Press ; Oxford University Press.

Barrett, E. P. *et al*. (1951). "The Determination of Pore Volume and Area Distributions in Porous Substances .1. Computations from Nitrogen Isotherms." Journal of the American Chemical Society **73**(1): 373-380.

Deitrick, G. L. *et al*. (1989). "Efficient Molecular Simulation of Chemical-Potentials." Journal of Chemical Physics **90**(4): 2370-2385.

Frenkel, D. and B. Smit (2002). Understanding molecular simulation : from algorithms to applications. London, Academic Press.

Gelb, L. D. and K. E. Gubbins (1999). "Pore Size Distributions in Porous Glasses: A Computer Simulation Study." Langmuir **15**(2): 305-308.

Gray, C. G. and K. E. Gubbins (1984). Theory of molecular fluids. Oxford, Clarendon.

Hill, T. L. (1986). Introduction to statistical thermodynamics. New York, Dover Publications.

Kolafa, J. and I. Nezbeda (1987). "Monte-Carlo Simulations on Primitive Models of Water and Methanol." Molecular Physics **61**(1): 161-175.

McQuarrie, D. A. (1975). Statistical mechanics. New York, Harper & Row.

Metropolis, N. *et al*. (1953). "Equation of State Calculations by Fast Computing Machines." Journal of Chemical Physics **21**(6): 1087-1092.

Metropolis, N. and S. Ulam (1949). "The Monte Carlo Method." Journal of the American Statistical Association **44**(247): 335-341.

Noss, K. R., A. D. Vaughan, et al. (2008). "Tailored binding and transport parameters of molecularly imprinted films via macromolecular structure: The rational design of recognitive polymers." Journal of Applied Polymer Science **107**(6): 3435-3441.

Sarkisov, L. and P. R. Van Tassel (2005). "Replica Ornstein-Zernike theory of adsorption in a templated porous material: Interaction site systems." Journal of Chemical Physics **123**(16): 164706:1-10.

Sciortino, F. *et al*. (2007). "Self-assembly of patchy particles into polymer chains: A parameter-free comparison between Wertheim theory and Monte Carlo simulation." Journal of Chemical Physics **126**(19): 164706:1-10.

Snurr, R. Q. *et al*. (1993). "Prediction of Adsorption of Aromatic-Hydrocarbons in Silicalite from Grand-Canonical Monte-Carlo Simulations with Biased Insertions." Journal of Physical Chemistry **97**(51): 13742-13752.

Spivak, D. A. (2005). "Optimization, evaluation, and characterization of molecularly imprinted polymers." Advanced Drug Delivery Reviews **57**(12): 1779-1794.

Wulff, G. *et al*. (1982). "Chirality of Vinyl-Polymers - the Preparation of Chiral Cavities in Synthetic-Polymers." Nouveau Journal De Chimie-New Journal of Chemistry **6**(12): 681-687.

Zhang, L. and P. R. Van Tassel (2000). "Configurational effects of templating on the adsorption isotherms of templated porous materials." Molecular Physics **98**: 1521-1527.

Zhang, Z. L. *et al*. (2005). "Self-assembly of patchy particles into diamond structures through molecular mimicry." Langmuir **21**(25): 11547-11551.

3.

Emergence of molecular recognition in a simple model of imprinted polymer

In this part of the thesis the model outlined in Chapter 2 is applied to a specific test system. The imprinted matrix generated is explored through adsorption simulations to evaluate the effectiveness of the imprinting process. The selectivity of the model matrix with respect to the template and an analogue is assessed. Further analysis is also made on the nature of pre-polymerization complexes and of binding sites for the adsorbate bound to the matrix.

3.1. Molecular model

In Chapter 2 we introduced the basic elements of the approach adopted in this work. Molecular species in this study are represented as hard spheres, or rigid clusters of hard spheres. Some of the hard spheres may also feature small association sites on their surface, with a prescribed set of rules on how these sites interact with each other. Using this language, the simplest model of an imprinted polymer capable of molecular recognition is constructed. The key requirement to achieve this is to consider a template molecule that is able to induce various *interaction patterns* with the functional monomers. In the model proposed, a template molecule (species *T*) is a rigid linear chain of three tangent hard spheres of the equal size σ (Figure 3.1). Two of these spheres also feature surface interaction sites in the arrangement shown in Figure 3.1a and can be viewed as functional groups (FG1 and FG2). Other species in the system are as follows.

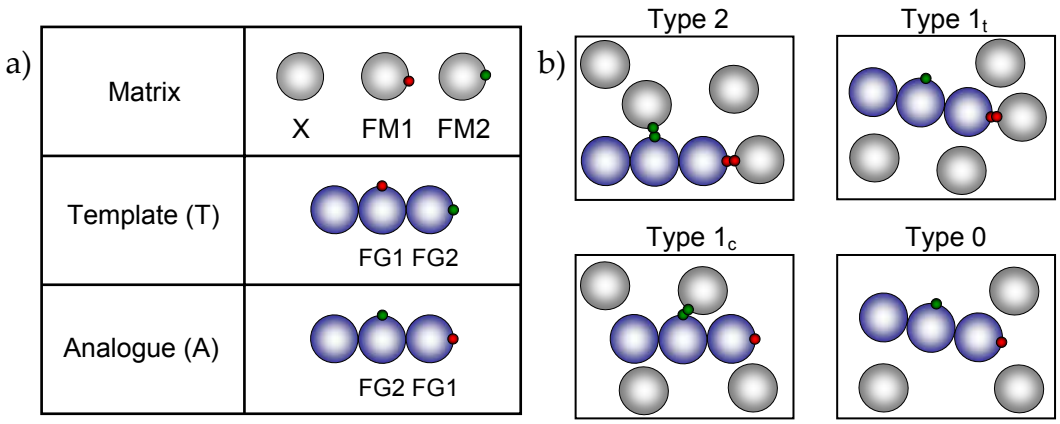

Figure 3.1: a) Representation of the species involved in the study. X corresponds to the cross-linker, FM1 and FM2 are the functional monomers. T indicates the template and A its analogue. b) Association types of either template or analogue.

The cross-linker is modelled as a hard sphere of size σ (species X). A functional monomer in this model is represented as a hard sphere of size σ with an interaction site on the surface. Functional monomers of two types, FM1 and FM2, are defined to complete the basic components of the pre-polymer mixture. Functional monomer FM1 can associate with functional group FG1, whereas functional monomer FM2 can associate with functional group FG2. The association between interaction sites is modelled via a square-well potential defined in equation II.45, with a well depth of $10 \times k_B T$ (typical magnitude for hydrogen bonds) and a range of $0.15 \times \sigma$. No functional monomers can associate with each other, and the same is true for the functional groups. Finally, for the analogue molecule, the location of the interaction groups is reversed. It is also clear, by comparing the template and analogue molecules that they differ only in this interaction pattern. This bears similarity to chiral molecules, featuring the same chemical groups, but with differing locations for functional groups and therefore different interaction patterns.

No solvent is modelled in this system (or other in this thesis) as this leads to lower number of associations between template and functional monomers. Modelling the presence of solvent is necessary for a realistic representation of its influence on the chemical equilibrium of the pre-polymerization mixture and of the porous space that results form said mixture. However, because we are primarily interested in studying molecular recognition, the focus is on obtaining a system that easily allows its study within a computationally simple simulation. Both large number of imprinted sites capable of recognition and the presence of solvent could be captured in larger and more computationally costly systems.

3.2. Characterization of pre-polymerization complexes

In the model presented here, associations form between the functional monomers and the functional groups of the template. In the pre-polymerization mixture composed by the species presented in Figure 3.1a, a template molecule can be observed in one of four possible coordination complex types. These are shown in Figure 3.1b. In the first type, labelled 0, the template molecule does not form any associations. Types 1_t and 1_c are characterized by a single association, with either the terminal or the central functional group of the template engaged in the association, respectively. (This notation was chosen, instead of using FG1 and FG2, since the location of these groups in the template and analogue molecules is swapped). Finally, the template can have associations established with both functional groups and this corresponds to complex of type 2. Type 2 sites should correspond to recognition capable sites, since these specify an interaction pattern, rather than an interaction point as in type 1 sites.

These types of association serve to describe the complexes established in equilibrium as well as the binding status of adsorbates. Computer simulations allow the monitoring of the population of these complexes during the equilibration of the matrix and also to relate these characteristics to various parameters of the system, such as composition or density. Once the system is quenched (imitating post polymerization MIP), the complexes are frozen in their structure. Template removal transforms these complexes into binding sites.

3.3. Simulation details

As we have already discussed in Chapter 2, the first stage of the proposed computational strategy considers an equilibrium mixture of the template, functional monomer and cross-linker components. Equilibration of the system is performed in the canonical *NVT* ensemble using the classical Metropolis sampling protocol. The number of canonical Monte Carlo steps (translations and rotations) required for equilibration is 1.7×10^5 per particle (on average), of these *ca.* 1.4×10^4 per particles (on average) are used to generate average properties of the system. A total of 3 different matrix realizations are generated.

Simulations of adsorption are performed using the grand canonical Monte Carlo scheme. In this ensemble, temperature T, volume of the system V, and the chemical potential μ of the adsorbing species are specified. A point on the adsorption isotherm corresponds to a simulation with *ca.* 10^8 steps performed. Insertions, deletions, rotations and translations are attempted with equal probability. These simulations are carried out for a range of increasing values of chemical potentials.

The first system considered here, MIP1, has characteristics such as the overall density, similar to those in the earlier studies of Sarkisov and Van Tassel (Sarkisov and Van Tassel 2005; Sarkisov and Van Tassel 2007). This system features 2400 cross-linker particles and 400 functional monomer particles of each type. The system is imprinted with 400 template molecules (Table 3.1). Therefore, the ratio of functional monomers ($N_{FM1}+N_{FG2}$) and functional groups ($N_{FG1}+N_{FG2}$) is in stoichiometric proportion. The pre-polymerization

mixture is placed in a cubic box of 20σ in length. The overall reduced density of the system, defined as:

$$\rho^* = \frac{N_{total}}{V}\sigma^3 \qquad \text{III.1}$$

is 0.55. Here $N_{total} = N_X + N_{FM1} + N_{FM2} + 3 \cdot N_T$ is the total number of hard sphere particles present in the system; N_X and N_T are the number of cross-linker and template particles, respectively; V is the volume of the system.

Table 3.1: Composition of the pre-polymerization mixture for MIP1.

	Number of molecules	ρ^*
FM1	400	0.05
FM2	400	0.05
T	400	0.15
X	2400	0.30
Total	3600	0.55

3.4. Results

3.4.1. Pre-polymerization matrix

The analysis of the equilibrated mixture, regarding the association types described in Figure 3.1b, can be performed towards obtaining an ensemble averaged property – a distribution of states of association. With this, one knows the composition at equilibrium. However, it is the final configuration of this mixture that forms the polymer matrix. Therefore, the final value of the distribution of association types is the value of interest, when characterizing the matrix. The energy, as well as the average distribution of

association types can be tracked. The system is deemed to be in equilibrium after evaluating there is no significant variation in the total energy of interaction, as shown in Figure 3.2 for MIP1.

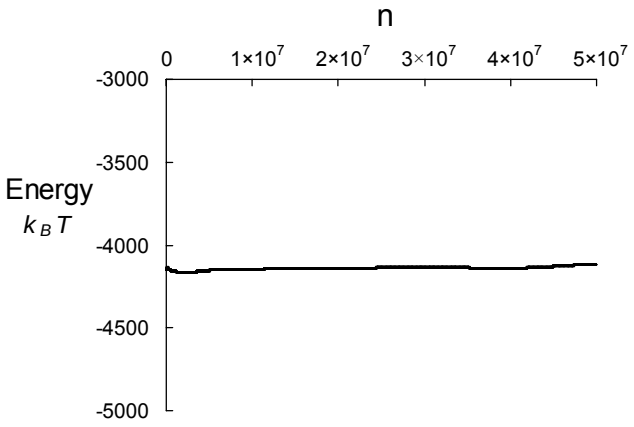

Figure 3.2: Total potential energy for MIP1 system (in units of $k_B T$) as a function of the number of Monte Carlo steps n in the production run.

Figure 3.3 summarizes the distribution of complexes observed in this pre-polymerization mixture, averaged over the three realizations. About 25% of templates are in complexes forming associations with two functional monomers. Other complexes are also observed with roughly the same percentage of 25%.

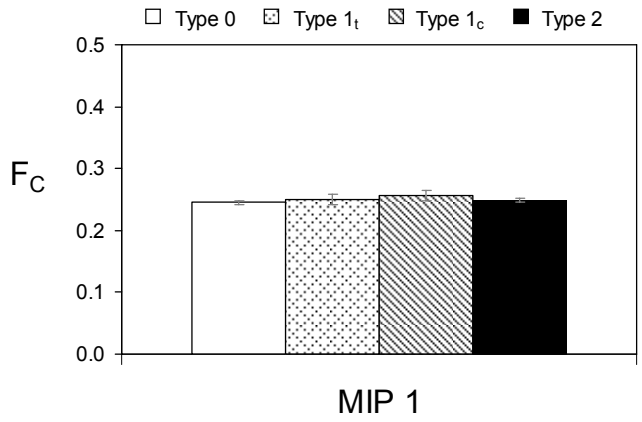

Figure 3.3: Distribution of different association types between template and functional monomers with the corresponding standard errors. F_C indicates the fraction of templates in a certain complex type.

In the next step in the simulation process, the final configuration of this mixture is saved and the template species are removed. The resulting structure represents a model MIP.

3.4.2. Adsorption in the model MIP structure

For each of the MIP matrix realizations, simulations of single component adsorption for both template and analogue are performed. Figure 3.4 shows adsorption isotherms for the template and analogue. Indeed, adsorption densities for the template are higher than those of the analogue throughout the whole range of chemical potentials sampled.

It is evident that at lower chemical potentials (expressed as $\beta\mu$), the difference in loading is larger. An intuitive way to characterize selectivity of a MIP is the separation factor, *S*, which is the ratio of adsorbed template and analogue densities at the same chemical potential. This ratio is plotted in Figure 3.4b.

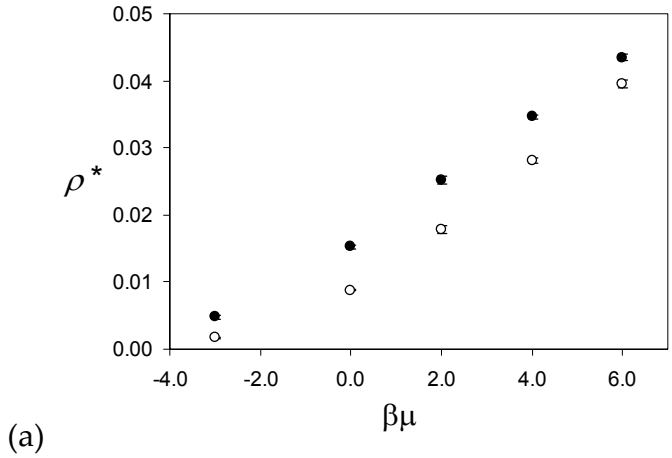

(a)

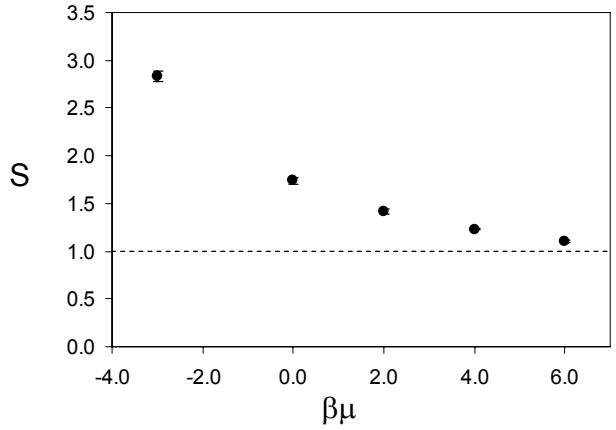

(b)

Figure 3.4: a) Isotherms obtained from the average of three matrix realizations and the corresponding standard errors; full circles correspond to the template adsorption and open circles are for the analogue. b) Selectivity expressed via the separation factor, as a ratio of averaged adsorbed density of template to averaged adsorbed density of analogue with the corresponding standard error.

For the whole range of chemical potentials this factor is greater than one, signifying the preferential adsorption of the template compared to the analogue. As expected, this factor is decreasing at higher loadings. The overall trend in selectivity can be explained by the highly specific binding

sites becoming occupied at lower chemical potentials and the remaining porous space not exhibiting any preferential adsorption.

The analogue is very similar to the template in terms of geometry and energy of interaction. The factor that makes the distinction between the two molecules possible must be the specific arrangement of interaction sites introduced in the matrix during the imprinting procedure. Although one can speculate that any individual association between adsorbed species and functional monomer is possible, the association of multiple functional groups for the analogue is expectedly less likely. Hence, we establish that the presented model is able to capture the molecular recognition effect.

3.5. Binding sites analysis

To understand the types of associations possible for the adsorbing species and how they might explain the selectivity observed, we employ the same analysis performed for the pre-polymerization mixture. Again, adsorbed molecules can be observed in different binding sites, with associations with functional monomers in the matrix similar to those depicted in Figure 3.1b.

All the graphics for adsorption binding analysis in this thesis are the result, for a specific matrix realization, of averaging the distribution of association types during the simulation of adsorption of template and analogue. Figure 3.5a summarizes the distribution of adsorbed template molecules among different types of association along the adsorption isotherm for MIP1.

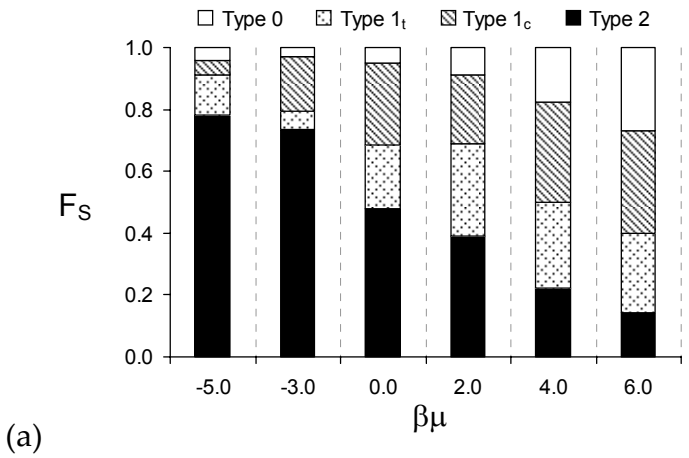

(a)

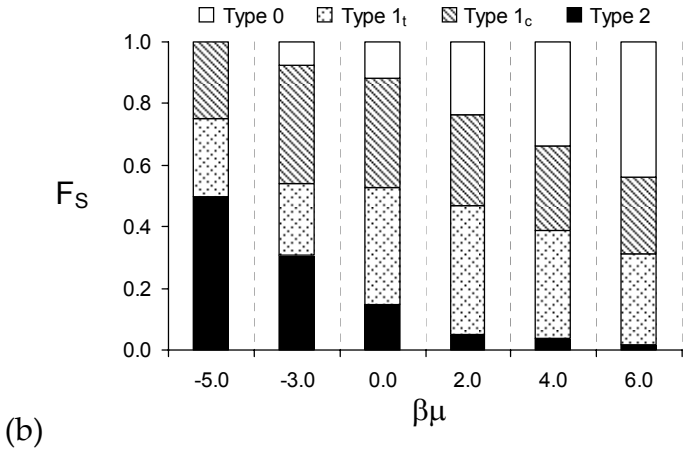

(b)

Figure 3.5: Fraction F_S of adsorbed template molecules (a) and analogue (b) in each binding site type as a function of the chemical potential $\beta\mu$, in MIP1.

For example, at the chemical potential $\beta\mu$ = -3.0, there are about 73% of adsorbed template molecules in type 2 sites, 6% in 1_t sites, 18% in 1_c sites and 3% not forming any associations (type 0). Overall, at lower values of the chemical potential, the majority of the adsorbed molecules form two associations with the matrix. As the loading of the material increases, progressively more and more molecules are able to form only one association with the matrix or no associations at all. Aside from specific cases, there is no indication of preferential binding between type 1 sites (terminal versus

central binding). Interestingly, at the highest loading the distribution of binding sites among different association types resembles the distribution of the complexes in the pre-polymerization mixture. It is also instructive to apply similar analysis to the analogue adsorption in the same material. Figure 3.5b shows distribution of adsorbed molecules among different binding sites for the analogue in MIP1. The most important feature of this result is that a significant fraction of analogue molecules are able to form two associations with the matrix, this despite the porous space being tailored to recognize the interaction pattern of the template. Examining the template and analogue species one can observe that association of analogues to functional monomers ordered in a templated site should be possible for a restricted set of orientations. This indicates that shape complementarity was not sufficient to create complete binding site fidelity.

It is important to recognize that not all association types of the adsorbed template in the matrix correspond to molecules located in binding sites formed during the imprinting step. For example, it is possible that an adsorbed molecule is associated with the matrix by *partially* binding to an imprinted site or by binding to FMs that did not take part in complexes in the pre-polymerization mixture. Specifically, it is instructive to know how many of the molecules in type 2 sites are actually located in the binding sites resulting from complexes of type 2. Computer simulations allow us, given a particular configuration, to examine the binding state of each molecule and also to make this distinction. The type of association, in pre-polymerization mixture, for each template is recorded and later compared to that observed during adsorption simulation.

The results of binding site analysis are shown in Figure 3.6, in which lighter shaded bars correspond to adsorbates re-binding in imprinted sites, and darker shades to adsorbates forming new (not originating from imprinting) associations of a particular type.

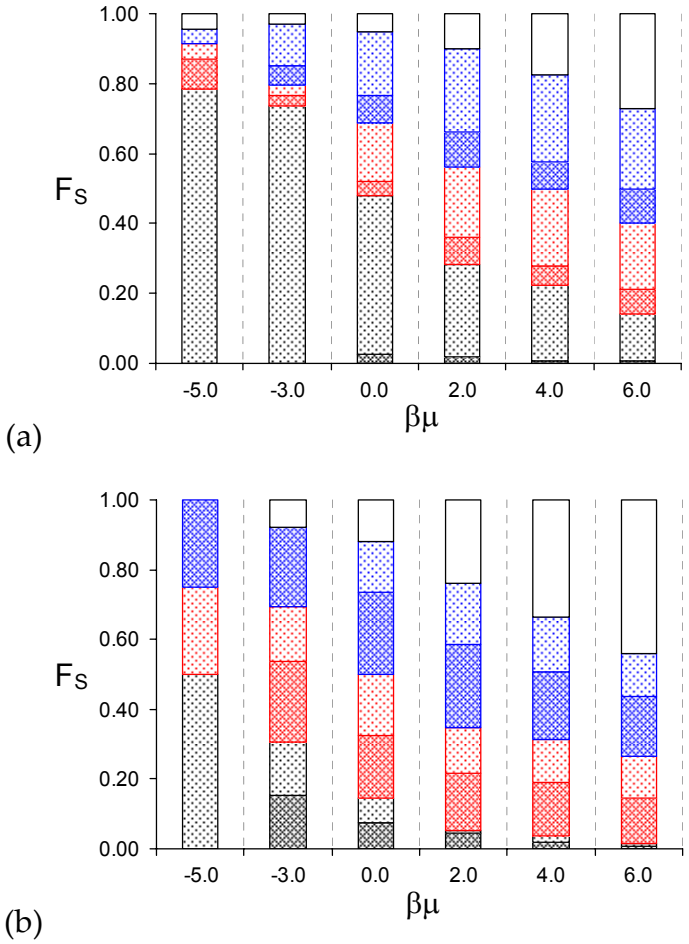

Figure 3.6: Fraction F_S of adsorbed template (a) and analogue (b) molecules, in each binding site type as a function of the chemical potential $\beta\mu$, in MIP1. The colour of each bar corresponds to a particular site type: grey for 2, blue for 1_c, red for 1_t and white for 0 sites, respectively. Lighter shades correspond to molecules located in the imprinted binding sites, whereas darker shades correspond to molecules forming alternative associations with the matrix. Data is shown for one matrix realization.

Let us first focus on type 1 sites. Analysis of Figure 3.6 reveals that the template tends to bind in the imprinted type 1 sites rather than occupy new sites. Analogues on the other hand are generally evenly split between the imprinted type 1 sites and non-imprinted sites of the same type. There is a slight favouring of binding of analogue in non-imprinted sites of the matrix. For sites of type 2, the difference is, overall, much more marked with the template binding almost exclusively to the imprinted sites while the analogue appears to split between the imprinted and non-imprinted sites. Although a substantial proportion of the analogue molecules seems to be in type 2 sites (including the imprinted kind), one must remember that this is for one matrix realization at very low total number of molecules adsorbed. Naturally sites with high energy of interaction will be occupied first.

3.6. Summary

This chapter outlines the first three-dimensional, disordered porous model of a MIP which exhibits molecular recognition and binding site heterogeneity. A system of template, cross-linker and functional monomers was simulated and analysed. Re-binding adsorption simulations show the model MIP to be selective towards the template used during the synthesis, when compared with the analogue species. The selectivity is owed to the specific interaction patterns imprinted into the model polymer matrix. This is observed from the analysis of the association types between template or analogue and the functional monomers in the polymer. The analysis of the distribution of the different sites clearly shows that the matrix possesses imprinted cavities. It also indicates that the high affinity sites are occupied at low loadings. At

higher loadings the relative contribution of high affinity sites diminishes and the less specific sites are being occupied. We also demonstrate that the model provides a wealth of information about the pre-polymerization and adsorption processes. Specifically, during these processes, individual complexes or binding site types for each molecule can be examined and linked to the overall behaviour of the system.

3.7. References

Sarkisov, L. and P. R. Van Tassel (2005). "Replica Ornstein-Zernike theory of adsorption in a templated porous material: Interaction site systems." Journal of Chemical Physics **123**(16): 164706:1-10.

Sarkisov, L. and P. R. Van Tassel (2007). "Integral equation theory of adsorption in templated materials: Influence of molecular attraction." Journal of Physical Chemistry C **111**(43): 15726-15735.

4.

Molecular recognition as a function of processing conditions and morphological modifications of MIPs

In the previous chapter the model was tested to establish its capability to exhibit molecular recognition. In the present chapter the behaviour of the model is explored as a function of various parameters and morphological

modifications of the imprinted matrix. This analysis is performed to help to understand the robustness of the molecular recognition effect.

4.1. Effect of density

The degree of cross-linking is a very important processing parameter in MIP studies. It has been shown that higher degrees of cross-linking lead to higher selectivity (Wulff *et al.* 1982; Srebnik and Lev 2002; Spivak 2005). This is due to the significant contribution of cross-linking to the higher rigidity of the polymeric matrix. A rigid matrix prevents the deformation of the binding cavity thus preserving its shape complementarity and therefore much of its affinity for the template. Density of the material may also have an important effect on molecular recognition, since a higher density is expected to lead to better defined, more specific binding sites. In general, on the bulk scale of a MIP material, the degree of cross-linking and the density of MIP are not *directly* related to each other. However, locally, in the vicinity of individual sites, we believe higher degree of cross-linking should lead to higher density. In our approach we do not model polymerization or cross-linking explicitly. (Polymerization and cross-linking are effectively captured by keeping the polymer particles frozen in space). Thus, only the matrix density effect can be explored in detail. However, since even the largest of our models operates on the scale comparable to the size of a binding site, we intend to investigate the effect of the density of the MIP on molecular recognition functionality and view this as an integrated impact of both higher local density and higher degree of cross-linking.

4.1.1. Model MIP systems of varying density

Two modifications of MIP1 were considered. Both of the systems feature the same composition as MIP1; however, MIP2 has lower overall density than MIP1 (75% of MIP1) and MIP3 has higher overall density than MIP1 (125% of MIP1). The resulting compositions are shown in tables 4.1 and 4.2. The simulation of these systems is otherwise the same.

Table 4.1: Composition of the pre-polymerization mixture for MIP2.

MIP2	Number of molecules	ρ*
FM1	300	0.03755
FM2	300	0.03755
T	300	0.11250
X	1800	0.22500
Total	2700	0.41250

Table 4.2: Composition of the pre-polymerization mixture for MIP3.

MIP3	Number of molecules	ρ*
FM1	500	0.0625
FM2	500	0.0625
T	500	0.1875
X	3000	0.375
Total	4500	0.6875

The analysis of the association complexes in the pre-polymerisation mixtures shows the expected shifts in the equilibrium at different concentrations of the components (Figure 4.1).

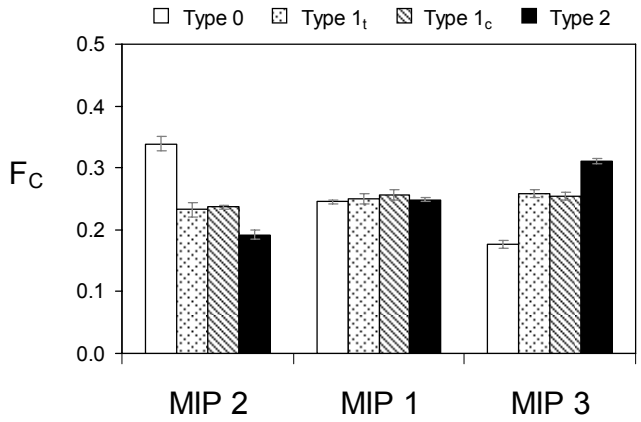

Figure 4.1: Distribution of different complexes between template and functional monomers in the final pre-polymerization configuration with the corresponding standard errors (obtained over 3 matrix realizations), for MIP1, 2 and 3.

Figure 4.1 reveals that higher density leads to a noticeably higher proportion of type 2 complexes observed in the mixture. The increase in type 2 complexes should promote more type 2 binding sites and these would increase selectivity.

Further characterization of model matrices is provided through porosity assessment. Porosity was determined by the method described in Chapter 2, with a total of 3×10^6 trial insertions. The probe molecule, shown in Figure 4.2 is similar to the template and analogue hard-sphere structure, but features no functional groups.

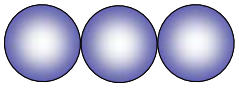

Figure 4.2: Schematic of the probe used to evaluate porosity.

Table 4.3: Apparent porosities, defined as a fraction of the system's volume, accessible to the probe in Figure 4.2, of MIP1, 2 and 3 (averaged over 3 matrix realizations), with respective standard error.

MIP2	$1.82\times10^{-2} \pm 4.46\times10^{-5}$
MIP1	$3.62\times10^{-3} \pm 2.00\times10^{-5}$
MIP3	$8.44\times10^{-4} \pm 9.68\times10^{-6}$

As expected, the increased density leads to the reduced pore volume accessible to the adsorbate species.

4.1.2. Adsorption in model MIPs of varying density

For both MIP2 and MIP3, simulations of single component adsorption for both template and analogue are performed. Simulations are performed in the grand canonical (μVT) ensemble via biased Monte Carlo as described in Chapter 2. The number of Monte Carlo steps (insertions, deletions, translations and rotations) required for the equilibration is between 2×10^8 and 3×10^8 (depending on the system), of these *ca.* 1×10^8 are used to generate average properties of the system. Figure 4.3 shows the adsorption isotherms for the template and analogue.

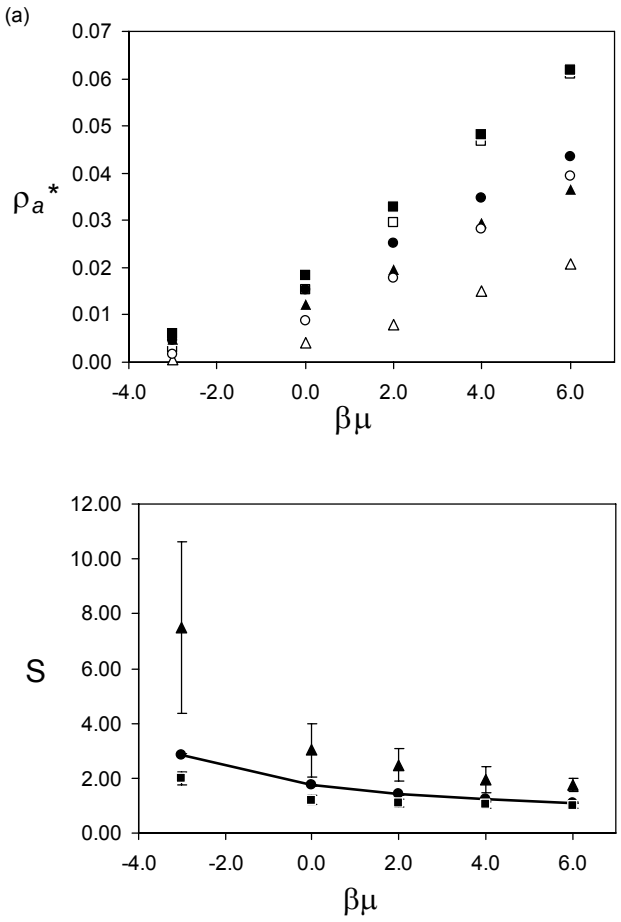

Figure 4.3: a) Adsorption isotherms for template (solid symbols) and analogue (open symbols) in MIP2 (squares), MIP1 (circles) and MIP3 (triangles). b) Selectivity expressed through the separation factor, averaged over three matrix realizations for MIP3 (triangles), MIP1 (circles) and MIP2 (squares), with the corresponding standard errors.

Adsorbate (either template or analogue) capacity decreases with the increased matrix density as is evidenced in Figure 4.3a. Although MIP3 has lower capacity due to the reduced porosity, this system exhibits significantly higher separation factors reaching more than 7 at the lowest value of the chemical potential shown in figure 4.3b. The opposite behaviour is observed for MIP2, where the selectivity is seen to fall below that of the reference MIP1, which is a higher density system compared to MIP2.

4.1.3. Binding sites characterization

As with MIP1, the analysis was performed of the association states of the template and analogue molecules adsorbed at each point on the isotherm, for MIP2 and MIP3.

This shows evidence that, for MIP3, templates are predominantly adsorbed in type 2 sites for a significant part of the isotherm (Figure 4.4a). Although some analogues also appear to be bound in type 2 sites, the fraction of these is relatively small throughout the isotherm. Also, it is very clear (more so than for MIP1) that the analogue binds predominantly to type 2 sites that did not originate from imprinting.

Figure 4.4 shows that there is a higher proportion of templates bound to high affinity sites, when compared to the analogue, whose behaviour at higher loadings is dominated by molecules not associated with any functional monomers. Thus, higher density leads to proportionally better functionalized porous structure and more pronounced effect of molecular recognition.

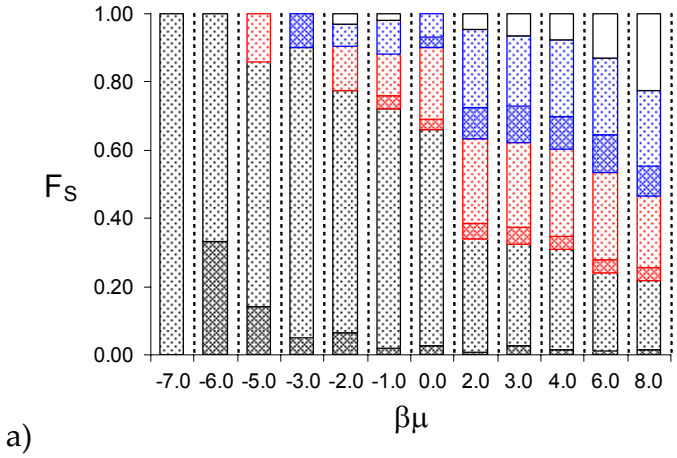

a)

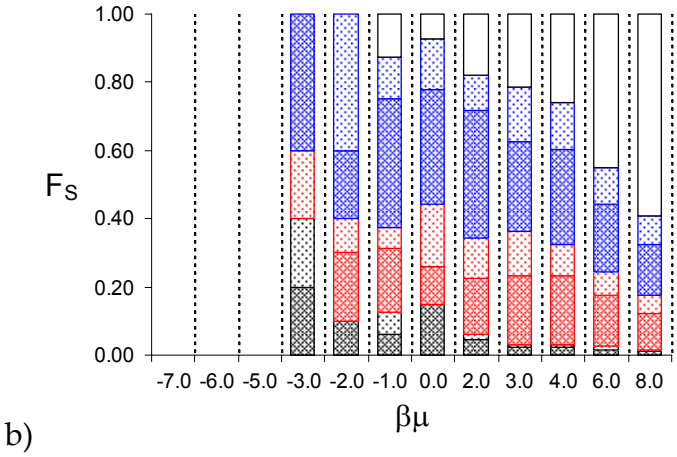

b)

Figure 4.4: Distribution of different association types between adsorbate and functional monomers for template (a) and analogue (b) in MIP3. Type 2 sites are shown in black, type 1_t is shown in red, type 1_c is shown in blue and type 0 sites are represented in white. Lighter shades correspond to molecules located in the imprinted binding sites, whereas darker shades correspond to molecules forming alternative associations of the same type with the matrix. Data is shown for one matrix realization.

Here, as in other figures throughout the thesis, simulations at very low values of chemical potential often led to low adsorbed density (particularly for the analogue) and thus to statistically poor results. Analysis of these points on the adsorption isotherms is omitted from the graphics related to association or binding site distribution analysis.

The behaviour of the less dense MIP2 is somewhat different (see Figure 4.5). Imprinted type 2 sites are still favoured by the template. The matrix is more open, this leads to more imprinted sites being accessible, but also of lower fidelity. Overall, the surface becomes less specific. This shows that having strong interaction patterns, with multiple functional groups associating, provides stronger and more stable binding sites that can be more specific.

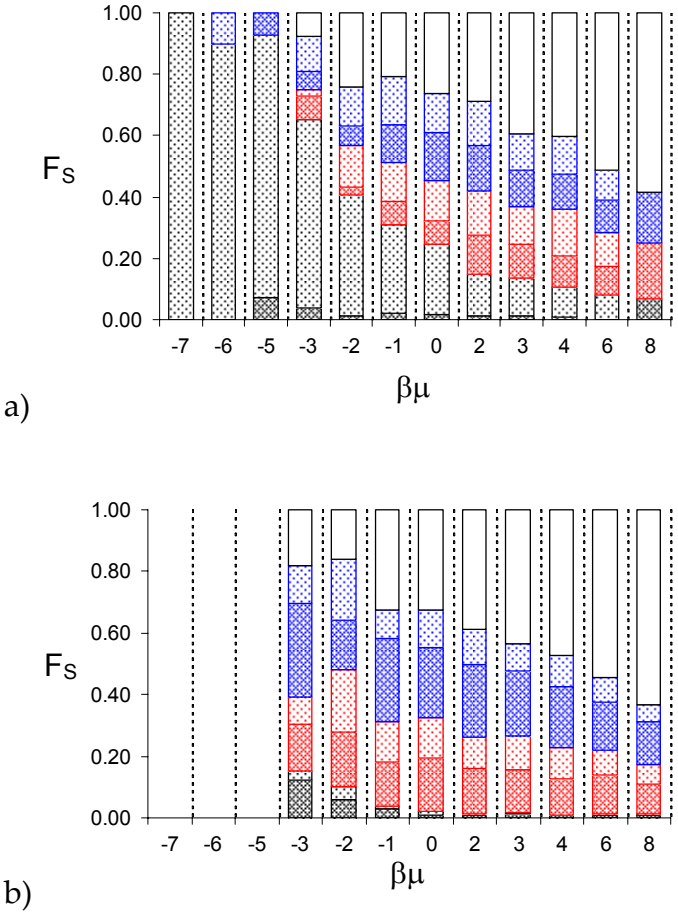

Figure 4.5: Distribution of different association types between adsorbate and functional monomers for template (a) and analogue (b) in MIP2. Type 2 sites are shown in black, type 1_t is shown in red, type 1_c is shown in blue and type 0 sites are represented in white. Lighter shades correspond to molecules located in the imprinted binding sites, whereas darker shades correspond to molecules forming alternative associations of the same type with the matrix.

4.2. Effect of composition

The composition of the pre-polymer mixture affects both the morphology and, very importantly, the chemical equilibrium. Both relative amounts of cross-linker to functional monomer (X:FM ratio) and functional monomer to template (FM:T ratio) are important and are inter-dependent. It has been observed in a number of studies that selectivity of MIPs goes through a maximum as these ratios are varied in a systematic way, exemplified in Figure 4.6 (Spivak 2005).

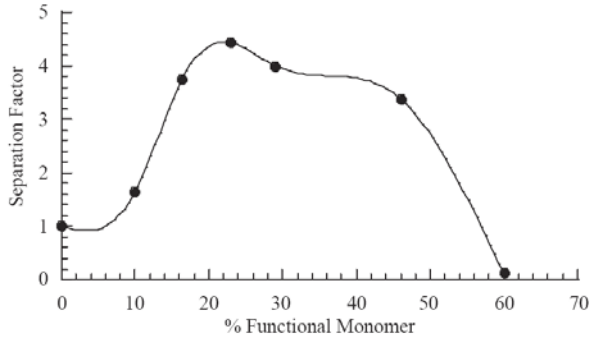

Figure 4.6: L-phenylalanine anilide versus D-phenylalanine anilide separation factor, in L-phenylalanine anilide templated MIPs at various ratios of MAA to EGDMA. Taken from (Spivak 2005).

4.2.1. Model MIP systems of varying composition

To explore the behaviour of our model, the X:FM ratio is varied, creating several systems derived from MIP1. The relative amounts of cross-linker and functional monomer are changed, while maintaining the overall density of the system and the amount of the template constant. We change the number of functional monomers simply by turning some of the cross-linker particles into functional monomers (or vice versa) as required. The reference MIP1 has a 3:1 ratio of cross-linker to functional monomer ($X=N_X$, $FM=N_{FM1}+N_{FM2}$).

Three variations of this ratio are explored. Compared to MIP1, the composition in MIP4 features half the number of functional monomers (X:FM ratio of 7:1), MIP5 has double the number of functional monomers (X:FM ratio of 1:1) and MIP6 has four times the number of functional monomers (X:FM ratio of 0:1). The pre-polymerization mixture of MIP6 consists of functional monomers and templates only, with no cross-linker particles. The details of these model materials are summarized in the table below.

Table 4.4: Composition of the pre-polymerization mixture composition for MIP1, MIP4, MIP5 and MIP6.

MIP	Number of molecules					ρ^*				
	FM1	FM2	T	X	Total	FM1	FM2	T	X	Total
MIP1	400	400	400	2400	3600	0.05	0.05	0.15	0.30	0.55
MIP4	200	200	400	2800		0.025	0.025	0.15	0.35	
MIP5	800	800	400	1600		0.1	0.1	0.15	0.2	
MIP6	1600	1600	400	0		0.2	0.2	0.15	0	

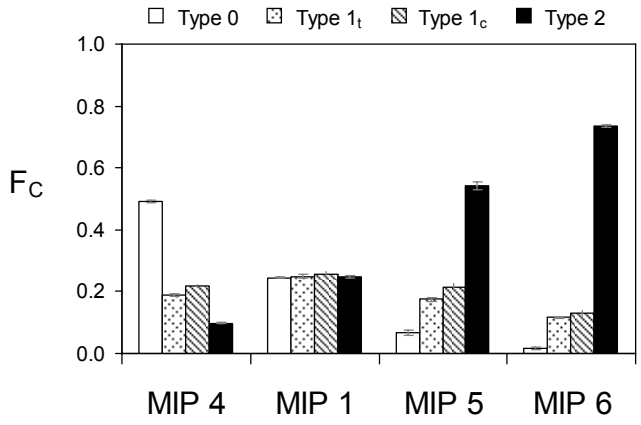

Figure 4.7: Distribution of different complexes between template and functional monomers in the final pre-polymerization configuration, with the corresponding standard errors (obtained from three independent realizations), for MIP1, 4, 5 and 6.

The equilibrium is shifted in the expected manner, with the excess of functional monomers substantially increasing the number of type 2 complexes. In MIP6, for example, almost 80% of template molecules are in type 2 complexes in the pre-polymerization mixture. Initially this is achieved at the expense of type 0 complexes and later of the less specific type 1 complexes. From what has been observed, these distributions should be reflected in the resulting MIPs selectivities, which have increased with higher fractions of type 2 sites.

Analysing the apparent porosities of these MIPs, there is an indication that changing the composition has affected the porosity of the material, although not by a large factor (less than 2 fold). The MIP systems in Table 4.5 are presented in increasing ratio of FM:T. The higher this ratio is, the higher the number of associations that are created between the components of the system. This in turn increases local density around the template, and consequently, around the resulting binding site. For this reason, the apparent porosity is decreased. A consequence of the increased local density would also be that the binding sites are more specific, though only slightly.

Table 4.5: Apparent porosity, defined as fraction of the system's volume, accessible to the probe in Figure 4.2, of MIPs 1 and 4 to 6 (averaged over 3 matrix realizations), with respective standard errors.

MIP4	$4.16\times10^{-3} \pm 2.15\times10^{-5}$
MIP1	$3.62\times10^{-3} \pm 2.00\times10^{-5}$
MIP5	$2.80\times10^{-3} \pm 1.76\times10^{-5}$
MIP6	$2.48\times10^{-3} \pm 1.66\times10^{-5}$

4.2.2. Adsorption in model MIPs of various compositions

By performing again the adsorption of template and analogue in the matrices created for these MIPs, one can attempt to establish a link between association complex distributions shown in Figure 4.7 and the resulting adsorption phenomena. For the following 3 figures, the full isotherm was studied for one realization, and is presented for illustrative purposes. The study of the selectivity is made for 3 matrix realizations at the region of interest (lower chemical potentials, higher selectivities).

First, we compare adsorption isotherms in MIP1 and MIP4 materials (Figure 4.8). From this data one can see that, for MIP4, the adsorbed density of the template is reduced. This is to be expected, since less functional monomers are present, and the surface has lower overall affinity.

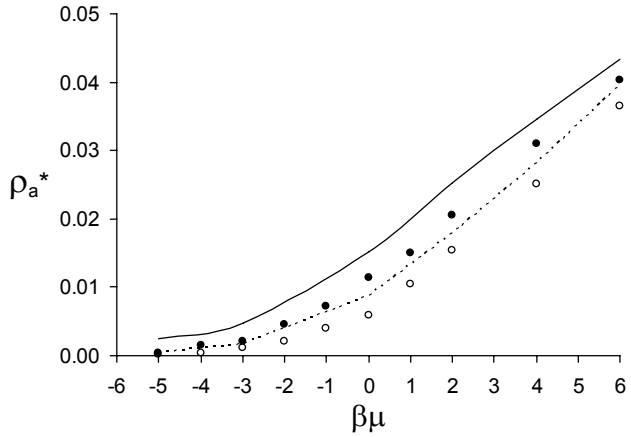

Figure 4.8: Adsorption isotherms for MIP1 (template: solid line, analogue: dashed line) and MIP4 (one realization, template: solid circles, analogue: open circles).

For MIP5, formed with double the number of functional monomers compared to MIP1, it is clear that the uptake of adsorbate is increased relative to MIP1 (Figure 4.9).

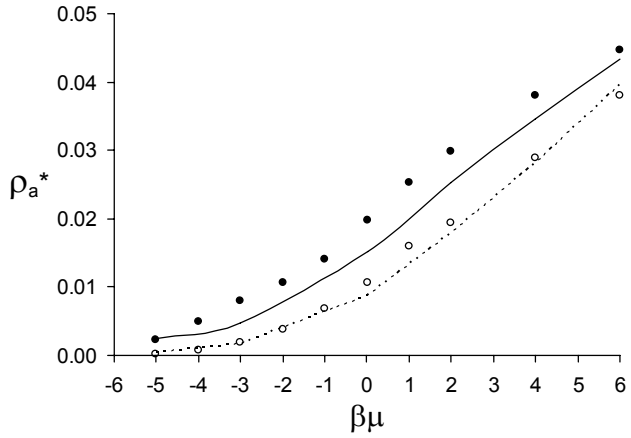

Figure 4.9: Adsorption isotherms for MIP1 (template: solid line, analogue: dashed line) and MIP5 (one matrix realization, template: solid circles, analogue: open circles).

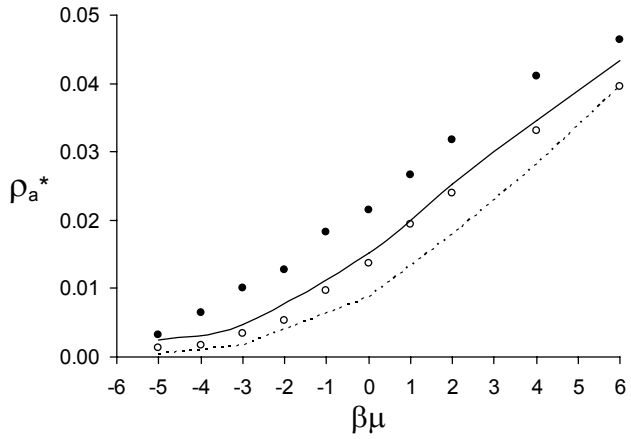

Figure 4.10: Adsorption isotherms for MIP1 (template: solid line, analogue: dashed line) and MIP6 (one matrix realization, template: solid circles, analogue: open circles).

Comparing MIP6 and MIP5 (see Figures 4.9 and 4.10) one can see some further increase in the adsorbate density but not a significant change.

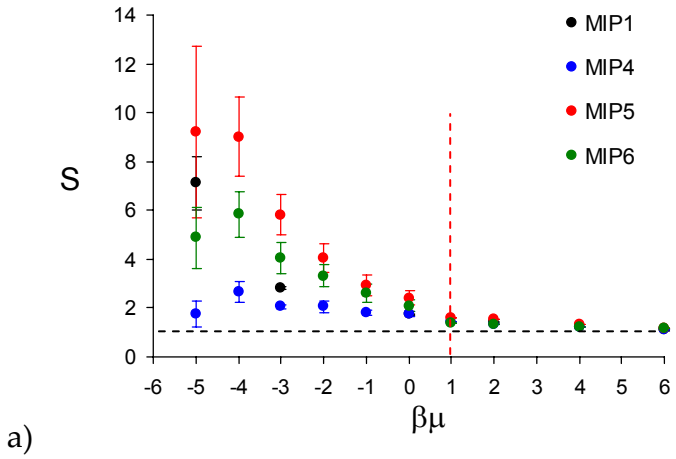

a)

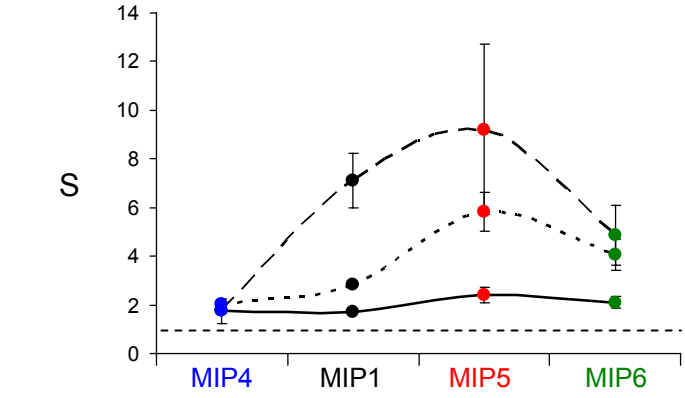

b)

Figure 4.11: a) Selectivity and associated standard error for MIP1, 4, 5 and 6 (the data points to the left of the red line are averaged over 3 matrix realizations). b) Selectivity sampled from 3 points on the isotherms: βμ = 0.0 (solid line), βμ = -3.0 (dashed line), βμ = -5.0 (broad-dash line).

A more convincing and intuitive way to assess the performance of various model materials is to compare their selectivities, defined throughout the thesis as the amount of template divided by the amount of analogue adsorbed at the same chemical potential. From Figure 4.11 it is clear that

MIP5, with an X:FM ratio of 1:1, and double the number of functional monomers (compared to MIP1) is the most selective MIP. We also observed from Figure 4.11b that as we decrease the X:FM ratio, from very high values to 0 (left to right in the figure) the selectivity goes through a maximum. This behaviour is particularly pronounced at the lower values of the chemical potential where adsorption takes place predominantly in very selective binding sites.

At first this observation seems odd, considering the results displayed in Figure 4.7. It is however in agreement with the experimental observations, exemplified in Figure 4.6 (Spivak 2005). The following picture has been proposed in order to explain these trends. At low concentration of monomers, there are simply not enough of them to form highly specific complexes with all the available templates. At the other extreme however, the excess of functional monomers leads to a different situation. Most template molecules have all the functional groups associated with the functional monomers. In addition to these, there are additional excess monomers not associated with any template. Upon polymerization, these free monomers become a part of the polymer structure inducing non-specific binding. This is why the selectivity goes through a maximum and diminishes for MIP6. This is further demonstrated in the binding site distribution analysis.

4.2.3. Binding sites distribution analysis for model MIPs of varying porosity

Here, the tools developed for the binding site characterization in Chapter 3 and 4, are applied to further highlight the differences between model materials MIP1, 4, 5, and 6.

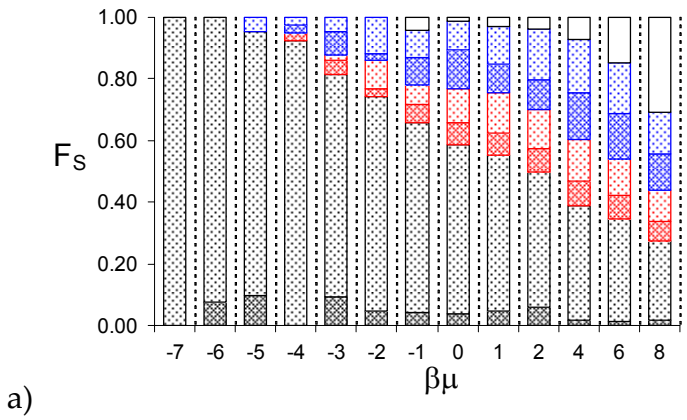

a)

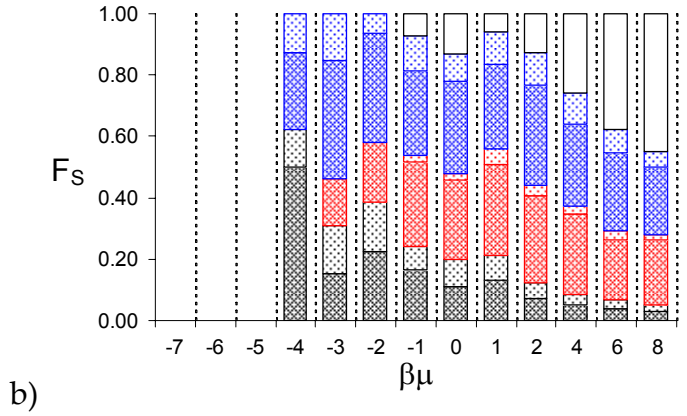

b)

Figure 4.12: Distribution of binding sites for MIP5, for adsorbed template (a) and adsorbed analogue (b). Type 2 sites are shown in black, type 1_t are shown in red, type 1_c sites are shown in blue and state 0 sites are represented in white, respectively. Lighter shades correspond to molecules located in the imprinted binding sites, whereas darker shades correspond to molecules forming alternative associations of the same type with the matrix.

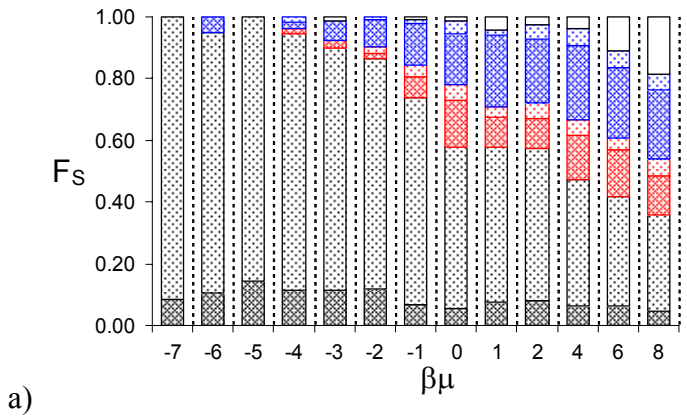

a)

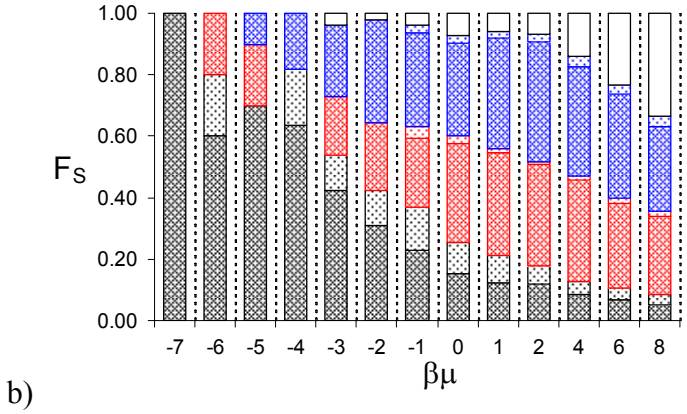

b)

Figure 4.13: Distribution of binding sites for MIP6, for adsorbed template (a) and adsorbed analogue (b). Type 2 sites are shown in black, type 1_t are shown in red, type 1_c sites are shown in blue and type 0 sites are represented in white, respectively. Lighter shades correspond to molecules located in the imprinted binding sites, whereas darker shades correspond to molecules forming alternative associations of the same type with the matrix.

It is clear, taking into account the behaviour seen in Figure 4.11 and comparing the binding sites distributions seen in Figures 3.6, 4.12 and 4.13, that the excess of functional monomers reduces the relative contribution of the imprinted sites to the adsorption behaviour. The extra functional monomers originate new, non-specific sites that compete with imprinted

ones. Naturally, there are more binding scenarios possible, with the analogue now allowed to bind to a large number of type 2 sites. Therefore, overall the surface becomes less selective with the excess functional monomers.

4.3. Theoretical model of chemical equilibria in MIPs

Findings in this chapter can be linked to a theoretical study of pre-polymerization association processes of Whitcombe and co-workers (Whitcombe *et al.* 1998). In their work, a chemical equilibrium between a template T which associates with equal affinity and independently to two equal functional monomers, M, is considered:

$$M + T \underset{K_1}{\Leftrightarrow} MT \qquad \text{IV.1}$$

$$MT + M \underset{K_2}{\Leftrightarrow} MTM \qquad \text{IV.2}$$

In this system, the equilibrium concentration of various complexes can be described by:

$$[MT] = K_1[M][T] \qquad \text{IV.3}$$

$$[MTM] = K_2[M][MT] \qquad \text{IV.4}$$

By substituting equation IV.3 in IV.4, if reaction IV.1 and IV.2 are considered to be independent, then $K = K_1 = K_2$, and the concentration of the fully coordinated complex can be described as:

$$[MTM] = K^2[M]^2[T] \qquad \text{IV.5}$$

This model allows one to investigate how the concentration of various complexes depends on the initial composition of the pre-polymerization mixture and on the equilibrium constant of template-monomer association reaction. In particular, two properties are important. [MTM] can be seen as

the total concentration of precursors for "well imprinted" sites, while [MTM]/{[M]+[MT]} is the ratio of "good" and "bad" sites, in the terminology of the authors, and should reflect the overall selectivity of the polymer. Indeed, according to the model, the first property increases with the equilibrium constant and degree of the monomer excess, whereas the second property goes through the maximum as a function of the monomer concentration, similar to Figure 4.11b.

The system studied in chapter 3 and variations of it explored in the present chapter closely resemble this theoretical system, if one treats the two kinds of functional monomers in our work as a single species [FM1]+[FM2]=[FM]. By taking the same assumption that the reactions of associations with the template are independent and equal to each other, the behaviour observed in our simulations should be described by the model presented by Whitcombe and co-workers.

Figure 4.14 shows that the results of the model of Whitcombe *et al.* with the equilibrium constant $K = 10M^{-1}$ and an initial template concentration $[T_0] = 0.1M$ can be compared to the MIP systems under study. In the study of Whitcombe and co-workers, as in these results, the equilibrium concentrations were determined numerically to minimize the difference between target and calculated values of K, wherein $K_1 \neq K_2$. It is clear the model predicts fairly well the equilibrium distribution of complexes in MIPs 1 to 6.

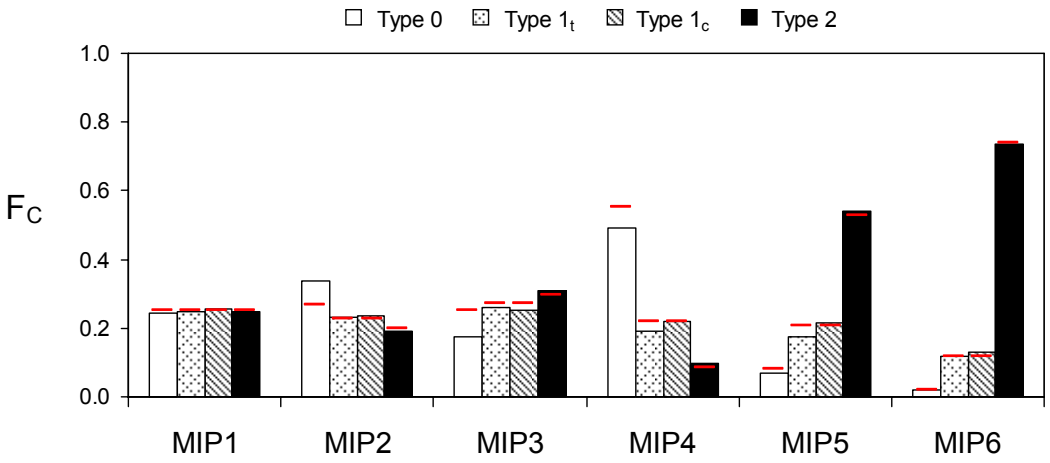

Figure 4.14: Distribution of different association types between the template and functional monomers, for various MIP systems. F_C indicates the fraction of complexes of a given type. Red lines indicate the same site type fraction calculated using the model of Whitcombe and co-workers (Whitcombe *et al.* 1998).

At the same time, the equilibrium in the MIP systems considered in this work is in fact more complex than that described by equation IV.1 through IV.5. There are two non-interchangeable functional monomers, which associate with the template to produce different complexes: type 1_t and 1_c (see Figure 3.1). Using data on ensemble average concentrations of the various species found in the pre-polymerization mixture, the association constants equivalent to K_1 and K_2 were calculated for the various systems. The results are reported in Table 4.6. The systems modelled are dimensionless, therefore $K_x \times 1/V$ is used.

Table 4.6: Values for K_1, K_2 and K (the association constant for [MTM] or type 2 complexes) for the different MIP systems considered.

$[M_0]/[T_0]$	MIP	$K_1 \times 1/V$ $\times 10^{20}$ mol^{-1}	$K_2 \times 1/V$ $\times 10^{20}$ mol^{-1}	$K \times 1/V$ $\times 10^{20}$ mol^{-1}
2	MIP1	31.24	7.40	15.21
2	MIP2	24.22	7.18	13.18
2	MIP3	40.36	8.43	18.44
1	MIP4	31.92	9.18	17.12
4	MIP5	34.57	8.22	16.87
8	MIP6	32.24	7.14	15.17

Table 4.6 shows that, with some variations, the association constants are consistent, for the systems of equal total density. However the assumption $K=K_1=K_2$ does not hold which helps clarify that the association reactions IV.1 and IV.2 are not independent. As expected, the results show that the formation of type 1 and 2 complexes cannot be considered as independent and equivalent processes with equal association constants. This shows that access to an available functional group of the template does depend on the association status.

To summarize, the key value of the theoretical model of Whitcombe and co-workers is that it provides a quick, analytical insight onto the formation of high quality complexes, as a function of the initial composition of the species. However, adsorption processes (including adsorption of analogues) is left outside of the scope of this model, as well as any information on the structural details of the complexes, the resulting binding sites and possible non-specific binding. These issues are tackled efficiently within the molecular simulation approach employed here.

4.4. Effect of expansion

The binding sites require the contribution of steric effects or geometric complementarity to achieve molecular recognition. As is confirmed in this work, the distribution of binding sites is heterogeneous in nature, is affected by the pre-polymerization equilibrium and can be linked to the structural qualities of the matrix surrounding the template. In addition to this, prior to, during and after polymerization, binding sites can be degenerated and their distribution is further perturbed. An example of this is swelling in MIPs. Swelling can occur for a number of reasons, such as temperature or pH variations, water or solvent intake, and these effects will be even more noticeable in imprinted hydrogels (Kim *et al.* 1992). This results in a loss of specificity of the binding sites and of the porous surface, consequently there is a reduction of the recognition effect in a MIP (Farrington and Regan 2007). Thus, this is an important effect that we chose to study using the proposed simplified model of MIPs.

4.4.1. Expanded polymer matrix

Of the several interactions responsible for molecular recognition, the establishment of hydrogen bonds and orientation of polar groups play a key role in creating a specific pattern of interaction. Swelling not only disrupts the shape of the binding site, but also this interaction pattern. With the disruption of this pattern, one can expect a change in the affinity and specificity which should reveal itself in the adsorption studies. The present model, although accounting only for the orientated hydrogen bond-like interactions, should present the same behaviour. Thus, within this model, it

should be possible to study adsorption behaviour in MIPs with varying porosity and binding site degeneration.

To model expansion of a model MIP, we adopted an approach traditionally employed in the studies of disordered quenched models of porous materials, where the size of the matrix particles (and other species) is simply scaled down (Figure 4.15). This captures the disruptive effect of swelling on the structure of the binding sites. It also captures the increased porosity of the material, which leads to higher capacity. This model of expansion is, of course, very crude since it operates on the particles not connected by chemical bonds to each other and omits several other important effects, but it will serve as a reasonable starting point given the type of the model adopted.

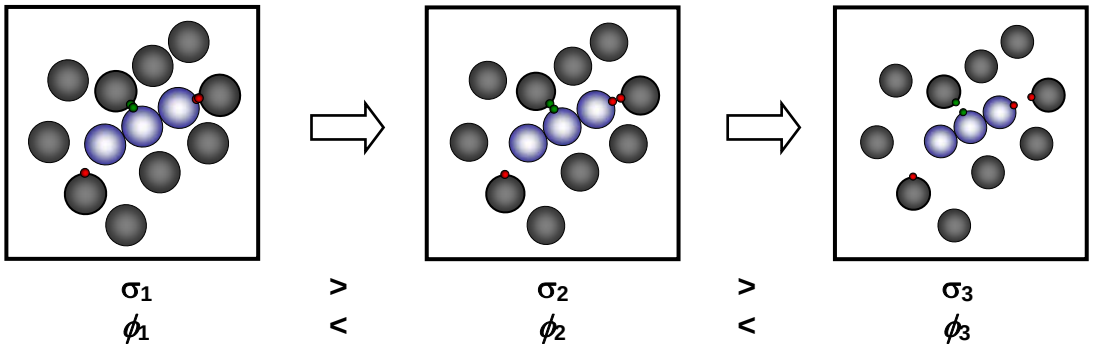

Figure 4.15: Schematic depiction of the expansion protocol. Systems 1, 2 and 3 have decreasing volume occupied by the molecules, and increasing porosity, ϕ. The volume of the system simulated is kept constant.

To explore the effect of swelling, MIP5, which presented the highest selectivity in the previous studies, is expanded to different extents. Four variations of a matrix of MIP5 were created: 5%, 10%, 20% and 40% equivalent volume expansion.

The volume does not actual expand, but rather, the sizes of the particles are decreased so that the variation in volume fraction occupied by the atoms is equivalent to an expansion in volume. New values of σ are then defined as:

$$\sigma_{new} = \left(\frac{1}{\frac{\Delta V}{V} + 1} \right)^{1/3} \sigma_{old} \qquad \text{IV.6}$$

where ΔV/V is the fraction of expansion.

Table 4.7: Apparent porosity, defined as a fraction of the system volume, accessible to the probe in Figure 4.2, for MIP5 and modified MIP5 systems resulting from the expansion, with respective standard errors. The left column shows the expansion as a percentage of the original volume of MIP5 system.

0% (MIP5)	$2.86\times10^{-3} \pm 3.07\times10^{-5}$
5%	$3.88\times10^{-3} \pm 3.59\times10^{-5}$
10%	$5.05\times10^{-3} \pm 4.09\times10^{-5}$
20%	$8.14\times10^{-3} \pm 5.19\times10^{-5}$
40%	$1.67\times10^{-2} \pm 7.40\times10^{-5}$

Table 4.7 summarises the porosities of the model materials as a function of the expansion extent. As expected, porosity increases with "expansion". It is also to be expected that the characteristics of the porous surface must change, not only concerning the binding sites, but also in terms of the surface density of functional monomers (and their binding points). Let us examine how these morphological changes manifest themselves in adsorption studies.

4.4.2. Adsorption in “expanded” MIP structures

Adsorption simulations reveal that selectivity drops as expansion increases, clearly depicted in Figure 4.16. This is the expected behaviour. However, what is interesting about this trend in the separation factor is that it happens in an apparently smooth fashion without any sudden or discrete transitions. This must be a reflection of averaging the behaviour of the material over binding sites of different types. Another notable observation is that even at 40% expansion, the expanded materials still exhibit some selectivity. The consistency between these curves gives credence to these observations. However, they must be taken as broad qualitative results and one must remain careful about the magnitude of these effects as these are results for one matrix realization only.

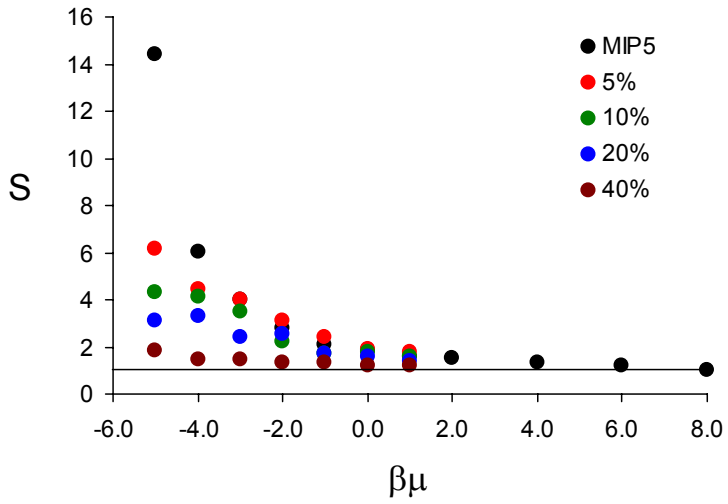

Figure 4.16: Selectivity for the original MIP5 matrix (0% expansion), compared to that for the matrices resulting from 5, 10, 20 and 40% expansion. Solid black line indicates S = 1, corresponding to no selectivity. Data is shown for one matrix realization.

4.4.3. Binding site analysis in the expanded matrices

The analysis of the associations made by adsorbing template and analogue helps to elucidate the points discussed. Comparing the binding site distributions for MIP5 (see Figure 4.12) and that for the matrix resulting from 5% expansion, we see that for the template the profiles are very similar, with a slight drop in type 2 sites at the very low values of the chemical potential. However, the analogue profiles are more distinct. Specifically, it is evident that in the expanded matrix, a higher percentage of analogue molecules bind to type 2 sites. This would explain the drop in selectivity at very low chemical potentials. Apparently, even with this small expansion, some steric restrictions are removed and therefore binding for the analogue becomes possible in a wider range of sites, including the imprinted ones.

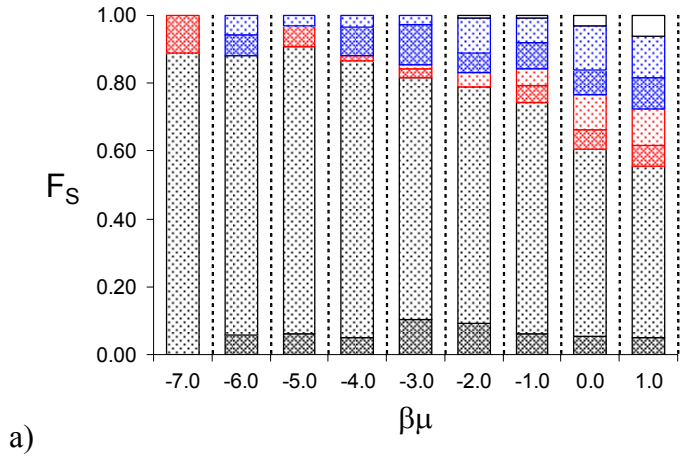

a)

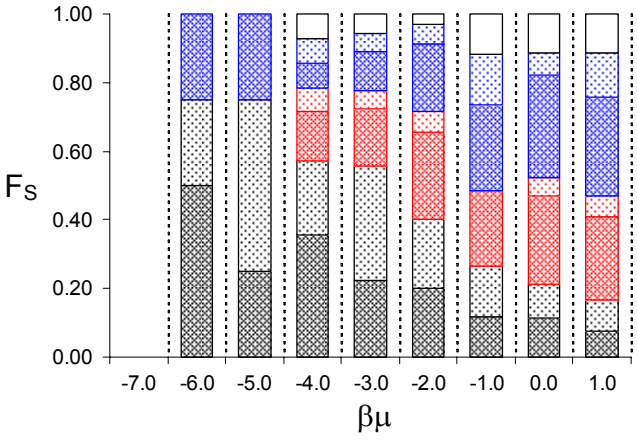

b)

Figure 4.17: Distribution of binding sites for 5% expansion of MIP5, for adsorbed template (a) and analogue (b). Type 2 sites shown in black, type 1_t sites are shown in red, type 1_c sites are shown in blue and type 0 sites are represented in white. Lighter shades correspond to molecules located in the imprinted binding sites, whereas darker shades correspond to molecules forming alternative associations of the same type with the matrix. Data is shown for one matrix realization.

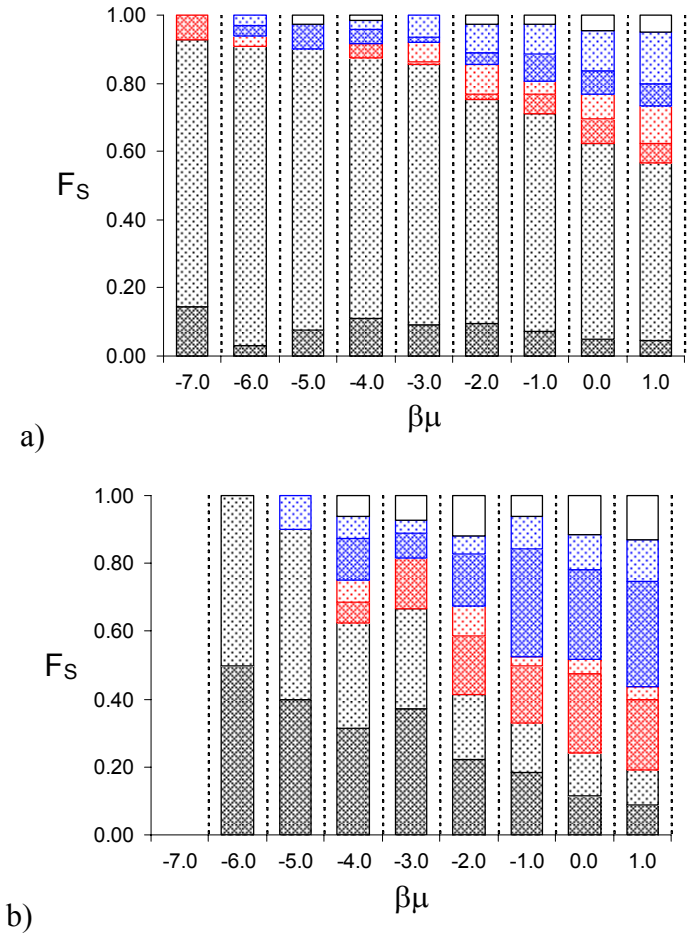

Figure 4.18: Distribution of binding sites for 10% expansion of MIP5, for adsorbed template (a) and analogue (b). Type 2 sites shown in black, type 1_t sites are shown in red, type 1_c sites are shown in blue and type 0 sites are represented in white. Lighter shades correspond to molecules located in the imprinted binding sites, whereas darker shades correspond to molecules forming alternative associations of the same type with the matrix. Data is shown for one matrix realization.

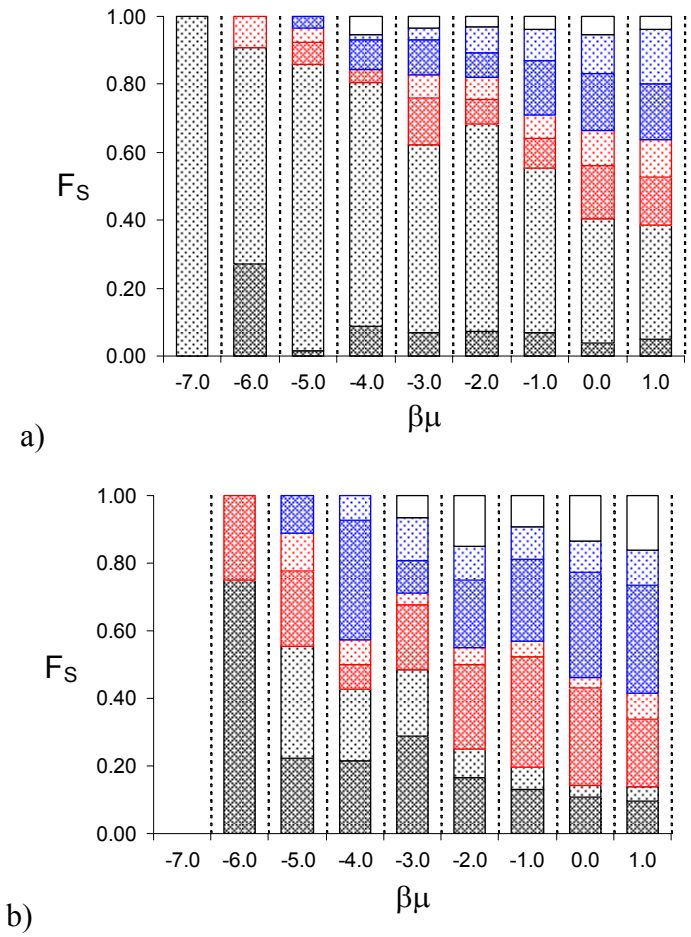

Figure 4.19: Distribution of binding sites for 20% expansion of MIP5, for adsorbed template (a) and analogue (b). Type 2 sites shown in black, type 1_t sites are shown in red, type 1_c sites are shown in blue and type 0 sites are represented in white. Lighter shades correspond to molecules located in the imprinted binding sites, whereas darker shades correspond to molecules forming alternative associations of the same type with the matrix. Data is shown for one matrix realization.

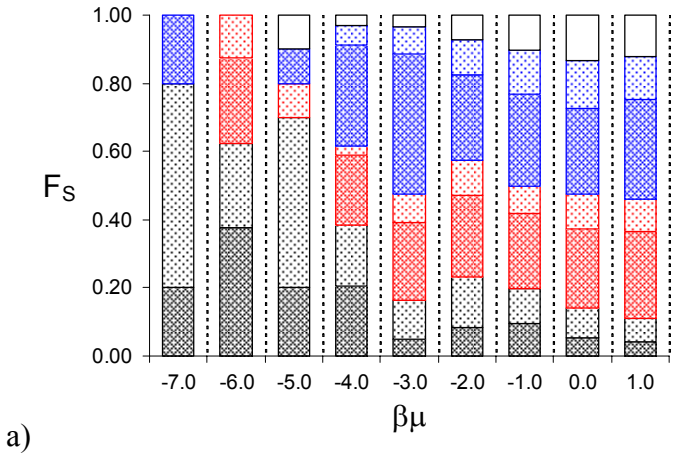

a)

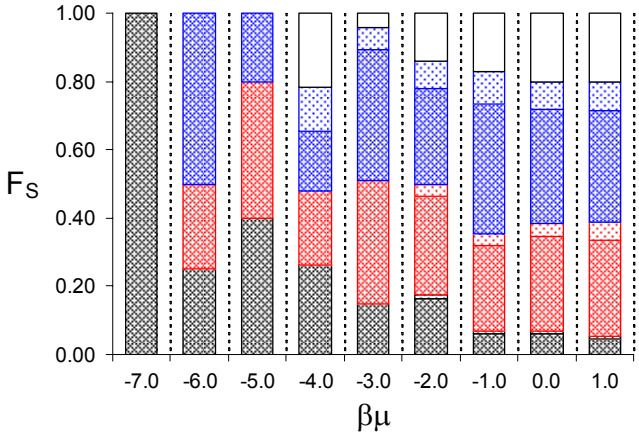

b)

Figure 4.20: Distribution of binding sites for 40% expansion of MIP5, for adsorbed template (a) and adsorbed analogue (b). Type 2 sites shown in black, type 1_t sites are shown in red, type 1_c sites are shown in blue and type 0 sites are represented in white. Lighter shades correspond to molecules located in the imprinted binding sites, whereas darker shades correspond to molecules forming alternative associations of the same type with the matrix. Data is shown for one matrix realization.

As the expansion level increases, it becomes clear that for the analogue species, new binding sites (*i.e.* sites that did not originate from the complexes in the pre-polymerization mixture) are increasingly favoured versus the imprinted binding sites. Expansion literally opens new opportunities for the analogue to bind, since it disrupts so greatly the complementarity of the sites.

In addition, some functional monomers, inaccessible in the original material become accessible upon expansion. For the case of the template, binding in the imprinted sites remains dominant up to 20% expansion. However, molecules bound to new type 1 sites start to play an important role at 20% expansion. At 40%, the binding in type 1 sites occurs mostly in new sites of this type, due again to the increased accessibility of the free functional monomers on the surface. Type 2 sites are more specific and impose certain geometrical restrictions; such an arrangement does not become readily available in the matrix, despite the expansion reaching high levels.

We can explicitly assess how many molecules actually *re-bind* to the type 2 binding sites that originate from the pre-polymerization mixture. This way, one can assess if expansion has improved access to imprinted type 2 sites. This analysis is provided below.

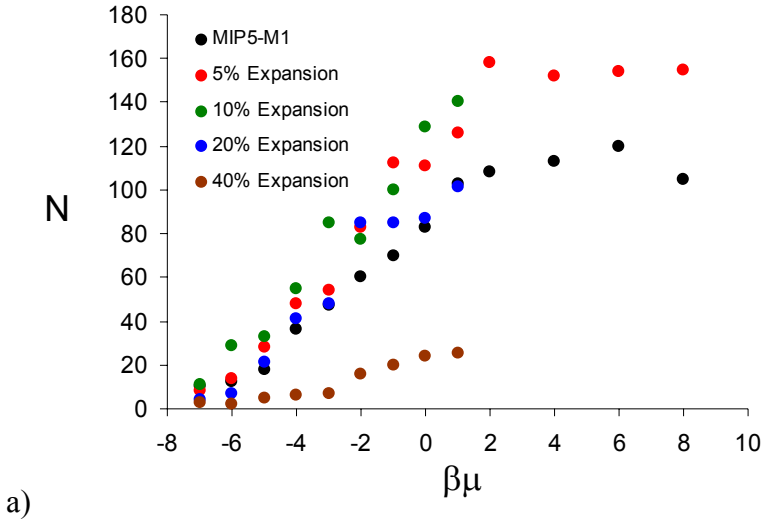

a)

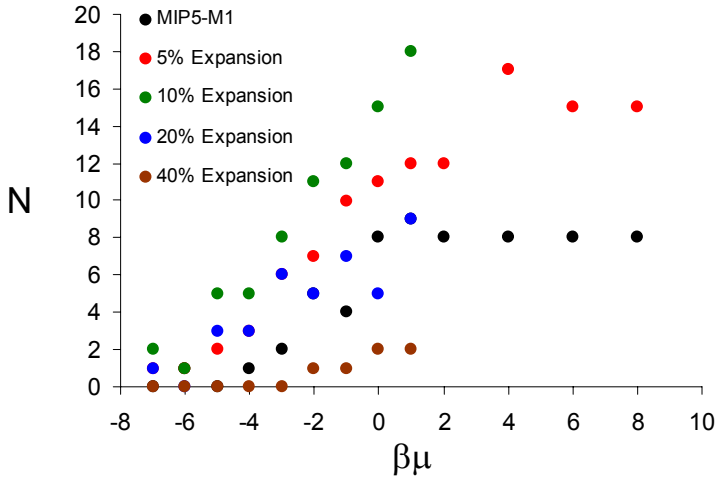

b)

Figure 4.21: Number of template (a) and analogue (b) molecules binding to type 2 binding sites formed by the imprinting process. Data shown for one realization of MIP5 system and expanded systems based on it.

In Figure 4.21, the amount of templates molecules found in imprinted type 2 binding sites is plotted as a function of chemical potential. For the systems under study, one can compare absolute values which results in a better direct evaluation of the effect of expansion. From Figure 4.21 it is evident that as expansion proceeds to 5 and then to 10%, both template and analogue are able to access a higher number of imprinted binding sites. At 20%, this number then drops, close to the values of the original matrix MIP5,

presumably because the original binding sites are now extremely expanded, leading to a large deformation of the interaction pattern within it, the result of which is that only a few sites still allow the double association with the template. This further drops dramatically at 40% expansion. In general, the effects associated with expansion are stronger for the analogue than for the template, *e.g.* at $\beta\mu = 0.0$ and 10% expansion the number of analogue molecules in type 2 sites nearly doubles compared to the original matrix MIP5 while for the template there is only a 60% increase. This indicates that there are two competing phenomena. On one hand, higher loadings of the template are possible due to lower steric restrictions and higher porosity. On the other hand, at a certain level of expansion, selectivity of binding sites starts to diminish due to the loss of geometric compatibility to the template.

4.5. Summary

In this chapter the molecular recognition behaviour in the proposed model is explored as a function of parameters of the system, and modifications of the porous morphology. The model exhibits higher selectivity for MIPs at higher density of the matrix, and this is attributed to higher binding site specificity as well as higher surface functionalization (in other words higher effective concentration of the monomers on the surface). Furthermore, molecular recognition was investigated as a function of pre-polymerization mixture composition. The model reproduces the experimentally observed trend in selectivity as a function of cross-linker to functional monomer ratio, with a maximum corresponding to a particular intermediate concentration of functional monomers. Using a simple molecular model, this behaviour is

explained based on the argument that in the low concentration of functional monomers regime, simply not enough specific binding sites form. With the excess of functional monomers the surface of the material becomes essentially non-specific. In between those two extremes an optimal composition of the pre-polymerization mixture exists.

A matrix was expanded to simulate MIP swelling and the results show the expected drop in selectivity. The analysis of the types of binding sites provides insights into different competing phenomena resulting from the matrix expansion. There is a loss of selectivity of the surface overall, due to higher number of non-specific sites being occupied by the template. One also discovers, however, that expansion may actually open (provide access) to some high affinity sites, previously inaccessible. This observation is useful in designing stimuli responsive MIPs. Previous studies have looked at the loading and release performance of MIPs under swelling, *e.g.* (Kim *et al.* 1992). This thesis presents the first study into the phenomenon of swelling in MIPs that analyzes possible effects at the scale of the binding sites, and provides clear evidence to suggest a mechanism for the observed adsorption behaviour.

4.6. References

Farrington, K. and F. Regan (2007). "Investigation of the nature of MIP recognition: The development and characterisation of a MIP for Ibuprofen." Biosensors & Bioelectronics **22**(6): 1138-1146.

Kim, S. W., Y. H. Bae, et al. (1992). "Hydrogels: Swelling, Drug Loading, and Release." Pharmaceutical Research **9**(3): 283-290.

Spivak, D. A. (2005). "Optimization, evaluation, and characterization of molecularly imprinted polymers." Advanced Drug Delivery Reviews **57**(12): 1779-1794.

Srebnik, S. and O. Lev (2002). "Toward establishing criteria for polymer imprinting using mean-field theory." Journal of Chemical Physics **116**(24): 10967-10972.

Whitcombe, M. J. *et al*. (1998). "Predicting the selectivity of imprinted polymers." Chromatographia **47**(7-8): 457-464.

Wulff, G., R. Kemmerer, et al. (1982). "Chirality of Vinyl-Polymers - the Preparation of Chiral Cavities in Synthetic-Polymers." Nouveau Journal De Chimie-New Journal of Chemistry **6**(12): 681-687.

5.

Alternative synthetic protocols for model MIP studies

In chapters 3 and 4, we proposed a simple model of imprinted polymers able to mimic molecular recognition behaviour. Within this model, it was possible to reproduce several known experimental observations for MIP behaviour, as well as to explain the underlying molecular mechanisms. In this chapter, the potential of the model is explored as a tool to predict and understand the behaviour of MIPs, as a function of synthetic protocols or post-synthesis modifications.

Two hypothetical synthetic protocols are of special interest: polymers templated with a species other than the target adsorbate and MIP post-

synthetic surface modification by removal of non-specific binding sites. Let us elaborate on why these two protocols are of interest.

In several applications one is interested in developing a MIP with molecular recognition towards some specific target. However, that target molecule need not be used as the template, sometimes it cannot be used or should not be used. An example of this approach is in molecularly imprinted catalysts. Ideally, a material imprinted with the transition state of a reaction of interest would provide a good catalyst. Since the transition state itself can not be directly used as the template because of its instability, a transition state *analogue*, very similar to the transition state, is generally employed instead. The binding sites produced are still molecularly complementary to the transition state and therefore promote a conversion from the reactant to the transition state, acting as artificial enzymes. This concept was first studied by Robinson and Mosbach (Robinson and Mosbach 1989). Another example of using an alternative template would be for the case of hazardous template species, where the use of a harmless species featuring similar structure provides a safer synthesis option.

In this study the use of alternative template (AT) is explored to address the issue of binding site accessibility. It has been discussed in several studies that during MIP synthesis some of the template molecules can be trapped inside inaccessible binding sites, or high quality binding sites become inaccessible for some other reason. It would be important to propose a route to improve accessibility of the binding sites in the MIP porous structure while retaining as much as possible its molecular recognition function. Such a route based on the alternative templates will be proposed and discussed on this chapter.

The heterogeneity of the binding site population in a MIP has been well recorded since the early studies in the area (Vlatakis *et al.* 1993) and its adverse effect on the applicability of MIPs is well known (Ramstrom and Ansell 1998). It has therefore been subject of many characterization and optimization studies (Umpleby *et al.* 2000; Umpleby *et al.* 2004; Yungerman and Srebnik 2006; Garcia-Calzon and Diaz-Garcia 2007). A synthetic protocol that could treat the surface in a way that reduces heterogeneity would be a great improvement in the field. The consequences of such a hypothetical protocol are studied here.

5.1. Alternative templates as means to control morphology of MIP materials

The idea of using an imprinting agent other than the target molecule has been proposed by Whitcombe and co-workers in a hybrid semi-covalent imprinting approach (Whitcombe *et al.* 1995). Their study revealed that very good recognition could be obtained from the MIP, but there is no insight on the effects of the spacer on morphology or accessibility of the binding sites. The strategy proposed here is the use of an alternative template as a means to increase binding site accessibility in the system, without loss of recognition towards the target molecule. To achieve this, the idea is to use a template consisting of two functional fragments. The first fragment features the interaction patterns of the target molecule (and is responsible for imprinting the actual binding sites. The purpose of the second fragment is to create pores, or voids, in the vicinity of binding sites. We study this concept here in

its simplest implementation and test, first of all, if such an alternative protocol leads to a significant loss of molecular recognition.

5.1.1. Polymer matrix analysis

The starting point of this analysis is again the system of species described in Chapter 3, Figure 3.1. We aim to design an alternative template molecule which could be used to prepare a model MIP with molecular recognition functionality towards the original template, or target molecule, but also with much more porous and open morphology. The simplest way to implement this idea is to keep the same structural motif of two functional groups (FG1 and FG2), but make the remaining fragment of the molecule (the terminal hard sphere featuring no surface association sites) much bulkier. This is schematically depicted in Figure 5.1 for the case when the size of the terminal site of the molecule is twice the original ($\sigma_{new} = 2.0\sigma$). In the following presentation of results and discussion, this species will be called Alternative Template (AT).

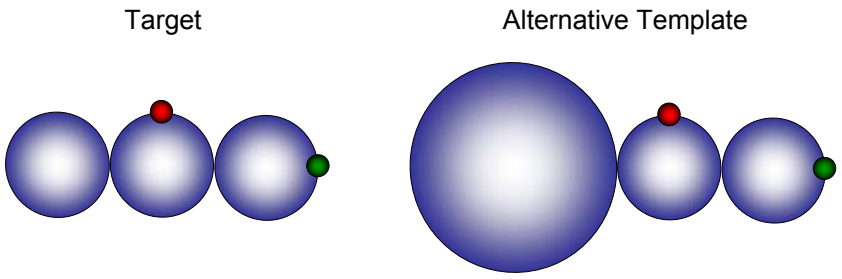

Figure 5.1: Representation of the target molecule (species template – T defined in chapter 3) and the alternative template (species AT).

A MIP system is created, based on the composition and density of MIP1, but using AT as the template. Because the alternative template AT has a different

volume than that of the original template, T, the simulation box is adjusted to maintain the same overall volume fraction of the mixture. The reason for this is to remove the effect of density, thus isolating the effect of the morphological differences of T and AT. Volume fraction of the mixture (η_v) for systems *i* and *j* is:

$$\eta_V = \frac{V_{MIP_i}}{L^3_{MIP_i}} = \frac{V_{MIP_j}}{L^3_{MIP_j}} \qquad \text{V.1}$$

where V stands for the volume occupied by all the hard-sphere particles in the MIP systems. The side of the box for the new system MIP7 can thus be related to the parameters of the reference system MIP1 using:

$$L_{MIP7} = \left(\frac{V_{MIP7}}{V_{MIP1}} L^3_{MIP1} \right)^{1/3} \qquad \text{V.2}$$

The ratio of the sum of the volumes of all the particles reduces to the ratio of the equivalent number of particles of radius σ. Given that the volume of the AT is equivalent to 10 particles of radius σ $\{V_{AT} = \pi/6[(2\sigma)^3+\sigma^3+\sigma^3]\}$, this results in:

$$\frac{V_{MIP7}}{V_{MIP1}} = \frac{\left(N_X + N_{FM1} + N_{FM2} + 10 \cdot N_{AT}\right)}{\left(N_X + N_{FM1} + N_{FM2} + 3 \cdot N_T\right)} = 1.6364 \qquad \text{V.3}$$

This means MIP7 will have a cubic simulation box with side $L = 23.56803 \times \sigma$. The resulting equilibrated matrix was analysed to determine the distribution of complexes.

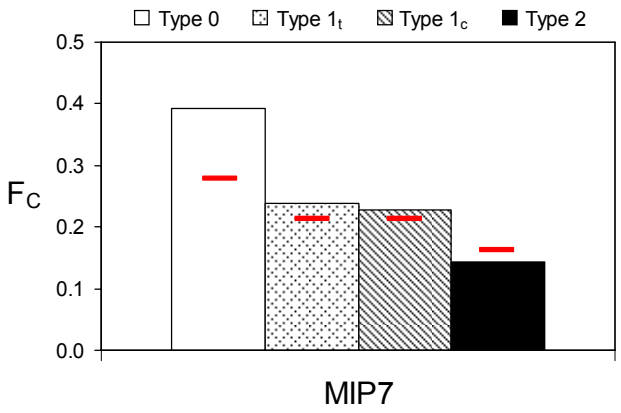

Figure 5.2: Distribution of different association types between the alternative template and functional monomers, for MIP7. F_C indicates the fraction of complexes of a given type. Data is shown for one matrix realization. Red lines indicate the same site type fraction calculated using the model by Whitcombe and co-workers (Whitcombe *et al.* 1998).

This analysis shows that a lower fraction of templates establishes associations compared to the reference system MIP1. This effect is not so pronounced for the "intermediate" complexes, 1_c and 1_t, but is very notable for complexes of type 2. Because the volume was adjusted, the concentrations are now different when compared to MIP1, therefore this shifts the equilibrium. Comparing these values with the data in Figure 4.14, MIP7 has a ratio $[M_0]/[T_0]=2$. Fc is equivalent to the ratio between equilibrium concentrations to initial template concentration). However, we must remember we are dealing with a different species as a template here.

As expected, using the alternative template AT leads to larger porosity (or accessible volume fraction) with this property for MIP7 being 6.66×10^{-2}, compared to 3.62×10^{-3} in MIP1 (calculated in the same fashion and with the same probe as in Chapter 3).

5.1.2. Adsorption studies

Adsorption simulations of the target molecule (T), and its analogue (A) are performed on the matrix MIP7 imprinted with the alternative template, AT.

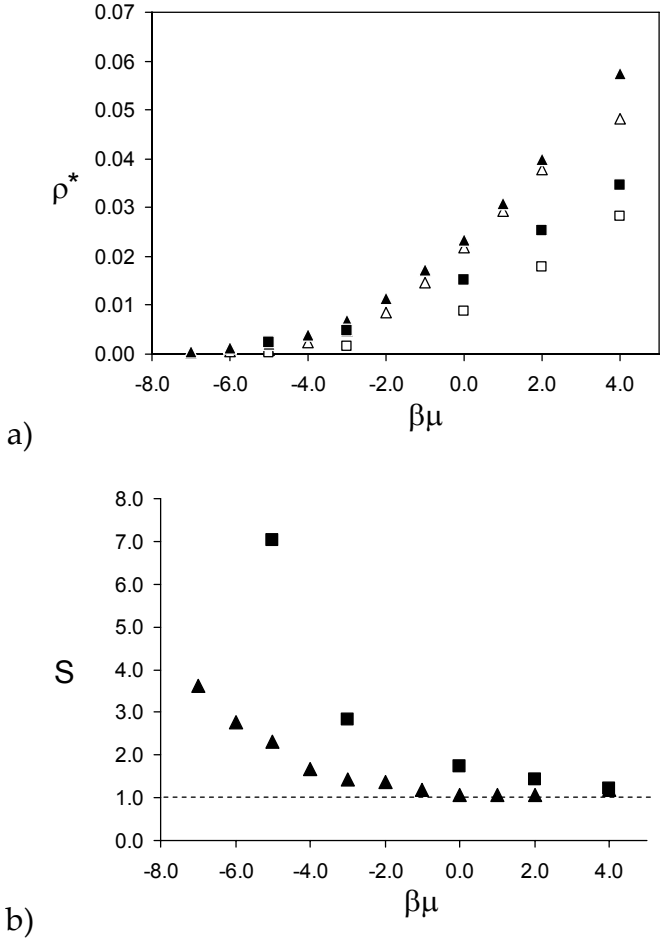

Figure 5.3: a) Isotherms obtained for a single matrix realization of MIP7 (triangles) and for MIP1 (squares; averaged over 3 matrix realizations). Closed symbols correspond to the template and open symbols to the analogue. b) Selectivity expressed through the separation factor, for MIP7 (triangles) and MIP1 (squares, averaged over 3 matrix realizations).

With a higher porosity, MIP7 has a higher capacity as expected. However, there is a large drop in selectivity, which given the considerations mentioned

in previous chapters, is to be expected. MIP7 has a lower number of complexes established and these are of lower affinity. Moreover, for a system of higher porosity, the surface is proportionally of lower affinity overall. Nonetheless, MIP7 maintains a significant level of selectivity at lower chemical potentials.

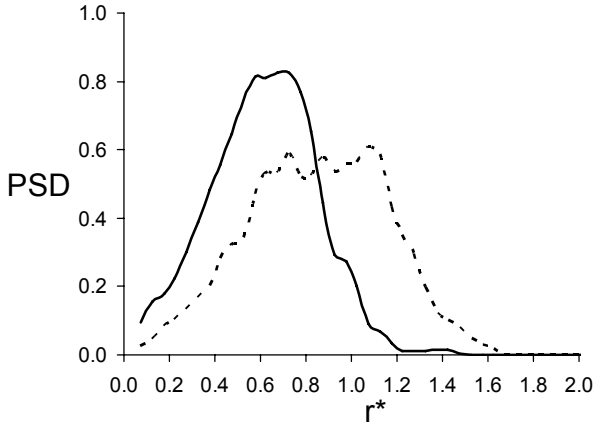

Figure 5.4: Pore size distribution (PSD) for MIP1 (solid line) and MIP7 (dashed line).

The assessment of the pore size distribution (defined on p.71) for MIP7 shows that compared to MIP1, the pore range is increased to higher pore radii while the distribution is broadened and shifted to the right (Figure 5.4).

5.1.3. Binding sites analysis

The analysis of the association status of the adsorbates T and A, show that for this higher porosity matrix of MIP7, a higher proportion of the adsorbate is not binding to functional monomers, which is to be expected from the lower selectivity values. It is interesting to note that within the lower affinity and less specific binding sites (types 1_t and 1_c) there is a shift in the fractions of adsorbates associated with the imprinted and non-imprinted binding sites, with the latter ones now being more prominent. If one compares Figure 5.5 with the same analysis for MIP1 (see Figure 3.5), it is also clear that the analogue (and to some extent also the template) now binds more preferentially to non-imprinted binding sites of type 2, 1_t and 1_c. It seems that making porous space more open, invariably also opens additional access to some binding sites that would be inaccessible in the reference system MIP1.

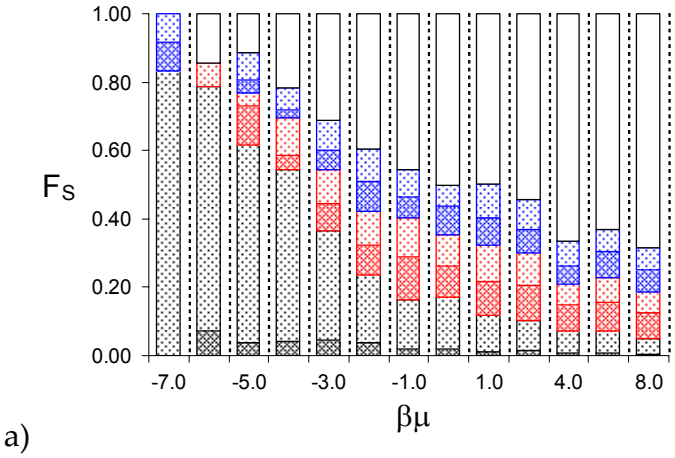

a)

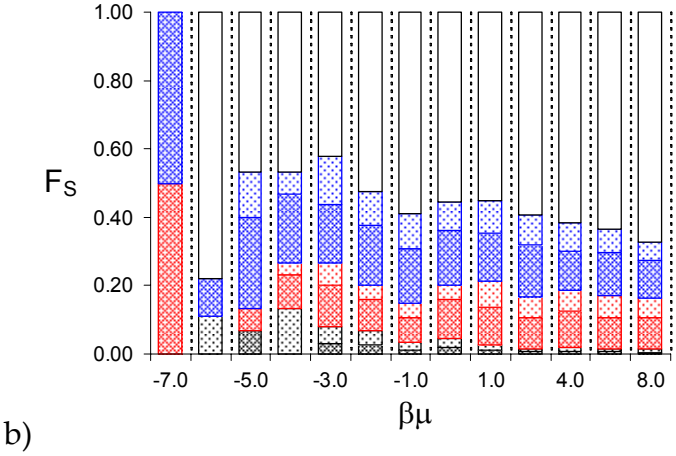

b)

Figure 5.5: Fraction F_S of adsorbed template molecules in each binding state as a function of the chemical potential $\beta\mu$ in MIP7. Colour of each bar corresponds to a particular binding site type: grey for 2, blue for 1_c, red for 1_t and white for 0. Lighter shades correspond to molecules located in the imprinted binding sites, whereas darker shades correspond to molecules forming alternative associations of the same type with the matrix. Data is presented for one matrix realization.

By studying the functional monomers in complexes, at the pre-polymerization stage, that subsequently form associations with adsorbing molecules, one can have an indication of how many complexes are re-occupied by templates.

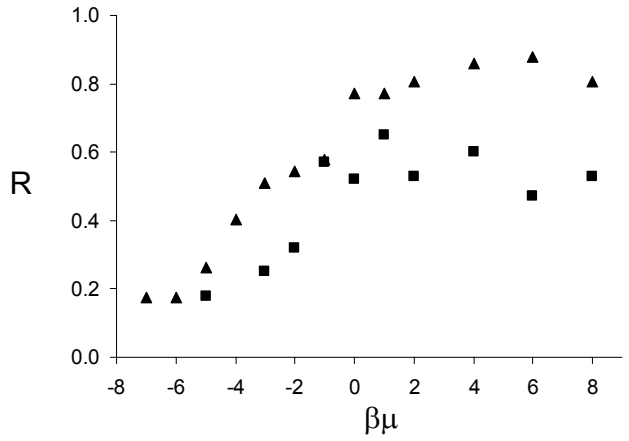

Figure 5.6: Fraction R of complexes of type 2 leading to binding sites of type 2 occupied at the stage of adsorption. Data is presented for adsorbing template in one matrix realization of MIP7 (triangles) and one matrix of MIP1 (squares).

Figure 5.6 shows the fraction R, of complexes of type 2 that form binding sites of type 2 occupied by the template. This is higher for MIP7 than MIP1 throughout the isotherm. Thus it is shown that the use of the alternative templates has increased the number of more favourable imprinted binding sites available. This shifts the affinity of the surface towards higher values, albeit not its selectivity.

Another curious observation can be made from the comparison of MIP7 system to MIP5 at 40% expansion considered in the previous chapter. Although porosity of MIP7 is *higher* than that of MIP5 at 40% expansion (6.66×10^{-2} *vs*. 1.67×10^{-2}), the selectivity of MIP7 is higher than that for MIP5 at 40% of expansion in the lower half of the isotherm. Thus, one may say that the objective of this alternative "synthetic" protocol has been achieved: a significantly more open or sparse matrix has been obtained without such a drastic loss of molecular recognition as would be expected from other,

indiscriminate processes that lead to higher porosity. This difference is all the more pronounced if one remembers that MIP7 is prepared on a less favourable stoichiometry when compared with MIP5. This is the intended result and to be expected, as the introduction of the spacer group in the alternative template leads to a particular localized effect, which does not affect the interaction pattern, whereas expansion is uniform throughout the matrix and disrupts this pattern in imprinted binding sites.

5.2. Binding site distribution optimization

The results presented thus far reiterate the observation that heterogeneity of the binding sites lead to a loss of selectivity. It was shown in Chapter 3 that the principal source of this loss of selectivity is functional monomers in the structure of an imprinted MIP that do not belong to any specific imprinted binding site. These are able to form both alternative associations with the rebinding template and associations with the analogue molecules. This naturally suggests that a simple way to alleviate the problem is to remove all functional monomers in the final MIP structure that are not involved in highly specific imprinted sites. This concept is depicted in Figure 5.7, where functional monomers (blue and red groups on the surface) not associating in strong complexes with the template (shown in grey) are removed to generate a homogeneous surface in terms of binding sites.

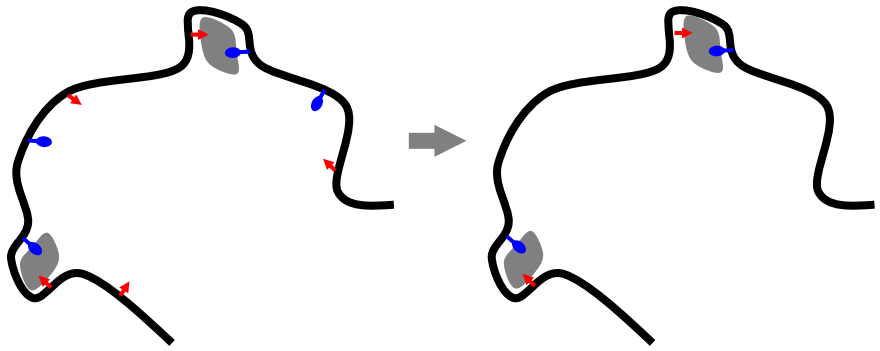

Figure 5.7: Schematic representation of the surface modification model.

We speculate that the process depicted in Figure 5.7 could be realized through some chemical cleaving of free monomers. Provided the functional monomers in binding sites are stabilized, some form of cleaving followed by washing of the polymer might result in less heterogeneous surface in the MIP. Alternatively, one could take advantage of the fact that high affinity sites will retain the template very strongly. With the high affinity sites occupied the remaining porous surface could be chemically treated to block the free functional monomers.

5.2.1. Polymer matrix

For this study, MIP5 is taken as the basis system to create MIP8. For MIP8, functional monomers not involved in any complexes of type 2 are turned into cross-linker particles by removing their surface association sites. (This is not equivalent to a system of extreme X:FM ratio though, since such a system would lead to a different chemical equilibrium.) The system has therefore the same composition and volume density, but association types can only be of two types: type 2, for fully formed complex (in these FMs were not removed), and type 0 for the templates that are now not associated to

functional monomers. The process removes approximately half the functional monomers from the system.

5.2.2. Adsorption

Adsorption simulations of template T and analogue A were performed on MIP8.

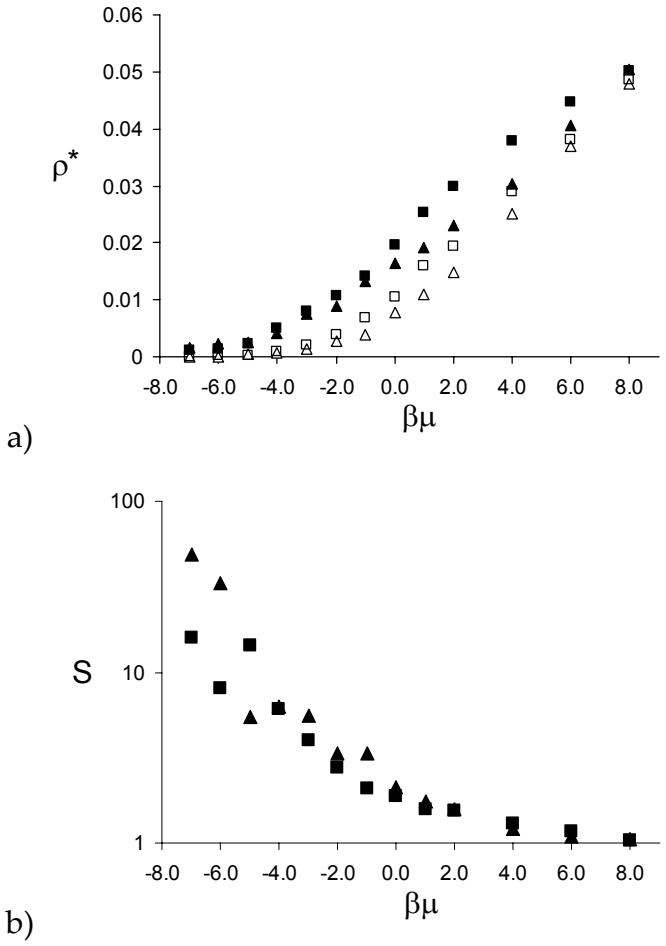

Figure 5.8: a) Adsorption isotherms obtained for a single matrix realization of MIP8 (triangles) and for MIP5 (squares). Closed symbols correspond to the template and open symbols to the analogue. b) Selectivity expressed by the separation factor, for MIP8 (triangles) and MIP5 (squares).

The adsorption data in Figure 5.8 (for one matrix realization, a MIP5 matrix was transformed to generate a matrix of MIP8) shows that for both template and analogue adsorbed densities are lower than in MIP5, at the same value of the chemical potential. This accounts for the lower overall number of attractive association sites in the matrix after the performed treatment.

The selectivity of MIP8 is considerably increased compared to the original MIP5 matrix, but this is only observed at very low chemical potentials, and considering the statistical uncertainty of these data, due to very low adsorbed density of the analogue, this observation must be taken with some care. Nonetheless, it corresponds to the behaviour expected, since binding to the surface can only be made at the imprinted binding sites.

5.2.3. Binding sites

To complete the picture, the association status of the adsorbate molecules is analyzed, and the results are presented in Figure 5.9.

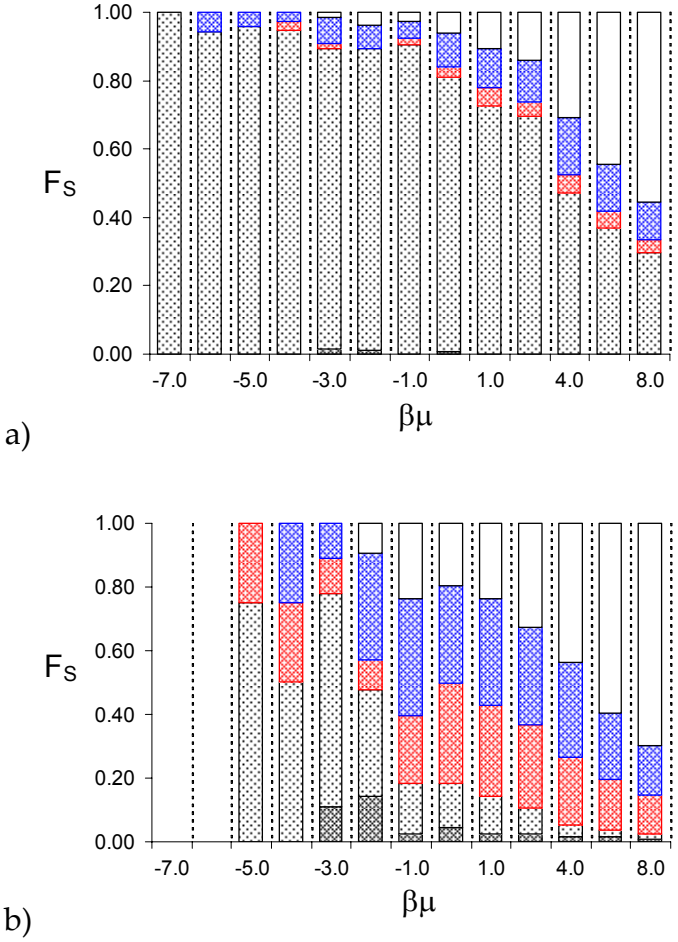

Figure 5.9: Fraction F_S of adsorbed template molecules in each binding type as a function of the chemical potential $\beta\mu$ in MIP8. The colour of each bar corresponds to a particular binding site type: grey for 2, blue for 1_o, red for 1_t and white for 0. Lighter shades correspond to molecules located in the imprinted binding sites, whereas darker shades correspond to molecules forming alternative associations of the same type with the matrix. Data is presented for one matrix realization.

From Figure 5.9a one observes that most templates re-bind in the imprinted binding sites of type 2 rather than form lower affinity associations (type 1); this happens in a much higher proportion than observed in the original MIP5 matrix. The existence of template molecules bound to type 1 sites reminds us that one cannot expect the distribution of complexes at equilibrium to be reflected directly in adsorption. The presence of template molecules in non-imprinted type 2 is residual (see $\beta\mu = -3$). Despite the improved distribution of binding sites, the analogue still manages to bind to some imprinted sites. Although specific, the type 2 complexes do not lead to imprinted binding sites that are sufficiently specific to prohibit *any* form of analogue association within them. To summarize, this proposed concept to manipulate binding site distribution seems to be of limited effectiveness, especially where it concerns separations since selectivity is only increased at lower loadings and overall affinity is reduced. However, very high selectivity at low loadings is promising for applications where only high association constants are of interest, such as certain drug delivery applications or sensing.

5.3. Summary

An alternative template protocol, using a species with a spacer group successfully produced a model MIP material which maintained some level of selectivity for the target molecules (versus its analogue). At the same time, analysis of the material and its properties shows that porosity is increased as well as the average pore size, leading to higher adsorption capacity. It is also observed that more high affinity binding sites are accessible, in the MIP imprinted via the new protocol, compared to the reference system. The

analysis laid out in this chapter is, to the best of the author's knowledge, the first study on the effects of alternative template, specifically spacer molecules, on the integrity the binding sites molecular recognition properties. Further understanding of the effects of the alternative template as a facilitator of binding site accessibility would require more specific studies of the binding site structure, connectivity of the porous network and accessibility of the binding sites. Higher porosity and binding site accessibility would be beneficial for most applications of MIPs.

The optimization of the affinity distribution, through the removal of the functional monomers that generate lower specificity sites, is shown to be effective in increasing selectivity. Unfortunately, the effect is restricted to lower concentration ranges. At higher loadings, association types other than type 2 become prevalent, and the specificity of the MIP is reduced. For its reduced effective range of chemical potentials, this protocol would serve MIP based sensing devices or to extend the applicability of MIPs as monoclonal pseudo-immunoassays.

5.4. References

Garcia-Calzon, J. A. and M. E. Diaz-Garcia (2007). "Characterization of binding sites in molecularly imprinted polymers." Sensors and Actuators B-Chemical **123**(2): 1180-1194.

Ramstrom, O. and R. J. Ansell (1998). "Molecular imprinting technology: Challenges and prospects for the future." Chirality **10**(3): 195-209.

Robinson, D. K. and K. Mosbach (1989). "Molecular Imprinting of a Transition-State Analog Leads to a Polymer Exhibiting Esterolytic Activity." Journal of the Chemical Society-Chemical Communications(14): 969-970.

Umpleby, R. J. *et al*. (2004). "Characterization of the heterogeneous binding site affinity distributions in molecularly imprinted polymers." Journal of Chromatography B, Analytical Technologies in the Biomedical and Life Sciences **804**(1): 141-149.

Umpleby, R. J. *et al*. (2000). "Measurement of the continuous distribution of binding sites in molecularly imprinted polymers." Analyst **125**(7): 1261-1265.

Vlatakis, G. *et al*. (1993). "Drug assay using antibody mimics made by molecular imprinting." Nature **361**(6413): 645-647.

Whitcombe, M. J. *et al.* (1995). "A New Method for the Introduction of Recognition Site Functionality into Polymers Prepared by Molecular Imprinting - Synthesis and Characterization of Polymeric Receptors for Cholesterol." Journal of the American Chemical Society **117**(27): 7105-7111.

Yungerman, I. and S. Srebnik (2006). "Factors Contributing to Binding-Site Imperfections in Imprinted Polymers." Chem. Mater. **18**(3): 657-663.

6.

Towards Atomistic Models of Adsorption in Molecularly Imprinted Polymers

In this chapter, the general approach developed earlier in Chapter 2 is extended to realistic models of MIPs. These models are based on accurate molecular force-fields available in the literature. Model imprinted polymers, templated with small organic molecules are simulated and studied. Comparison of different types of interactions is made and their role in imprinting and recognition performance of the model MIP is assessed. The applicability of the affinity distribution as a characterization method for MIPs is explored.

6.1. Introduction

In chapter 2, a general strategy to model MIPs was described; this same strategy is applied throughout the whole thesis. In Figure 2.1, it is proposed that different levels of detail can be explored within the framework of this general approach. Chapters 3 to 5 explored a relatively simple level of detail in the description of molecular species and their interactions. With this approach, some useful qualitative results and insights have been extracted.

More elaborate and realistic potentials can be employed in the modelling of molecular interactions. In order to understand the motivation to explore more complicated and thus more computationally intensive models, it is probably beneficial to review the limitations of the simple models of MIPs, considered in Chapters 3 to 5.

The simple molecular model used hard-sphere potentials to define interactions between atoms. This interaction potential neglects weak attractive forces and results, for example, in unrealistic adsorption isotherms which do not comply with any isotherm model commonly used to characterize MIPs. Another limitation is the fact that, because the simple model deals with abstract molecular species, there is no direct parallel with any real compounds (or their properties). Although more than one association was possible in the complexes studied in the simple models, they were of the same nature (square-well potentials of equal strength). The intention of these simple potentials was to mimic the presence of hydrogen bonding. A more realistic picture would involve attractive interaction

potentials of different types. At this point it seems natural to turn our attention to atomistic modelling.

Atomistic models can describe molecules with varying degrees of detail, but they are overall realistic in the representation of the molecule's geometry and types of interactions between the atoms and molecules. In principle, this opens a possibility for quantitative predictions and analysis. For example, one can discriminate between different types of realistic interactions, such as Coulombic and non-Coulombic terms (dispersion or van der Waals interactions), and subsequently understand their role in the recognition behaviour of MIPs. Within this level of detail, pre-polymerization mixtures can now be modelled in even greater complexity (*i.e.* under realistic conditions and compositions), association constants between various species can be calculated as well as other equilibrium and adsorption properties.

However, atomistic modelling simulations have the drawback of being computationally expensive. This constrains the scale of the simulations, and if one were performing molecular dynamics, the time span one could cover. This is a serious issue in the simulation of disordered porous materials because such simulations require a sufficiently large sample of the structure or averaging over several matrix realizations.

Many detailed descriptions of the template and functional monomer interactions have been done using these atomistic force-fields for the analysis of the forces governing template - functional monomer association, *e.g.* (Chianella *et al.* 2002; Chianella *et al.* 2006). Studies into the pre-polymerization mixture and its chemical equilibrium have also been

performed (Yungerman and Srebnik 2006; Huang and Li 2008; Karlsson *et al.* 2009). While very detailed modelling of template - functional monomer interactions have been a subject of intense research efforts for some time, only recently a realistic model of MIP has emerged based on capturing the processes of MIP formation and function (Herdes and Sarkisov 2009; Karlsson *et al.* 2009).

Although the general approach as shown in Figure 2.1 remains largely the same, the actual implementation of the models based on detailed atomistic potentials requires more advanced simulation techniques, such as Ewald summation methods for the calculation of Coulombic interactions. In this part of the studies, the simulation tools and methods used have been developed in other research groups. Therefore the details of the implementation of the methods are presented without any in-depth description of their statistical mechanical foundations.

6.2. Methodology

The methodology employed by the author draws directly from the approach and model originally used by Herdes and Sarkisov in simulation studies of adsorption of pyridine, benzene and toluene in imprinted polymers (Herdes and Sarkisov 2009).

The overall modelling approach is the same as for the simple model, with the exception of the simulation tools used. Molecular Dynamics (MD) simulations were performed in the (NPT) ensemble (constant number of

molecules, pressure and temperature) to realistically mimic laboratory conditions. This is used to model the equilibrium mixture prior to polymerization.

The MD simulations were run using the open source software GROMACS (Lindahl *et al.* 2001) - http://www.gromacs.org. Adsorption simulations are performed using MuSiC (Multipurpose Simulation Code), developed in the group of Snurr (Gupta *et al.* 2003) and available under the GPL licence. For a comprehensive review of the foundations of molecular dynamics, the reader is referred to several well known sources (Allen and Tildesley 1987; Kendrick *et al.* 1997; Frenkel and Smit 2002).

6.2.1. Molecular Model

The focus of this particular study is the generation of realistic model MIPs, insofar as the generation of template binding sites is concerned. For this reason, model MIPs are constructed replicating a typical synthetic protocol, with **m**eth**a**crylic **a**cid (MAA) as the functional monomer and **e**thylene **g**lycol **di**meth**a**crylate (EGDMA) as the cross-linker (Figure 6.1). These components are very commonly used to prepare MIPs as they are well suited for non-covalent imprinting. In this study model MIPs imprinted with pyrazine or pyrimidine (shown in Figure 6.1) are investigated. This system features relatively simple species, and therefore provides a suitable starting point for the atomistic simulation studies. These species are isomers, they differ only in the interaction pattern they create in the complex with functional monomers. This follows the line used in the simple model studies of testing molecular recognition by using model MIPs to try and distinguish between two very similar species, the template and its chemical analogue.

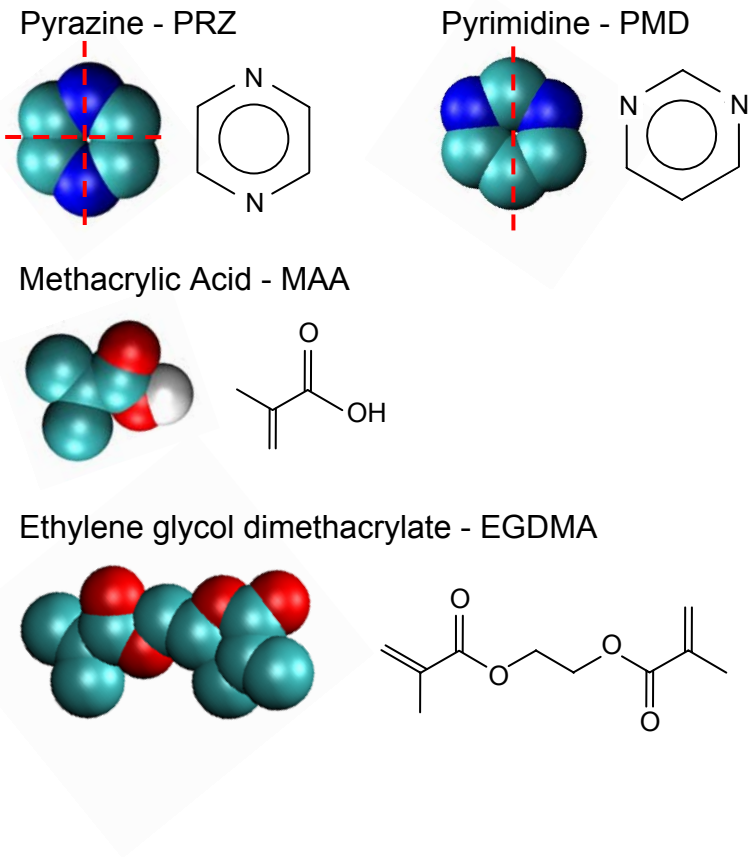

Figure 6.1: Graphic representation of the species involved in the atomistic simulations of the model MIP. Cyan corresponds to carbon based united atoms (C, CH_x), blue indicates nitrogen atoms, the red colour shows the location of oxygen atoms and white defines an explicit hydrogen atom.

Red dashed lines across the templates, pyrazine and pyrimidine help to delineate the axes of symmetry of these molecules. For greater degree of realism, the proportions of the components in the pre-polymerization mixture were selected to mimic experimental conditions. Herdes and Sarkisov considered a system of pyridine, MAA and EGDMA in 1:4:20 molar proportions to reflect a real MIP material prepared by Dr. Peter Cormack

and co-workers at the University of Strathclyde (Herdes and Sarkisov 2009). Here similar proportions are used.

Unlike pyridine, pyrazine and pyrimidine have two functional groups, therefore the interaction pattern they create should be stronger. To maintain the same proportion of functional monomers per functional group as in the original work of Herdes and Sarkisov, twice the amount of functional monomers in the system is used here. The composition of the systems is presented below in Table 6.1. In principle, solvent such as chloroform could be included in the system as well. Herdes and Sarkisov varied the amount of solvent as a way to control porosity and showed that lower amounts of solvent led to higher densities and selectivities of the model materials. Here, for simplicity, an extreme case of no solvent at all is investigated.

Table 6.1: Composition (number of molecules of each species) of model MIPs templated with pyrazine (MIP_PRZ) and pyrimidine (MIP_PMD).

Species	MIP_PRZ	MIP_PMD
Template	10 PRZ	10 PMD
Functional Monomer	80 MAA	80 MAA
Cross-linker	200 EGDMA	200 EGDMA

One may view the templates chosen as ideal species for the theoretical studies of imprinting and molecular recognition effects. They are simple, rigid, and differ only in the interaction pattern (*i.e.* in the location of the nitrogen atoms). The goal is to verify whether atomistic models of MIPs, imprinted with these molecules, are capable of molecular recognition.

The force-field parameters for the species in this study are taken from the TraPPE force-field of Siepmann and co-workers (Martin and Siepmann 1998; Chen and Siepmann 1999; Martin and Siepmann 1999; Wick *et al.* 2000; Chen *et al.* 2001; Stubbs *et al.* 2004; Lubna *et al.* 2005; Wick *et al.* 2005; Rai and Siepmann 2007). Pyrazine and pyrimidine parameters are taken directly form TraPPE, whereas the MAA parameters where taken from TraPPE and a TraPPE-like model by Clifford for saturated carboxylic acids (Clifford *et al.* 2006). This was validated by Herdes and Sarkisov by the simulation of MAA vapour-liquid equilibrium data (Herdes and Sarkisov 2009). In the same work, EGDMA was modelled as two MAA molecules and a bridging ethylene glycol (Herdes and Sarkisov 2009). Parameters for ethylene glycol were also taken from TraPPE directly. Liquid EGDMA was modelled at 1 atm and 298 K, to obtain a reasonable agreement (in terms of density) with the experimental data. Molecular interaction parameters are shown in the following table.

Table 6.2: Force-field parameters and graphic representation of the charge distribution for the species in the model MIPs. Black patterns for negative charges, red patterns for positive charges. Stronger shaded patterns indicate stronger charges.

PRZ

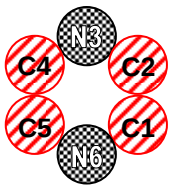

n	TraPPE ID	Atom ID	σ nm	ε kJ·mol^{-1}	Charge eV
1	CHN	C1	0.374	0.399	0.33
2	CHN	C2	0.374	0.399	0.33
3	N	N3	0.345	0.233	-0.66
4	CHN	C4	0.374	0.399	0.33
5	CHN	C5	0.374	0.399	0.33
6	N	N6	0.345	0.233	-0.66

PMD

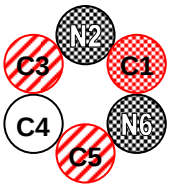

n	TraPPE ID	Atom ID	σ nm	ε kJ·mol^{-1}	Charge eV
1	CN2	C1	0.39	0.391	0.66
2	N	N2	0.345	0.233	-0.66
3	CHN	C3	0.374	0.399	0.33
4	CHaro	C4	0.370	0.420	0.00
5	CHN	C5	0.374	0.399	0.33
6	N	N6	0.345	0.233	-0.66

MAA

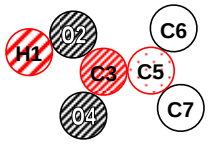

n	TraPPE ID	Atom ID	σ nm	ε kJ·mol^{-1}	Charge eV
1	Hdm	H1	0	0	0.37
2	OH	O2	0.302	0.773	-0.46
3	CO	C3	0.390	0.341	0.42
4	OC	O4	0.305	0.657	-0.45
5	Csp2	C5	0.385	0.166	0.12
6	CH_2sp2	C6	0.368	0.707	0.00
7	CH_3	C7	0.375	0.815	0.00

EGDMA

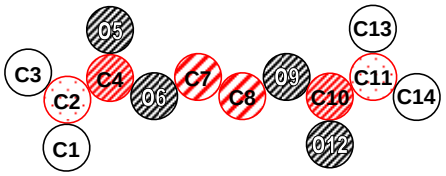

n	TraPPE ID	Atom ID	σ nm	ε kJ·mol^{-1}	Charge eV
1	CH_2sp2	C1	0.368	0.707	0.00
2	Csp2	C2	0.385	0.166	0.12
3	CH3	C3	0.375	0.815	0.00
4	CO	C4	0.390	0.341	0.42
5	OC	O5	0.305	0.657	-0.45
6	OH	O6	0.302	0.773	-0.46
7	CH_2sp3	C7	0.395	0.382	0.37
8	CH_2sp3	C8	0.395	0.382	0.37
9	OH	O9	0.302	0.773	-0.46
10	CO	C10	0.390	0.341	0.42
11	Csp2	C11	0.385	0.166	0.12
12	OC	O12	0.305	0.657	-0.45
13	CH_3	C13	0.375	0.815	0.00
14	CH_2sp2	C14	0.367	0.707	0.00

6.2.2. Simulation of pre-polymerization mixture using NPT molecular dynamics

Two MIP systems are modelled, templated with pyrazine and pyrimidine and denominated MIP_PRZ and MIP_PMD, respectively. The systems are initialized by mixing the components: 200 EGDMA, 80 MAA and 10 template (PRZ or PMD) molecules. The initial configurations of the systems are prepared by placing all the molecules in a simulation box, using a simple Monte Carlo code. In this process, the atoms are all defined as hard spheres and Monte Carlo moves are performed to relax the system and bring it closer to the final equilibrium state.

The system is then equilibrated via molecular dynamics simulations in the (NPT) ensemble. In these simulations, temperature is set to T = 298 K and pressure is set to P = 1 atm, to reflect laboratory conditions. Simulating (NPT) makes it easier to mimic laboratory conditions realistically because pressure is set as constant (as it would be in the lab) rather than volume (as in the NVT ensemble). Equilibration is done with the time step of 0.002 ps and at least 5×10^6 time steps for each realization (10 ns). Three realizations are generated for each MIP system. Periodic boundary conditions are used for the simulation box in all dimensions (xyz). The LINCS algorithm is employed to constrain the molecular bonds. The Berendsen coupling scheme is adopted for isotropic baro- and thermostat (Berendsen *et al.* 1984). The Particle Mesh Ewald (PME) method is used for electrostatic calculations with xyz periodic boundary conditions (Darden *et al.* 1993; Essmann *et al.* 1995). The systems created measured about 4.20 nm in size (edge of the cubic box). The model polymer templated with PRZ has a density of 1045.4 ± 5.6 $g\cdot l^{-1}$; while the polymer templated with PMD registered a density of 1048.2 ± 3.9 $g\cdot l^{-1}$ (values averaged over three realizations). Bulk PRZ and PMD

systems were also simulated, using 300 molecules, at 1 atm, and 298 K. For PRZ, density of 1005.2 ± 5.2 $g \cdot l^{-1}$ was observed which compares favourably with the experimental value of 1031 $g \cdot l^{-1}$. For PMD the density observed was 1030.0 ± 3.3 $g \cdot l^{-1}$, with the experimental value being 1016 $g \cdot l^{-1}$.

6.2.3. Adsorption simulation

The modelling approach is the same as before, where the matrix is created simply by taking an equilibrated configuration from MD simulations, "freezing" the coordinates of the components, and removing the template molecules. The resulting rigid structure of functional monomer and cross-linker serves as a model porous matrix in the subsequent adsorption studies. To gather better statistics, adsorption simulations are performed in a 2x2x2 supercell for each matrix realization (Figure 6.2).

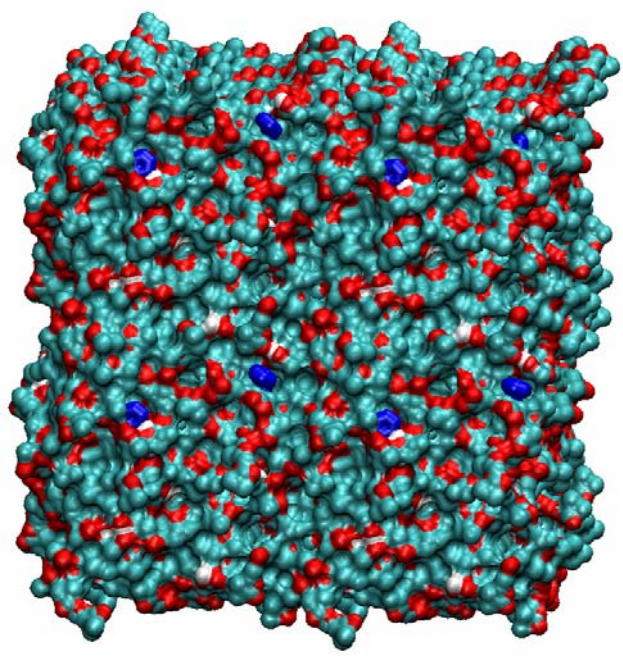

Figure 6.2: Visual representation of a single configuration of pyrazine (in blue) adsorbing in a MIP_PRZ matrix. Visualization obtained using the VMD software (Humphrey *et al.* 1996).

Adsorption simulations are performed at T = 300 K. Simulation of adsorption in a dense system using conventional Monte Carlo is often inefficient due to a significant proportion of rejections of trial insertions and translations. Again, as previously discussed in Chapter 2, an energy biased grand canonical Monte Carlo (EB-GCMC) protocol is employed, as proposed by Snurr and co-workers (Snurr *et al.* 1993). Before the adsorption simulation is started, energy maps are constructed to bias insertions and deletions. The moves (insertions, deletions, rotations, translations) are given equal probability of selection. Simulation runs correspond to at least 20×10^6 moves per point on the isotherm, with half of the moves being sampled to average properties. In Figure 6.2 a typical snapshot for MIP_PRZ with pyrazine adsorbing, is shown. Figure 6.2 helps to convey the disordered, microporous nature the matrix.

6.2.4. Data Analysis

The new, atomistic level of the model detail opens a substantially wider scope for the kind of analysis that can be performed and information that can be extracted from the simulations. First, it is possible to investigate in detail various contributions to the potential interaction energy (Coulombic, non-Coulombic) between different species, individual molecules and atoms. One can inspect what molecules and how many form associations with each other via hydrogen bonds, link this information to the equilibrium constants of various association reactions and examine how these processes depend on the structure of components and so on. Besides the establishing of hydrogen bonds, one can study the arrangement of molecules in the mixture via radial distribution functions.

For the simple model, binding site distributions were constructed based on the type of associations created between adsorbate and functional monomers in the matrix. The model now features continuous, realistic potentials of interaction, so it is more appealing to analyse the distribution of energies of interaction between matrix and adsorbing fluid.

Furthermore, because the molecular structure and interaction potentials are realistic, for this model one can obtain adsorption isotherms that conform (in shape) to typical isotherms observed in experiments. This can be used to understand the link between an adsorption isotherm and the binding site distribution that induces it. In particular, one can treat the simulated adsorption isotherm as an experimental result, apply the conventional methods for binding site characterization to it (Langmuir-Freundlich isotherm for example), and investigate to what extent the generated binding site distribution reflects "true" binding site heterogeneity. The "true" heterogeneity can be explicitly known from the molecular model.

6.3. Results

6.3.1. MIP pre-polymerization mixture

The analysis begins with the examination of how various species interact with each other in the pre-polymerization mixture. The values of Coulombic and non-Coulombic interactions of the template with its surrounding polymer mixture (functional monomer + cross-linker) are obtained from averaging over all template molecules in the mixture and over 3 independent

realizations. The results are shown in Figure 6.3a. In addition, in Figure 6.3b, results are shown for the final configurations of the 3 independent simulations (these are used as matrix realizations).

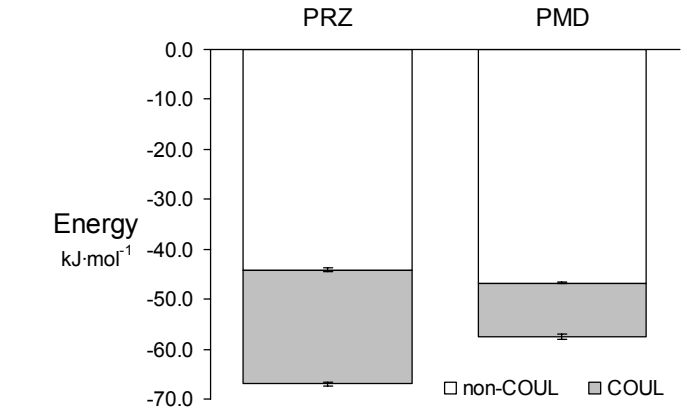

a)

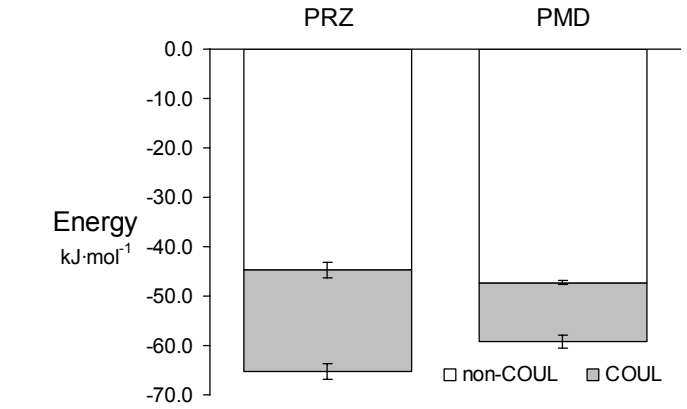

b)

Figure 6.3: Average energy of interaction between one template molecule and polymer mixture components, for two MIP systems imprinted with pyrazine (PRZ) and pyrimidine (PMD). Non-Coulombic contribution is represented by the white area; Coulombic contribution is represented by the grey shaded area. a) Energies averaged from molecular dynamics simulation over 10 ns and over 3 independent simulations (lines correspond to the standard error). b) Energies in the final configurations averaged over 3 matrix realizations (lines correspond to the standard error).

The first thing to notice in Figure 6.3 is that the final configurations of the mixtures (used as matrix realizations) are good representatives of the equilibrium mixture, featuring very similar distribution of the total energy of interaction between Coulombic and non-Coulombic terms.

Between the two templates, the total interaction energies do not differ greatly, which is not surprising considering the similarity between pyrazine and pyrimidine. The total interaction energy for the pyrazine in the pre-polimerization mixture is circa 15% more negative than that of pyrimidine. The difference lies in the Coulombic interactions which are stronger in the pre-polymerization mixture with pyrazine, approximately double that of the pyrimidine mixture. This difference is observed for both interaction with MAA and EGDMA (see Figure 6.4).

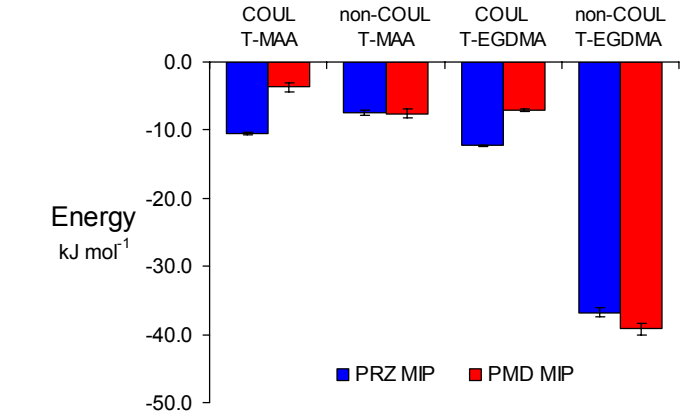

a)

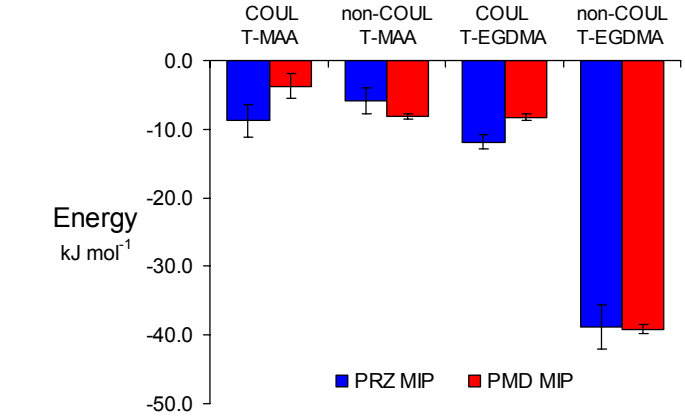

b)

Figure 6.4: Energy of interaction between template (T) and polymer mixture components (MAA, EGDMA) for two MIP systems: imprinted with pyrazine (PRZ, in blue) and pyrimidine (PMD, in red). Non-Coulombic (non-COUL) and well as Coulombic (COUL) interactions are represented for template-MAA and template-EGDMA interaction pairs. a) Energies averaged from molecular dynamics simulation over 10 ns and over 3 independent simulations (lines correspond to the standard error). b) Energies in the final configurations averaged over 3 matrix realizations (lines correspond to the standard error).

Rather than the whole pre-polymerization mixture, it is the specific association of templates and functional monomers that are of greater interest. The mixture was also analyzed to determine if any hydrogen bonds are

established between the carboxyl group of the methacrylic acid and the secondary amine group of the templates. Hydrogen bonds describe a particular geometric arrangement of polar atoms. As usual, these atoms will also interact via dispersion (van der Waals) forces. From the analysis of Coulombic and non-Coulombic terms presented earlier, it is difficult to extract what proportion of these interactions is associated with hydrogen bonds specifically. However, the number of hydrogen bonds present in the system can be counted using a simple geometric criteria based on the first minimum in the corresponding atom-atom radial distribution function, observed during the molecular dynamics run. Hydrogen bonds are said to be established if the hydrogen and nitrogen atoms are within a 2.5 Å distance. Here the complexes are classified in the same manner as for the simple model. Type 0 complexes correspond to pyrazine or pyrimidine not engaged in any hydrogen bonding, types 1_{N1} and 1_{N2} correspond to one of the nitrogens of either template involved in a hydrogen bond, type 2 complexes corresponds to templates where both nitrogen groups are establishing hydrogen bonds.

The analysis of the energies of interaction revealed that pyrazine templated MIPs will produce a matrix that is more energetically attractive to template (versus pyrimidine MIPs). The analysis of hydrogen bonds points to a similar picture (see Figures 6.5 and 6.6). In MIP_PRZ, there is a higher number of complexes established than in MIP_PMD. Naturally, the establishment of these hydrogen bonds should be the defining feature of the particularly stronger arrangement of Coulombic interactions.

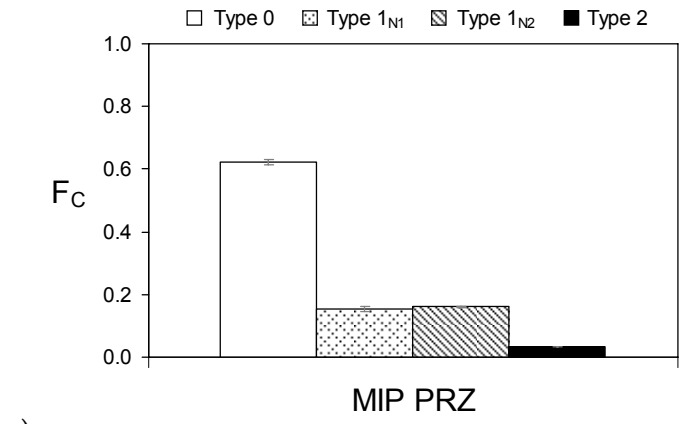

a)

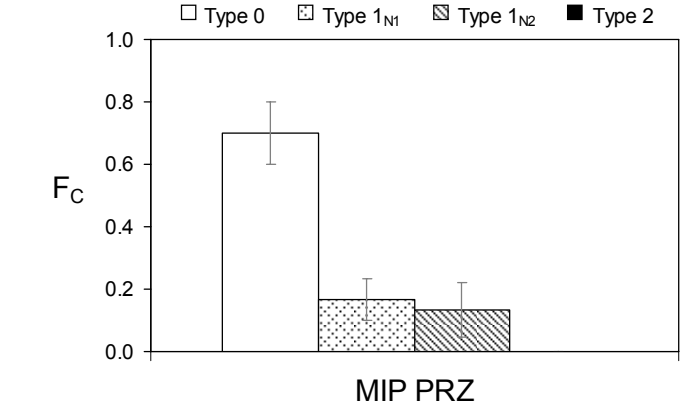

b)

Figure 6.5: Distribution of different association types between the template and functional monomers with the corresponding standard errors, for pyrazine templated system (MIP PRZ). F_C indicates the fraction of complexes of a certain type. a) F_C over 1000 equilibrium molecular dynamics configurations, in 3 independent realizations. b) F_C is determined for the configuration saved as matrix and averaged over the 3 matrix realizations.

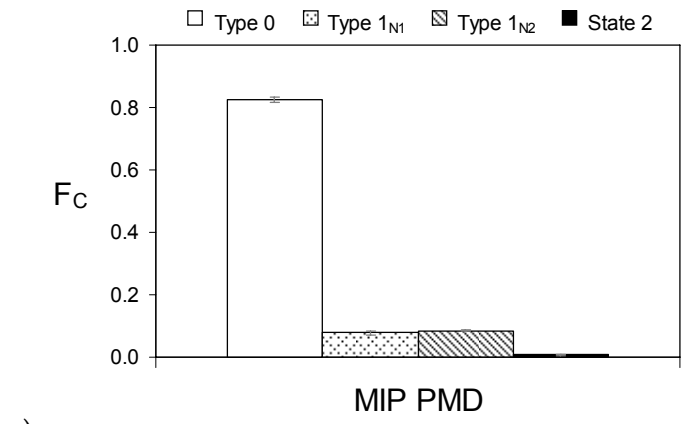

a)

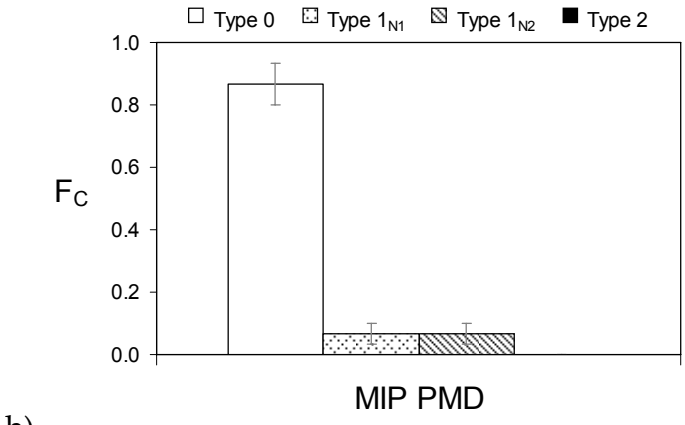

b)

Figure 6.6: Distribution of different association types between the template and functional monomers with the corresponding standard errors, for pyrimidine templated system (MIP PMD). F_C indicates the fraction of complexes of a certain type. a) F_C over 1000 equilibrium molecular dynamics configurations, in 3 independent realizations. b) F_C is determined for the configuration saved as matrix and averaged over the 3 matrix realizations.

The distribution of complexes obtained from averaging snapshots over the course of molecular dynamics simulation (Figures 6.5a, 6.6a) and extracted from the final configurations used as matrices (Figures 6.5b, 6.6b) are similar. This assures that one can solidly interpret of the results obtained in the adsorption studies of these matrices, in the light of pre-polymerization

equilibrium data. The analysis of hydrogen bonds in the equilibrium indicates that most templates do not establish associations with MAA complex, and only a residual number of them establish type 2 complexes. This is even more noticeable in the pyrimidine system. Pyrazine produces almost double the number of type 1 complexes when compared to pyrimidine. Analysing Figures 6.3-6 together, one finds the distribution displayed is in agreement with the difference in interaction energy, observed earlier. However the equilibrium energies of interaction do not seem to explain the large difference in equilibrium concentrations of complexes for the two systems (MIP_PRZ and MIP_PMD). This seems to hint that besides enthalpic, there are important entropic contributions to the binding event between these templates and the functional monomers (see Equation I.5).

To investigate this issue further, the energies of interaction for template - functional monomer and template - cross-linker pairs were evaluated. Annealing was simulated using GROMACS, from 298 to 100K, in 6 ns, for the following 4 systems: 1 PRZ + 1 MAA, 1 PRZ + 1 EGDMA, 1 PMD + 1 MAA, 1 PMD + 1EGDMA. The energies presented below are the result of averaging the energies over 2 ns at 100 K. With this, one can evaluate the most energetically favourable configurations of these pairs (examples of these in Figure 6.7).

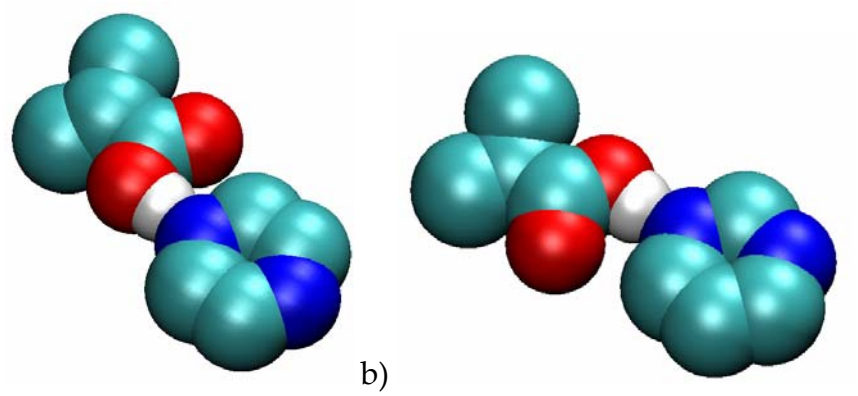

a) b)

Figure 6.7: Representation of the favourable configurations observed from annealing simulations. a) pyrazine and methacrylic acid; b) pyrimidine and methacrylic acid.

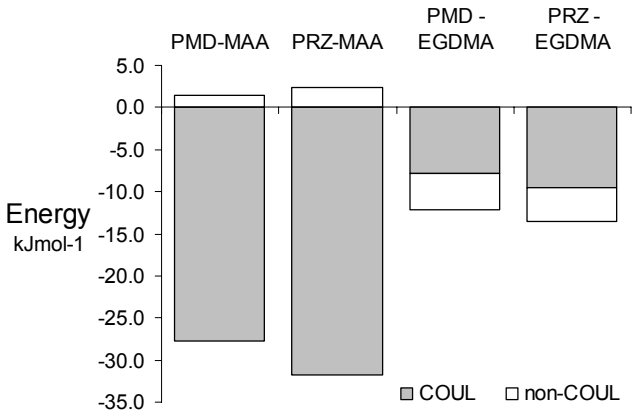

Figure 6.8: Energies of interaction for the 4 pairs, obtained from one annealing simulation realization, averaged over 2 ns (at 100K). Coulombic contribution is shown in grey and non-Coulombic contribution is shown in white.

This analysis reveals that even in its most favourable association, the difference between PRZ-MAA and PMD-MAA interactions is small.

However, it is important to analyse this difference in the context of its impact on the assocation process.

Consider a process of association between PRZ and MAA:

$$PRZ+MAA \rightleftharpoons PRZ\text{-}MAA \qquad \text{VI.1}$$

The equilibrium state of this association process is characterized by the association constant (in low concentration and ideal solution regimes)(Gilson *et al.* 1997) :

$$K_C = \frac{C^o C_{PRZ-MAA}}{C_{PRZ} C_{MAA}} = e^{-\Delta G^o / RT} \qquad \text{VI.2}$$

where, C^O is standard concentration, C_i is the equilibrium conctration of species *i*, and ΔG^0 is the free energy of binding that reflects the change in the free energy as PRZ and MAA form the complex.

Applying this equation for both PRZ-MAA and PMD-MAA associations, one can obtain the following ratio:

$$\frac{K_{PRZ}}{K_{PMD}} = \frac{e^{-\frac{\Delta G^0_{PRZ}}{RT}}}{e^{-\frac{\Delta G^0_{PMD}}{RT}}} = e^{-\frac{\Delta\Delta G^0}{RT}} \qquad \text{VI.3}$$

where $\Delta\Delta G^0 = \Delta G^0_{PRZ} - \Delta G^0_{PMD}$. In principle, each term ΔG^0_i involves enthalpic contributions associated with the change in the inter- and intramolecular interactions as the molecule forms a complex, as well as the entropic effects. For the sake of the analysis here, we equate $\Delta\Delta G^0 = \Delta G^0_{PRZ} - \Delta G^0_{PMD} \approx \Delta U_{PRZ} - \Delta U_{PMD} = \Delta\Delta U$, where $\Delta\Delta U$ is the difference in the potential energy between PRZ-MAA and PMD-MAA complexes in their lowest energy conformations, thus ignoring for the moment entropic and conformational contributions and the interactions with other molecules in the pre-polymerization mixture. This is not an unreasonable approximation, as the template species are very similar to each other, and in the double free energy difference $\Delta\Delta G^0$, many of these effects should cancel. From this $\Delta\Delta G^0$ results in the difference in the total energy of interaction between the two associations, -3.10 kJmol^{-1}. For

these annealing simulations, $\Delta\Delta G^0$ is 1.25 times larger than RT. This results in $K_{PRZ}/K_{PMD} \approx 3.5$. For the equilibrium conditions this factor would be lower (by about an order of magnitude), but it is easy to see that a small difference in the interaction energy does indeed lead to a large variation in the equilibrium concentrations.

A simple, albeit, indirect way of analysing the arrangement of molecules in a mixture is the analysis of the radial distribution function. With molecular simulations, one can determine the average density of any atom (or molecule) in the system relative to any other atom (or molecule).

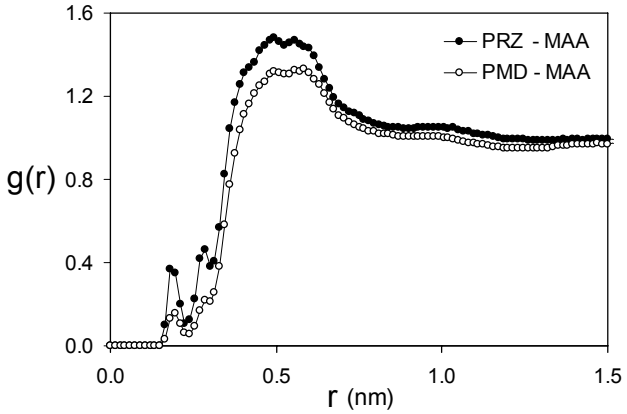

a)

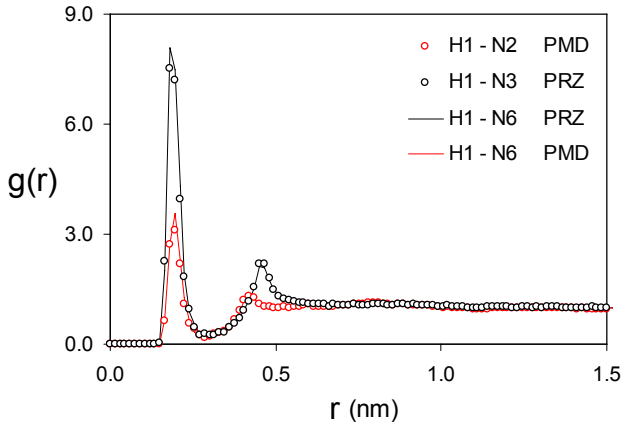

b)

Figure 6.9: Radial distribution function for: a) the templates and methacrylic acid in their respective mixtures, calculated from the centres of mass of the molecules; b) Atom H1 (in MAA) and nitrogen atoms in PRZ and PMD.

Figure 6.9 reinforces the previous observations. From the first peak in the g(r) in Figure 6.9a, pyrazine is found associating with methacrylic acid more often than pyrimidine. The graphic in Figure 6.9b reveals the presence of the hydrogen bonds; particularly for pyrazine there is approximately double the number of hydrogen bonds established (from the first peak of g(r)).

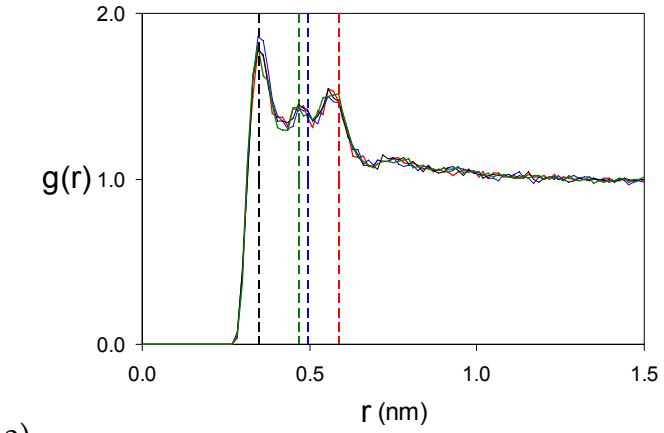

a)

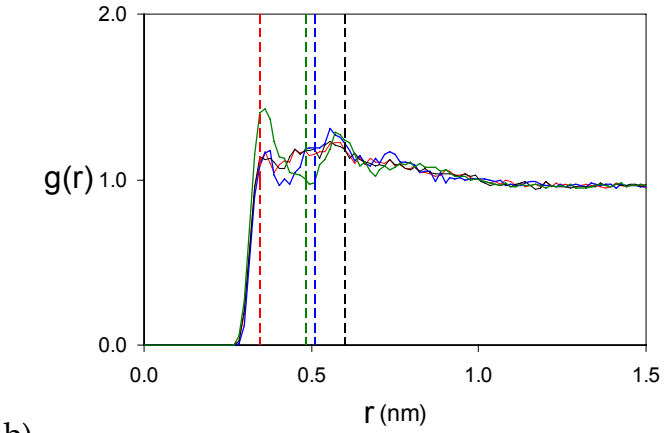

b)

Figure 6.10: Radial distribution functions for: a) Atom O4 (in MAA) and carbon atoms in PRZ. b) Atom O4 (in MAA) and carbon atoms in PMD. C1 in blue, C2 and C3 in red, C4 in green, C5 in black. Vertical dashed lines indicate the location of the peaks for the same g(r) measured from the annealing simulations (at 100 K).

Figure 6.10 shows that for PRZ-MAA interaction, the configuration such as the one shown in Figure 6.7a is observed with equal probability as mirror images across both axes of symetry (overlaping peaks in g(r)). For PMD-MAA interactions, the radial distribution functions indicate that although the configuration shown in Figure 6.7b is likely to occur, as well as its mirror configuration along the axis of symetry, there are other possible configurations for associating PMD and MAA (or multiple MAA molecules). This is made clear by the peak for O4 and C4, and the disagrement with the location of the atoms in the complex observed from the annealing simulations. These radial distribution functions also hint to why PRZ can establish hydrogen bonds with both of its functional groups (although not very often), while PMD cannot. Forming two associations with the nitrogen atoms of the template imposes strong restriction on its rotational degrees of freedom. In case of PRZ, if two MAA molecules bind to the opposite nitrogen atoms, the molecule still possesses some rotational degrees of freedom along the axis connecting the two nitrgen atoms. In case of PMD, formation of the two hydrogen bonds restricts greatly any rotation, thus leading to a significant loss of the degrees of freedom.

It is therefore clear that pyrazine is allowed a higher degree of freedom while associating with methacrylic acid. It pays a smaller penalty in the $\Delta G_{trans+rot}$ contribution to the free energy of the phenomena, than does pyrimidine (see Equation I.5). Naturally the binding event during adsorption should reflect this observation as well.

6.3.2. Adsorption simulations in pyrazine and pyrimidine imprinted model MIPs

GCMC simulations were performed using the MuSiC Fortran program. The four classical grand-canonical moves (translations, rotations, insertions, deletions) are performed with equal probability and in a total of 20 to 40 × 10^6 steps for each point on the isotherms.

The first system considered in adsorption studies is MIP_PRZ, for which pyrazine is the template and pyrimidine is the analogue. In Figure 6.11 the adsorption isotherms for these species are represented with the corresponding standard deviations from the 3 matrix realizations.

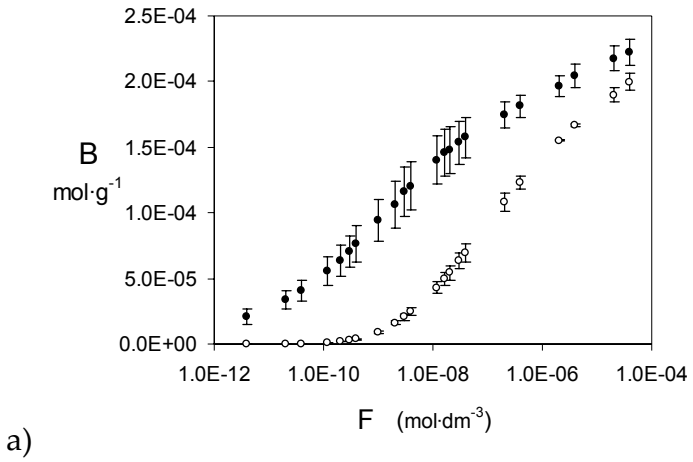

a)

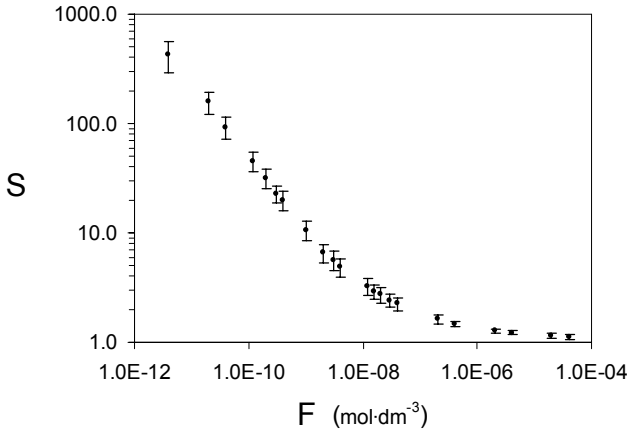

b)

Figure 6.11: a) Adsorption isotherms in model MIP imprinted with pyrazine (MIP_PRZ). Data shows the amount of adsorbate per gram of adsorbent, B, plotted against the adsorbate concentration, F (on logarithmic scale). Data for pyrazine adsorption is shown as closed circles and for pyrimidine adsorption as open circles. b) Separation factor, S, as a function of adsorbate concentration (on logarithmic scale). Data is averaged over three realizations and presented with respective standard errors.

MIP_PRZ exhibits favourable adsorption of template versus the analogue, which is better expressed by the separation factor S shown in Figure 6.11b. S is displayed in semi-log scale to show more clearly that this MIP exhibits extremely high selectivity at very low values of concentration. The graph also

shows an extremely high uncertainty associated with the separation factor, due to generally very small number of molecules adsorbed at those values of the free adsorbate concentration, and hence poor statistics.

The values of selectivity exhibited in the model MIP_PRZ material (order of 10^2) are one order of magnitude higher than what would be typically observed in the experiments (10^1). Naturally, a question arises how we can rationalize these behaviour. For this we perform the following simplified analysis. The equilibrium between the adsorbed species and unbound, free species in solution (or the gas phase) can be expressed through the partition coefficient (or the equilibrium constant):

$$K = \frac{B_i}{F_i} \qquad \text{VI.4}$$

where, B_i is the moles of adsorbed species *i* per gram of the material, and F_i is the concentration of the unbound species *i* in the gas or liquid phase. Selectivity between pyrazine and pyrimidine at the same value of the bulk concentration F can be expressed as:

$$S = \frac{B_{PRZ}/F_{PRZ}}{B_{PMD}/F_{PMD}} \qquad \text{VI.5}$$

This partition coefficient and the selectivity depend on the bulk concentration and describe a process associated with the binding sites from a particular region of the binding site distribution. Here we are interested in the most specific binding sites corresponding to low values (dilute regime) of the bulk concentration F. Using the equilibrium constants, selectivity can then be expressed by:

$$S = \frac{K_{PRZ}}{K_{PMD}} \qquad \text{VI.6}$$

Since K can be related to the free energy of binding ΔG (see equation VI.2), this can be introduced in the previous equation to give:

$$S = \frac{e^{-\Delta G_{PRZ}/RT}}{e^{-\Delta G_{PMD}/RT}} \qquad \text{VI.7}$$

If we recall Equation I.5

$$\begin{aligned}\Delta G_{bind} &= \Delta G_{trans+rot} + \Delta G_{rotors} + \Delta G_{conform} \\ &\quad + \Delta G_{polar} + \Delta G_{vdW} + \Delta G_{hydro} + \Delta G_{vib}\end{aligned} \qquad \text{I.5}$$

it would be reasonable to expect that most terms contributing to the free energy of binding will be the same, or very similar for pyrazine and pyrimidine as these species are very similar. Indeed, these are small rigid molecules and we speculate that we can ignore ΔG_{rotors}, $\Delta G_{conform}$, ΔG_{vib} terms. Analysis of the various energy terms indicate that ΔG_{vdW} is very similar for the two species. As we consider adsorption from a gas-like phase (no solvent), there are no effects associated with dissolution. The remaining terms are $\Delta G_{trans+rot}$ and ΔG_{polar}. So, S can be expressed as:

$$S = \frac{e^{-\left(\Delta G_{trans+rot}+\Delta G_{polar}\right)_{PRZ}/RT}}{e^{-\left(\Delta G_{trans+rot}+\Delta G_{polar}\right)_{PMD}/RT}} \qquad \text{VI.8}$$

or

$$S = e^{\frac{-\Delta\left(\Delta G_{trans+rot}+\Delta G_{polar}\right)}{RT}} \qquad \text{VI.9}$$

It is enough for $-\Delta\left(\Delta G_{trans+rot}+\Delta G_{polar}\right)$ to be *ca.* 6 times larger than RT for S to be equal to 450; this equates to approximately a 15 kJ·mol^{-1} difference in the free energy of binding between pyrazine and pyrimidine. This is comparable to the difference in the values of the Coulombic energy term between pyrazine and pyrimidine interacting with the functional monomers and cross-linkers in pre-polymerization mixture. We argue, that in solution, these differences in the average Coulombic interaction result from both slightly more

favourable interactions that pyrazine can form *and* higher entropic losses for pyrimidine due to restricted rotation. Similar combined effects upon binding lead to substantial values of selectivity.

The second system considered reverses the roles of pyrimidine and pyrazine. Adsorption simulations of pyrimidine as *template* and pyrazine as *analogue* in 3 matrix realizations of MIP_PMD were performed, again using MuSiC with the same simulation parameters as for the study on MIP_PRZ. The isotherms for MIP_PMD shown in Figure 6.12a indicate that the material does not appear to be selective.

The simulated isotherms for pyrazine and pyrimidine imprinted MIPs are similar, and their shape is quite characteristic of microporous adsorbents. An indication that the model material has a very small pore volume is the fact that it is nearly saturated at very low concentrations (F = 40 μM).

Analysing the selectivity of these MIPs, it becomes apparent that these model polymers are quite different. For MIP_PRZ the imprinting process was successful in generating binding sites capable of molecular recognition which exhibit selectivity towards the template (pyrazine) versus the analogue (pyrimidine). On the other hand, MIP_PMD exhibits a very different selectivity profile.

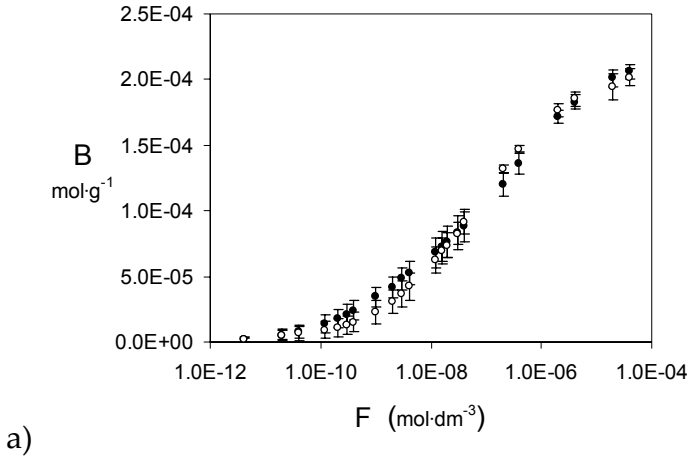

a)

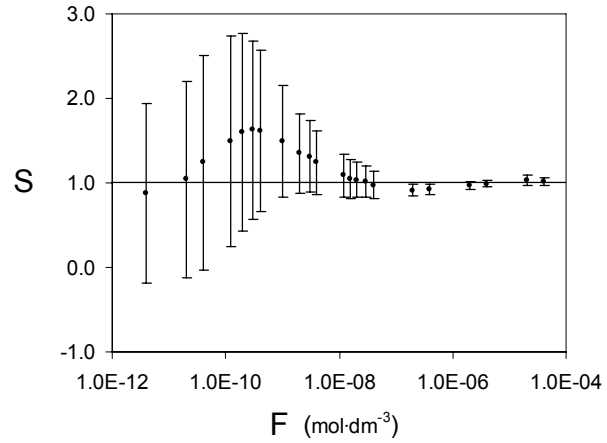

b)

Figure 6.12: a) Adsorption isotherms in model MIP imprinted with pyrimidine (MIP_PMD). Data for pyrimidine adsorption is shown as closed circles and for pyrazine adsorption as open circles. b) Separation factor S as a function of the adsorbate concentration, F (in log scale). Solid line corresponds to 1 (no selectivity). Data is averaged over three realizations and presented with respective standard errors.

The separation factor varies, exhibiting no selectivity at first, and then it shows a small preference towards the template which then disappears. Due to the very large uncertainty in the results for this MIP, we cannot extrapolate from this observation, other than it is safe to assume that MIP_PMD exhibits no molecular recognition.

This is a fascinating observation and we would like to explore it in more detail. The higher fidelity of the imprinting protocol for pyrazine as the template must be associated with the stronger interaction between this template and polymer components, or, more specifically, it must be associated with stronger Coulombic interactions and the ability of pyrazine to form more of these favourable associations due to lower rotational restraints resulting from the complexation. As hydrogen bonds are, essentially, a particular type of Coulombic interactions, not surprisingly this also correlates with the higher number of hydrogen bonds established in this system compared to that for pyrimidine.

6.3.3. Energy histogram analysis of the adsorbed species

Further insights on the role of various interaction terms in the binding processes in model MIPs can be gained from the analysis of the energy histograms for adsorbed molecules. For a particular value of bulk adsorbate concentration (F) and the corresponding adsorbed density, an energy histogram shows the distribution of adsorbed molecules over different values of interaction energy.

These results for pyrazine imprinted MIP are summarized in Figure 6.13. Specifically, Figure 6.13a presents energy histograms for pyrazine (solid lines) and pyrimidine (dashed lines) in pyrazine imprinted MIP_PRZ at 4 different values of concentration, whereas Figure 6.13b and Figure 6.13c show this data, separately, for Non-Coulombic and Coulombic terms, respectively.

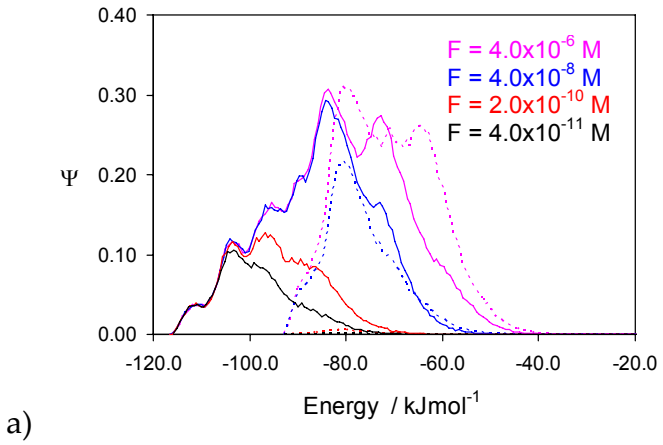

a)

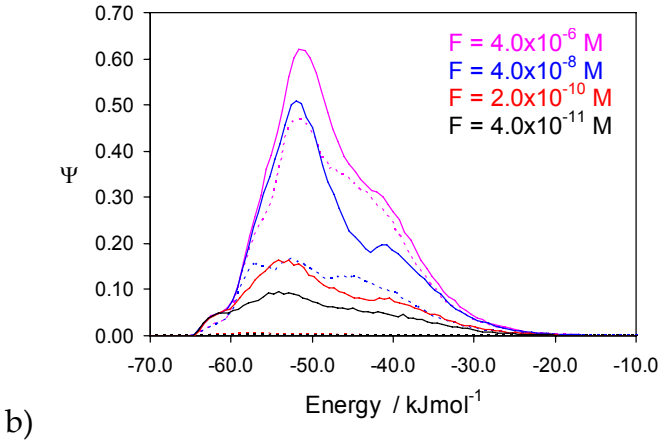

b)

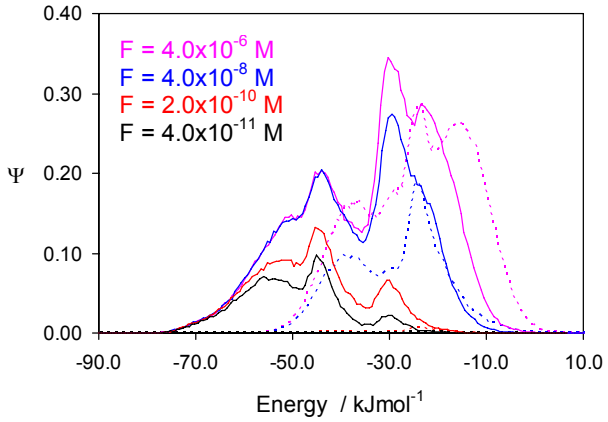

c)

Figure 6.13: Energy histograms for interaction energy between adsorbate (pyrazine in solid lines and pyrimidine in dashed lines) and pyrazine imprinted matrix, MIP_PRZ. Cumulative values sampled over 10^6 configurations (equilibrated) at different loadings, averaged over three matrix realizations. a) Total interaction energy. b) Non-Coulombic interaction contribution. c) Coulombic interaction contribution.

Several things are important to observe from these figures. First, let us consider total energy histograms presented in Figure 6.13a. For both pyrazine and pyrimidine, these histograms are unimodal and expanded towards higher (less favourable) values of energy as F (and therefore bound concentration) increases. However, for pyrazine adsorbing in MIP_PRZ these histograms reach towards lower energies by 10-30 $kJ \cdot mol^{-1}$ compared to pyrimidine, signifying stronger interaction of pyrazine with pyrazine-templated sites in the matrix. This also reveals that the population of sites being occupied is quite different from the average as this energy gap is larger than that observed in pre-polymerization energies analysis. Furthermore it shows there are binding sites so specific they are only accessible to pyrazine, which constitutes a clear evidence of the recognition phenomenon.

What is the nature of these differences in the histograms? For this, we turn our attention to Figure 6.13b and 6.13c. Figure 6.13b shows the Non-Coulombic energy distribution for pyrazine and pyrimidine adsorbed in MIP_PRZ. From these graph the two species are, not surprisingly, indistinguishable. However, Coulombic energy histograms in Figure 6.13c reveal a remarkable difference in the behaviour between pyrazine and pyrimidine.

The key feature of the pyrazine energy histogram in Figure 6.13c is its bimodal shape, developing as the concentration increases. This means that there is a group of pyrazine molecules interacting very strongly with the matrix (apparently sitting in very specific binding sites) and another group occupying the remaining, less energetically favourable space. In contrast, this bimodality of the distribution is less pronounced and the whole distribution is shifted towards less favourable energies for pyrimidine. Thus, it is clear

that Coulombic interaction (and as we argue, hydrogen bonds) is responsible for the specificity of binding sites and for molecular recognition of pyrazine in MIP_PRZ material.

The same analysis for pyrimidine imprinted MIP (see Figure 6.14) informs us that the energy histograms are centred much closer, and very notably, the range of possible interaction energies, never reaches values as low as in MIP_PRZ (for either adsorbate). This latter observation is in agreement with the earlier analysis of the interaction energies observed for the complexes in the equilibrated pre-polymerization mixture. It shows also why pyrazine isotherm in MIP_PMD is much lower compared to MIP_PRZ, and correlates with the lack of selectivity of this material towards either component. Furthermore, unlike MIP_PRZ, for MIP_PMD there is no bimodal distribution for the Coulombic energy histogram, and its peak is found in higher (less favourable) energy values. One can conclude that although the imprinting process enabled the establishing of some complexes, the resulting binding sites still lack specificity. Overall, the imprinting process was not successful in producing molecular recognition capabilities in the model MIP, and this is due to inability of pyrimidine to form fully coordinated complexes in solution (due to less favourable interaction energy and entropic effects).

These are, in the author's best knowledge, the first application of energy histograms for adsorption in MIPs. These provide a wealth of information about the population of binding sites and to a level of detail not obtained by commonly used analysis, including the assessment of the affinity distribution.

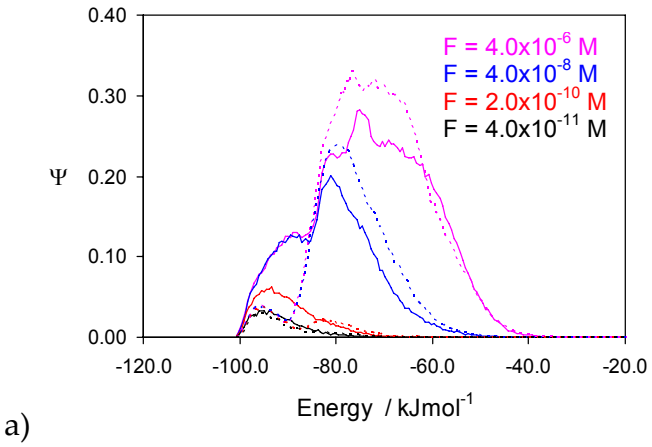

a)

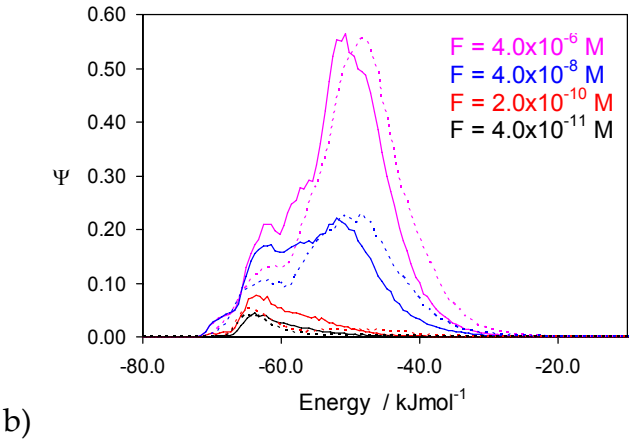

b)

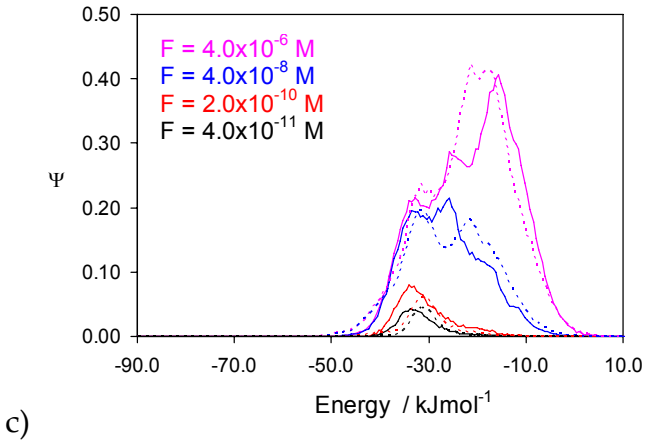

c)

Figure 6.14: Energies histograms for interaction energy between adsorbate (pyrimidine in solid lines and pyrazine in dashed lines) and pyrimidine imprinted matrix, MIP_PMD. Cumulative values sampled over 10^6 configurations (equilibrated) at different loadings, averaged over three matrix realizations. a) Total interaction energy. b) Non-Coulombic interaction contribution. c) Coulombic interaction contribution.

It is important to note, that despite the clear differences of energy of interaction, the difference in selectivities between the two MIPs is due in great part to entropy differences between the PMD and PRZ.

6.3.4. Affinity distribution analysis

The affinity distribution (AD) is often used as a tool for characterization of MIPs and its binding site heterogeneity (Umpleby *et al.* 2001; Garcia-Calzon and Diaz-Garcia 2007). The advantage of the AD analysis is that it provides a visualization of the range and relative weight of the different binding sites on the surface of the porous MIP. It has been proposed that this allows one to understand and evaluate the imprinted binding sites and use this information as a tool for more efficient MIPs optimization. The methodology of the AD analysis has been outlined in section 1.4. In principle, the free energy landscape inside a porous material could be estimated using umbrella sampling and other advanced approaches such as those used by Dubbeldam and co-workers in the context of adsorption in zeolites (Dubbeldam and Smit 2003). This is however a computationally demanding approach.

Here we limit ourselves to a simper task. The simulated adsorption isotherms allows the calculation of the ADs for model materials and the examination of what type of information can be obtained from them, using additional data on the detailed structure of these solids.

The Langmuir-Freundlich isotherm (equation I.4) has been shown to give the best fit to experimental adsorption data and provide intuitively meaningful affinity distribution curves (Umpleby *et al.* 2001). Here, this isotherm model is fitted to the results from simulations for template rebinding in MIP_PRZ

and MIP_PMD, and for comparison, to the analogue adsorption as well. The software Origin 8 from OriginLab© was used for this task.

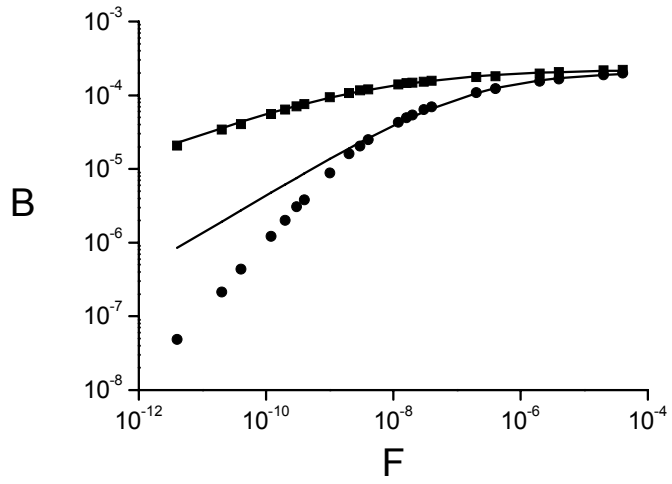

Figure 6.15: Adsorption isotherms for the pyrazine templated MIP_PRZ, on logarithmic scale. Points indicate the simulated adsorption isotherm (squares for pyrazine, circles for pyrimidine), solid lines correspond to the fitting of the LF adsorption isotherm.

Table 6.3: Fitting parameters for the LF isotherm to adsorption of PRZ and PMD on MIP_PRZ.

Parameters	PRZ	PMD
M	0.332 ± 0.011	0.515 ± 0.023
A	$676.14 \pm 162.61\ M^{-1}$	$3041.38 \pm 1252.92\ M^{-1}$
N_t	$2.25 \times 10^{-4} \pm 2.98 \times 10^{-6}\ mol \cdot g^{-1}$ (*ca.*10 molecules)	$2.05 \times 10^{-4} \pm 4.34 \times 10^{-6}\ mol \cdot g^{-1}$ (*ca.* 10 molecules)
K_0	$3.32 \times 10^{8} \pm 3.22 \times 10^{8}\ M^{-1}$	$5.87 \times 10^{6} \pm 6.20 \times 10^{6}\ M^{-1}$

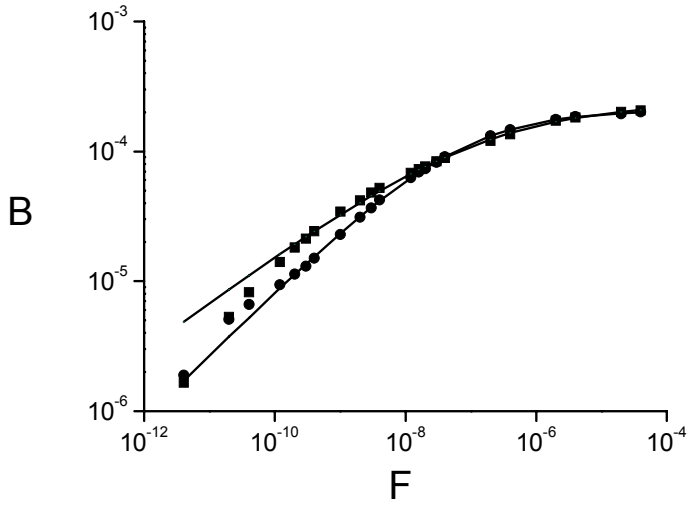

Figure 6.16: Adsorption isotherms for the pyrimidine templated MIP_PMD, on logarithmic scale. Points indicate the simulated adsorption isotherm (squares are for pyrimidine, circles for pyrazine), solid lines correspond to the fitting of the LF adsorption isotherm.

Table 6.4: Fitting parameters for the LF isotherm to adsorption of PRZ and PMD on MIP_PMD.

Parameters	PRZ	PMD
m	0.492 ± 0.005	0.367 ± 0.009
a	$3369.29 \pm 332.55\ M^{-1}$	$322.40 \pm 58.63\ M^{-1}$
N_t	$2.09 \times 10^{-4} \pm 9.44 \times 10^{-7}\ mol \cdot g^{-1}$ (*ca.* 10 molecules)	$2.34 \times 10^{-4} \pm 3.74 \times 10^{-6}\ mol \cdot g^{-1}$ (*ca.* 11 molecules)
K_0	$1.47 \times 10^{7} \pm 3.92 \times 10^{6}\ M^{-1}$	$6.93 \times 10^{6} \pm 4.36 \times 10^{6}\ M^{-1}$

For the case of heterogeneous surfaces, one can extract the affinity distribution, N(K), by solving the Langmuir adsorption integral equation:

$$\frac{B}{R} = \int_{-\infty}^{+\infty} \frac{N(K)FK}{1+FK} d(\log K) \qquad \text{VI.10}$$

where B, F and R are the concentration of the bound and free template and total number of binding sites, respectively. $N(K)\mathrm{d}(\log K)$ is the probability of a binding site having an association constant between log K and log K + d(log K) (Umpleby *et al.* 2000).

This is a general equation and does not assume R or its distribution. However, this is an example of a Fredholm integral, an ill-posed problem, for which there is no analytical solution. A method to solve this integral, which does not rely on assumptions, was developed by Hunston (Hunston 1975). The approximations used here are those adopted by Umpleby and co-workers, developed from their application and analysis of several MIP systems (Umpleby *et al.* 2001). The result of their analysis is the following general function for the affinity distribution $N(K_i)$:

$$N_i = N_t am\left(\frac{1}{K_i}\right)^m \times \frac{1 - m^2 + 2a\left(\frac{1}{K_i}\right)^m + a^2\left(\frac{1}{K_i}\right)^{2m} + 4am^2\left(\frac{1}{K_i}\right)^m - a^2\left(\frac{1}{K_i}\right)^{2m}}{\left(1 + a\left(\frac{1}{K_i}\right)^m\right)^4} \quad \text{VI.11}$$

Although the AD is theoretically valid throughout the range of concentrations, in practice its validity is assumed only in the range of concentrations of the isotherm experiment.

The affinity distributions were calculated based on the parameters obtained from fitting the LF isotherm; the results are displayed in Figure 6.17, within the range of log K where they are applicable. The limits of the affinity distribution for these isotherms are 2.49×10^{11} to 249×10^{4} M^{-1}, set by $K = 1/F$, for F_{min} and F_{max}, respectively.

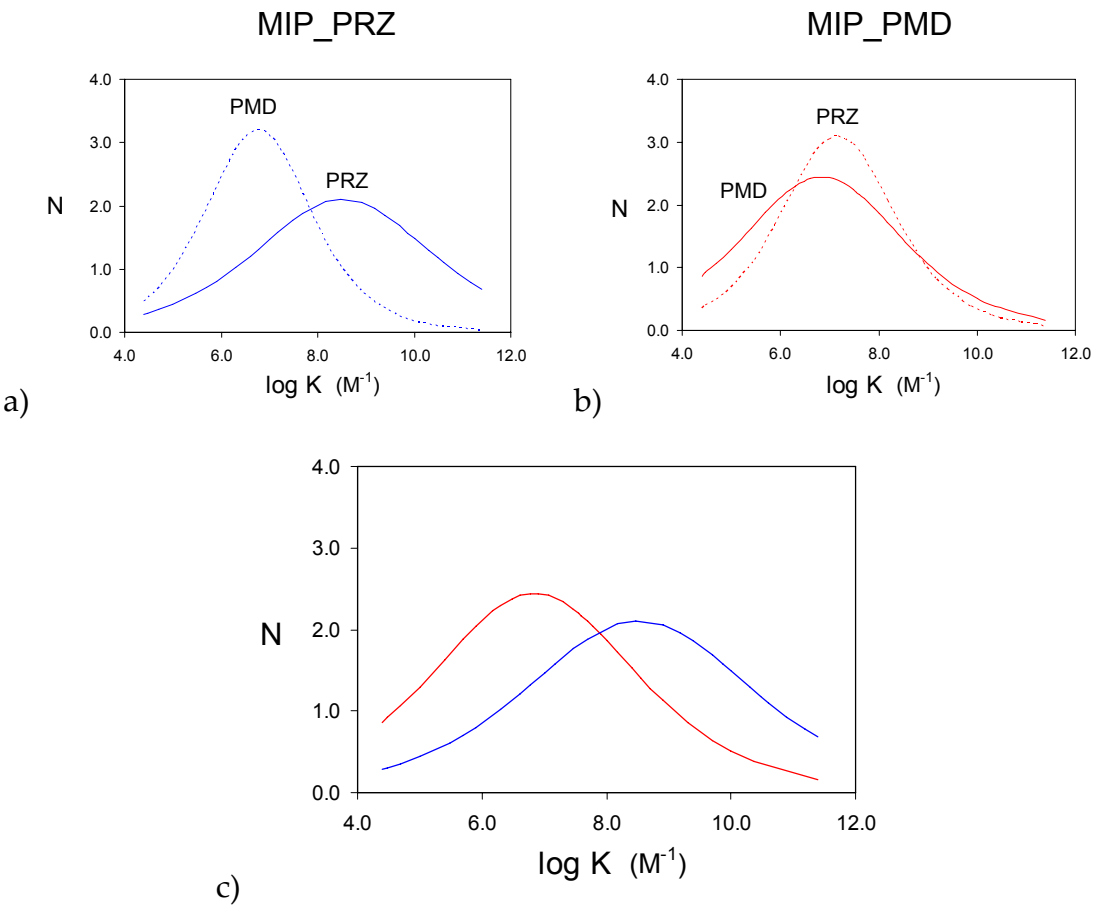

Figure 6.17: Affinity distributions (ADs) obtained from the fitting of the Langmuir-Freundlich isotherms. a) AD for pyrazine rebinding in MIP_PRZ (solid line), and pyrimidine adsorption in MIP_PRZ (dashed line). b) AD for pyrimidine rebinding in MIP_PMD (solid line), and pyrazine adsorption in MIP_PMD (dashed line). c) Comparison of the characteristic ADs (from template rebinding) for both MIP_PRZ and MIP_PMD.

The affinity distributions for pyrazine and pyrimidine in MIP_PRZ are quite different, with the AD for pyrazine being broader and its peak shifted towards higher values of log K (Figure 6.17a). This indicates that when pyrazine adsorbs in MIP_PRZ, it samples a much more heterogeneous surface and reaches higher affinity sites, than does the analogue. This is to be

expected. As exemplified before by the energy histograms, analogue binds to a narrower range of binding sites. Higher median K_0 for pyrazine also signifies that it binds stronger and to more specific sites, compared to pyrimidine. These observations are perfectly in tune with the results on selectivity and characterization of MIP_PRZ shown earlier.

It now becomes apparent that, remembering the analysis done for MIP_PMD, one should not be surprised to observe the affinity distributions presented for MIP_PMD in Figure 6.17b. As before, the analogue shows a more homogeneous distribution; ADs for the template and analogue are of similar range and median affinity. In fact the median affinity is somewhat higher in the AD extracted from the analogue adsorption data.

Comparing the ADs obtained from the rebinding simulations (Figure 6.17c), it is clear that MIP_PRZ and MIP_PMD are of similar heterogeneity. This is not surprising if one takes into account the fact that they are imprinted with the same number of very similar molecules. However, similar heterogeneity of the distributions does not imply similar site populations.
The affinity distribution reiterates what the study of the equilibrium concentrations and energies (in the pre-polymerization mixtures) were indicating. The two MIPs have different distributions of binding sites, with MIP_PRZ having noticeably more sites with strong energy of interaction.

One can interpret affinity distributions in terms of molecular recognition functionality in this specific case due to a particular choice of the system. The porous materials have very similar morphology; analogue and template species are structurally identical and differ only in interaction patterns. In

general, there is no unambiguous link between an AD and molecular recognition. Thus, for two very different types of MIPs or two very different adsorbing species, comparison of two ADs may not necessarily provide an insight on the adsorption behaviour. In this case, an AD characterizes the heterogeneity of binding site distribution (*i.e.* broadness) and this is the original function AD analysis was meant for.

Consequently, the AD is limited as a single characterizing feature. But one must remember, unlike almost all other tools to characterize MIPs, it is not concentration dependent. Despite its limitations, if it is considered in the context of MIP optimization, where MIPs of different formulation but with common characteristics are being tested towards a particular target, then this analysis becomes more applicable and presents itself very attractive.

6.4. Summary

In this chapter, we further developed an atomistic model of adsorption and binding phenomena in molecularly imprinted polymers. Two model imprinted MIPs were prepared using pyrazine (MIP_PRZ) and pyrimidine (MIP_PMD) as templates. The imprinting results in MIP_PRZ having high selectivity for the template versus the analogue (pyrimidine), thus exhibiting molecular recognition. This was not the case for MIP_PMD, where no significant evidence is found for the selective behaviour.

We investigated complex formation and molecular interactions in these model MIP materials to understand the nature of molecular recognition in

MIP_PRZ and lack of this functionality in MIP_PMD. We showed that the formation of more stable complexes in solution and resulting highly specific binding sites is governed by stronger Coulombic interactions of pyrazine with the components of the matrix, combined with lower entropic penalties in the association with methacrylic acid. Non-Coulombic interactions do not play a significant role in binding site specificity. In other words we confirmed the dominating role of electrostatic (polar) interactions in the molecular recognition phenomena. This should be expected for all competing pairs of template and analogue of very similar dimensions and conformation. This provides conclusive evidence for the general rule of thumb that stronger interactions improve molecular recognition in MIPs.

The Langmuir-Freundlich isotherm model was fitted to the simulated adsorption isotherms and the affinity distribution was determined for both MIPs. The results indicate the expected shift of the distribution towards higher affinities in the AD for MIP_PRZ versus MIP_PMD, as well as a higher median affinity. For comparison, ADs based on the analogue adsorption isotherms were generated. These ADs are narrower and shifted to lower values of affinities, which correlates with the results observed from the adsorption studies and the analysis of energies of interaction for adsorbing molecules.

The AD is believed to be a good method to characterize MIPs provided it is used for MIPs of comparable nature. Hopefully this will clarify the role AD analysis can play in studying MIPs, and with appropriate application, MIP optimisation can be accelerated.

6.5. References

Allen, M. P. and D. J. Tildesley (1987). Computer simulation of liquids. Oxford, Clarendon Press ; Oxford University Press.

Berendsen, H. J. C., J. P. M. Postma, et al. (1984). "Molecular-Dynamics with Coupling to an External Bath." Journal of Chemical Physics **81**(8): 3684-3690.

Chen, B., J. J. Potoff, et al. (2001). "Monte Carlo calculations for alcohols and their mixtures with alkanes. Transferable potentials for phase equilibria. 5. United-atom description of primary, secondary, and tertiary alcohols." Journal of Physical Chemistry B **105**(15): 3093-3104.

Chen, B. and J. I. Siepmann (1999). "Transferable potentials for phase equilibria. 3. Explicit-hydrogen description of normal alkanes." Journal of Physical Chemistry B **103**(25): 5370-5379.

Chianella, I., K. Karim, et al. (2006). "Computational design and synthesis of molecularly imprinted polymers with high binding capacity for pharmaceutical applications-model case: Adsorbent for abacavir." Analytica Chimica Acta **559**(1): 73-78.

Chianella, I., M. Lotierzo, et al. (2002). "Rational design of a polymer specific for microcystin-LR using a computational approach." Analytical chemistry **74**(6): 1288-1293.

Darden, T., D. York, et al. (1993). "Particle mesh Ewald: An N-log(N) method for Ewald sums in large systems." Journal of Chemical Physics 98: 10089–10092.

Dubbeldam, D. and B. Smit (2003). "Computer simulation of incommensurate diffusion in zeolites: Understanding window effects." Journal of Physical Chemistry B **107**(44): 12138-12152.

Essmann, U., L. Perera, et al. (1995). "A smooth particle mesh ewald potential." Journal of Chemical Physics 103: 8577–8592.

Frenkel, D. and B. Smit (2002). Understanding molecular simulation : from algorithms to applications. San Diego ; London, Academic.

Garcia-Calzon, J. A. and M. E. Diaz-Garcia (2007). "Characterization of binding sites in molecularly imprinted polymers." Sensors and Actuators B-Chemical **123**(2): 1180-1194.

Gupta, A., S. Chempath, et al. (2003). "Object-oriented programming paradigms for molecular modeling." Molecular Simulation **29**(1): 29-46.

Herdes, C. and L. Sarkisov (2009). "Computer Simulation of Volatile Organic Compound Adsorption in Atomistic Models of Molecularly Imprinted Polymers." Langmuir **25**(9): 5352-5359.

Huang, X. and S. J. Li (2008). "Rationally designing molecularly imprinted polymers toward a highly specific recognition by using a stoichiometric molecular self-assembly." Journal of Inorganic and Organometallic Polymers and Materials **18**(2): 277-283.

Humphrey, W., A. Dalke, et al. (1996). "VMD: Visual molecular dynamics." Journal of Molecular Graphics **14**(1): 33-&.

Hunston, D. L. (1975). "2 Techniques for Evaluating Small Molecule-Macromolecule Binding in Complex System." Analytical Biochemistry **63**(1): 99-109.

Karlsson, B. C. G., J. O'Mahony, et al. (2009). "Structure and Dynamics of Monomer-Template Complexation: An Explanation for Molecularly Imprinted Polymer Recognition Site Heterogeneity." Journal of the American Chemical Society **131**(37): 13297-13304.

Kendrick, J., E. Robson, et al. (1997). "Molecular modelling of novel energetic materials." Waste Management **17**(2-3): 187-189.

Lindahl, E., B. Hess, et al. (2001). "GROMACS 3.0: a package for molecular simulation and trajectory analysis." Journal of Molecular Modeling **7**(8): 306-317.

Lubna, N., G. Kamath, et al. (2005). "Transferable potentials for phase equilibria. 8. United-atom description for thiols, sulfides, disulfides, and thiophene." Journal of Physical Chemistry B **109**(50): 24100-24107.

Martin, M. G. and J. I. Siepmann (1998). "Transferable potentials for phase equilibria. 1. United-atom description of n-alkanes." Journal of Physical Chemistry B **102**(14): 2569-2577.

Martin, M. G. and J. I. Siepmann (1999). "Novel configurational-bias Monte Carlo method for branched molecules. Transferable potentials for phase equilibria. 2. United-atom description of branched alkanes." Journal of Physical Chemistry B **103**(21): 4508-4517.

Stubbs, J. M., J. J. Potoff, et al. (2004). "Transferable potentials for phase equilibria. 6. United-atom description for ethers, glycols, ketones, and aldehydes." Journal of Physical Chemistry B **108**(45): 17596-17605.

Umpleby, R. J., S. C. Baxter, et al. (2001). "Characterization of molecularly imprinted polymers with the Langmuir-Freundlich isotherm." Analytical chemistry **73**(19): 4584-4591.

Umpleby, R. J., M. Bode, et al. (2000). "Measurement of the continuous distribution of binding sites in molecularly imprinted polymers." Analyst **125**(7): 1261-1265.

Wick, C. D., M. G. Martin, et al. (2000). "Transferable potentials for phase equilibria. 4. United-atom description of linear and branched alkenes and alkylbenzenes." Journal of Physical Chemistry B **104**(33): 8008-8016.

Wick, C. D., J. M. Stubbs, et al. (2005). "Transferable potentials for phase equilibria. 7. Primary, secondary, and tertiary amines, nitroalkanes and nitrobenzene, nitriles, amides, pyridine, and pyrimidine." Journal of Physical Chemistry B **109**(40): 18974-18982.

Yungerman, I. and S. Srebnik (2006). "Factors Contributing to Binding-Site Imperfections in Imprinted Polymers." Chem. Mater. **18**(3): 657-663.

7.

Conclusions and prospective research paths

This thesis outlines the first model of a three-dimensional disordered porous MIP which exhibits molecular recognition and binging site heterogeneity and where these characteristics are explored in MIP application (adsorption) as well as formation. Several MIP systems composed of templates, cross-linker and functional monomers were simulated and analysed. The simulations follow a modelling approach which is, simply put, the modelling of all stages of MIP formation and function. We find this necessary because the optimization of biomimetic molecular recognition through molecular imprinted polymers is a complicated subject. It requires the knowledge of the effects of many varied factors influencing the formation of binding sites, the porous network, accessibility, binding site types and population distribution,

etc. The model must allow us to correlate their effects, during synthesis and application, with each other so that they can be interpreted with the view of their benefits and disadvantages towards different applications.

The modelling approach can be implemented with varying levels of detail. In the present work, two distinct forms were investigated. The fundamental differences are that one provides qualitative answers from generalized molecular species, while the second is more realistic and gives quantitative results which can more directly be compared with real MIPs.

A simplified model, described by hard-sphere and square-well interactions, was implemented to describe model MIPs were hydrogen bond – like associations are mimicked to imprint interaction patterns onto a MIP matrix. The model successfully mimics behaviour of MIPs with regards to variations of density and stoichiometry of the pre-polymerization mixture. The study of the associations between template or analogue and the functional monomers reveals more selective binding sites, and consequently, a higher selectivity MIP is favoured with higher number of fully complexed templates in the pre-polymerization mixture. The selectivity is shown to ultimately dependent on the relative weight of imprinted selective sites to non selective sites in the adsorbent model MIP.

Novel optimization protocols were tested in simulations. Model MIPs were imprinted with alternative templates featuring a spacer group. These showed increased binding site accessibility while retaining selectivity for the target molecule versus its analogue.

Large increases in the selectivity of model MIPs were achieved for low loadings, by incapacitating the association of adsorbates with functional monomers not present on high specificity binding sites. This reduction in the heterogeneity provides a great boost in selectivity, but at the cost of lowered capacity.

This model detail is simple, but it has proven that it can mimic and study with some depth MIP materials capable of molecular recognition and of displaying binding site heterogeneity. It makes a likely candidate to link with and test theory or as a stepping stone to more detailed simulations or experiments.

A different study in this thesis saw the same approach used with realistic model detail. MIPs were modelled by imprinting polymers composed by MAA and EGDMA with pyrimidine and pyrazine. The results showed the imprinting to be successful for only the pyrazine templated MIP. The study of the equilibrium in the pre-polymerization stage, together with the discrimination of the energetic contribution of Coulombic and non-Coulombic interactions reveals the distinguishing characteristics that led to the different behaviour. In the pyrazine templated MIP, template – functional monomer complex is governed by stronger interactions. The difference in the energy of interaction is due to the Coulombic contribution, but it does not explain the differences in the behaviour by itself. Because of the nature of the two adsorbates, pyrazine has a lower entropic penalty (loss of rotational degrees of freedom) in the binding event. Together these effects are responsible for higher propensity of pyrazine to form complexes in the pre-

polymerization mixture, and higher selectivity of the binding sites resulted from these complexes towards pyrazine.

With the use of realistic force-fields, adsorption isotherms were analyzed to extract the affinity distribution via the same methodology used for experiments. The AD conforms to the expected behaviour. The AD expresses the observations obtained from different analysis in a single, simpler form. But the complex issue of optimizing MIPs for different application requires information in detail for different factors influencing the phenomena; hence the AD should not be taken as a single figure of merit.

The current approach follows the accepted assumption that the pre-polymerization equilibrium is reflected in the binding site population. In this work this is done, by a simple quenching step. A more realistic simulation should include the modelling of polymerization. This could allow the understanding of what influence the process has on the nature of the complexes and ultimately its effects on the binding sites. Modelling of polymerization would also permit better representations of porous morphology. Once this capability is set up, it opens the door to the study of processes that affect the binding site since the formation of the complex to the binding in adsorption experiments. These can include: the polymerization process itself, solvent extraction, temperature changes and other effects. Furthermore, modelling polymerization would allow for a more detailed and realistic representation of the effects of expansion on the properties of binding sites and MIPs.

The natural next step is to evolve the model to a stage where solvent and/or porogen are included, polymerization is modelled and the model structure is a realistic percolating network (as opposed to fragments of the structure not connected to each other and essentially suspended in space). We speculate that the principal, qualitative observations obtained in this work will not change. However, areas such as the influence of expansion or cross-linking level would be considered from a different angle since different parameters would come into scrutiny due to more complex phenomena being captured. With a kinetic model of polymerisation, a realistic pore network could be examined and the issues of accessibility and structural characterisation of MIPs could be addressed in much greater depth and accuracy.

A subject of great interest is the use of molecular recognition to trigger events. Flexible MIPs have been shown to change their morphology in this way, under certain conditions. One could imagine a membrane filtration system in a nano-device with customizable filtration properties via an injection of template.

Other exciting applications relate to the use of molecular recognition in self-assembly and supra-molecular chemistry. For example, the use of molecular recognition, not only to aid the assembly of vesicles (for example for drug delivery), but also to allow interaction of these with biological structures. It would be a great achievement if molecular recognition triggered destruction of these vesicles could be made common place *in vivo*, as this would mean extremely targeted and safe drug delivery.